A GRAPHENE OXIDE NANOCOMPOSITE FOR NEURAL INTERFACING APPLICATIONS

by

Cassandra Lynn Weaver

B.A., Boston University, 2005

Submitted to the Graduate Faculty of

Swanson School of Engineering in partial fulfillment

of the requirements for the degree of

Doctor of Philosophy

University of Pittsburgh

2014

UNIVERSITY OF PITTSBURGH

SWANSON SCHOOL OF ENGINEERING

This dissertation was presented

by

Cassandra Lynn Weaver

It was defended on

March 31, 2014

and approved by

Guoqiang Bi, Ph.D., Professor, School of Life Sciences, University of Science and Technology of China

Kacey G. Marra, Ph.D., Associate Professor, Departments of Plastic Surgery and Bioengineering

Yadong Wang, Ph.D., Professor, Departments of Bioengineering, Chemical Engineering, and Surgery

Dissertation Director: Xinyan Tracy Cui, Ph.D., Associate Professor, Department of Bioengineering

A GRAPHENE OXIDE NANOCOMPOSITE FOR NEURAL INTERFACING APPLICATIONS

Cassandra Lynn Weaver, PhD

University of Pittsburgh, 2014

Advanced neural interfacing technologies have the ability to communicate with the central nervous system (CNS) and provide researchers with valuable information about the complex physiology of the brain. Traditional neural electrodes interact with nervous tissue electrically, either through recording or stimulation, but are limited in their potential to chemically interface with the CNS. This dissertation describes the development of a conductive neural biomaterial with the capability of recording neurochemical signals in addition to providing both immobilized and soluble chemical cues to influence cell behavior.

The material consists of a graphene oxide/conducting polymer (GO/CP) nanocomposite deposited onto the surface of metal or carbon electrodes for improved, multimodal interfacing capabilities with neurons and neural stem cells (NSCs). The GO/CP nanocomposite demonstrated good biocompatibility with neurons and NSCs and improved neuronal differentiation and neurite outgrowth as a result of its chemical and morphological properties. Additionally, the GO nanosheets present at the nanocomposite surface enabled patterning with bioactive molecules to further influence cell growth. The electrochemical properties of the GO/CP nanocomposite enabled highly controllable, on-demand drug delivery, and the chemical properties contributed by the GO nanosheets created a platform for highly sensitive and selective dopamine detection. With an eye toward developing a highly customizable device that

incorporates the versatile chemical interfacing capabilities of GO/CP with the electrical recording ability of planar multielectrode arrays, this body of work concluded with the characterization of an *in vitro* cultured neuronal network (CNN) damage model for investigating the pathobiology of neuronal injury. A crush injury applied to the CNN interrupted the normal activity patterns of the network and the addition of NSCs to the injury site demonstrated the ability to protect the network from developing dysfunctional circuitry, making the model an exciting platform for exploring neuronal regeneration. While the work here focuses solely on the potential of the nanocomposite in neural interfacing applications, its uses are not limited to the CNS but span all systems in the body and, as a result of its extremely unique chemical and electrical properties, extend to fields outside biomedicine.

TABLE OF CONTENTS

LIST OF TABLES

LIST OF FIGURES

PREFACE

This dissertation is dedicated to my parents who provided me with loving support over the years and always encouraged me to pursue my dreams. During the past six years, I often repeated to myself the words of advice my mom gave me when I was an undergraduate and I told her I was hesitant to apply for a scholarship because I did not think I would win it. "Nothing ventured, nothing gained," she said. With those four words, she taught me to have confidence in myself and reach for things that were outside of my comfort zone even if I was scared of failure. Those words served me well because I ended up winning that scholarship and it was during those two years I spent as a Beckman Scholar that I first truly discovered my passion for science. Thank you, Mom. And thank you, Dad, for inspiring me with your level-headedness and rational approach to addressing problems. These personality traits that I sometimes have the ability to master have helped me succeed as a scientist. I am so sorry you could not be here to see this day arrive.

A huge acknowledgement goes to my advisor, X. Tracy Cui, who supported me in countless ways during this experience. Thank you for accepting me into your laboratory six years ago and teaching me how to be a scientist, to always ask why, and to always think of the next experiment. The rest of the NTE lab, past and present, has helped me in numerous ways throughout the course of my work. Xiliang Luo originally conceived the idea of creating a composite material composed of graphene oxide and conducting polymer. Without the groundwork he laid for this project, none of this work would have been possible. Bill Stauffer showed me the ropes during my first year of graduate school and, along with a folder full of

uncommented MATLAB code, he passed on to me the responsibility of developing a project based on the multielectrode recording system. Trevor Sleight and Jeff Du helped me sort through that code and gave me the basic understanding of coding in MATLAB that got me though graduate school in a Bioengineering program. Takashi Kozai provided assistance with neural analysis and was always ready with some helpful advice about developing a career in science. Kasey Catt assisted me with network recordings and was always my go-to person for microfabrication advice. Noah Snyder reminded me of all of the important chemistry concepts that I had forgotten since freshman chemistry class and he surely saved me from creating a chemical explosion or two. James Eles was a constant source of entertainment, which was especially welcome during the final months leading up to my defense when I was so focused on finishing and needed some comic relief. Christi Kolarcik was a role model always ready with advice and encouragement. Her continual reminders that graduate school is temporary and I would soon be on the other side were always fortifying. I was lucky enough to have a number of great undergraduate students who were willing to donate their time to help me collect data for my projects: Jonathan Callan, Sanjeev Khanna, Huaxiu Li, Jaclyn LaRosa, and Linn Zhang.

I would not be in this position today if it were not for my previous scientific mentors. My undergraduate advisor, the late Mary S. Erskine, taught me the importance of mentoring and instilling excitement into young minds about the prospect of scientific discovery. Dave Lewis, my post-baccalaureate advisor, showed me what it means to dedicate a career to truly making a difference in the lives of individuals suffering from illness. Thank you to all of my mentors for setting an example and making me the scientist I am today.

My committee members, Guoqiang Bi, Kacey Marra, and Yadong Wang, were an important part of my graduate training. They provided support and advice over the years, and

entertained my often overly ambitious timelines without too much criticism. Guoqiang was especially helpful in providing insight into neural network analysis and was kind enough to make the trip from China to Pittsburgh to attend my committee meetings and dissertation defense.

Others from the University of Pittsburgh community provided various support over the years. Jonathan Franks and the Center for Biological Imaging supplied assistance with scanning electron microscopy. Susheng Tan and the Nanofabrication and Characterization Facility provided training and access to numerous characterization instruments that I so heavily relied on for all of my work. Lacey Cirinelli generously provided me with neurons and tissue for cell culture experiments.

Additionally, Christopher Matranga from the National Energy Technology Laboratory advised me during my time in the Oak Ridge Institute for Science and Education internship program. He taught me Raman spectroscopy and x-ray photoelectron spectroscopy, and introduced me to the foreign world of research inside of a government facility.

This work was supported by a number of funding sources over the years including the University of Pittsburgh Provost's Development Fund, the Oak Ridge Institute for Science and Education Professional Internship Program, National Science Foundation Grants 0748001, 0729869 and DGE-0549352, National Institute of Health R01NS062019, the Department of Defence TATRC grant WB1XWH-07-1-0716 and DARPA MTO N66001-11-1-4014. I would also like to thank the Center for the Neural Basis of Behavior for proving travel stipends each year.

Finally and most importantly, I need to thank Kevin for supporting me throughout the past four years. He motivated me during the early years of graduate school when I questioned my decision to continue along this path. He grounded me during the later years of graduate school

and reminded me that there is a world outside of the research lab. And during the last few hectic months of dissertation writing and job interviews he kindly endured my obsessive and frantic behavior, all while offering loving support and encouragement.

1.0 INTRODUCTION

While tremendous progress has been made in the fields of neuroscience and neurorehabilitation in the past several decades, the brain remains the most uncharted organ in the body. Composed of billions of electrically excitable neurons that form precise and intricate connections with each other, the brain embodies a high level of complexity that will require decades of work to unravel. Advanced neural interfacing technologies that have the ability to interact with the nervous system will be able to assist this endeavor by providing information about the physiology underlying the complex set behaviors and cognition characteristic to humans. Ultimately, advances in this area will generate the knowledge that is necessary to create life-changing therapeutics for nervous system damage and disease. The overarching goal of this dissertation is to further the efforts towards understanding the enigmatic brain physiology and creating therapeutics for injury and disease by developing and characterizing a novel neural material that can improve the ability to chemically interface with the nervous system.

1.1 INTERFACING WITH THE NERVOUS SYSTEM

Neural interfacing technologies can provide scientists and engineers a window into complex and intricate physiology of the brain. Traditionally, glass or metal electrodes have been used to record electrical signals from the central nervous system (CNS) in behaving animals, and these

types of recordings have been the basis for our current understanding of the neural control of behavior and cognition [1-3]. Additionally, neural electrodes are being developed for brain-machine interfaces that can restore function to the nervous system by electrically stimulating dysfunctional circuitry or by translating recorded signals to drive prosthetic devices. The state-of-the-art neural electrode systems are multi-channel arrays composed of metal that have the ability to simultaneously sample from or stimulate populations of neurons [4, 5]. The electrodes function by transducing the electrical signals that occur at the neuron-electrode interface, a process that is mediated by the transfer of charge between the electrode surface and the surrounding electrolyte solution [6]. While great progress has been made for neural interfacing devices in their ability to record electrical signals from nervous tissue, these devices lack the capability of multimodal interfacing. The goal of this dissertation is to describe a material that was developed as a neural electrode modification that will create the means to interface chemically with cells in the CNS by providing cues, either immobile or soluble, and by detecting neurochemical signaling. The novel nanocomposite material consists of graphene oxide (GO) nanosheets embedded in a conducting polymer (CP) matrix that has unique chemical and electrical properties amenable to chemical interfacing with nervous tissue. The following sections will introduce the unique properties of CPs and GO separately and briefly summarize their bioapplications.

1.2 CONDUCTING POLYMERS

The first reported synthesis of intrinsically conducting polymers (CPs) occurred in the mid-nineteenth century when British chemist, Henry Letheby, described the electrochemical

oxidation of polyaniline [7]. Since their modern development in the 1970s, CPs have found a wide range of applications in electronics [8], fuel cells [9], sensors [10, 11], biointerfacing [12], and tissue engineering [13]. Because of their intrinsic conductivity of both electrons and ions, CPs lend themselves particularly well to neural interfacing applications, in which responsiveness to electrical signaling is a necessary component of interfacing materials [14-19]. Two of the most commonly studied CPs, and the two which will be the focus of this dissertation, are polypyrrole (PPy) and poly(3,4-ethylenedioxythiophene) (PEDOT) (Figure 1.1).

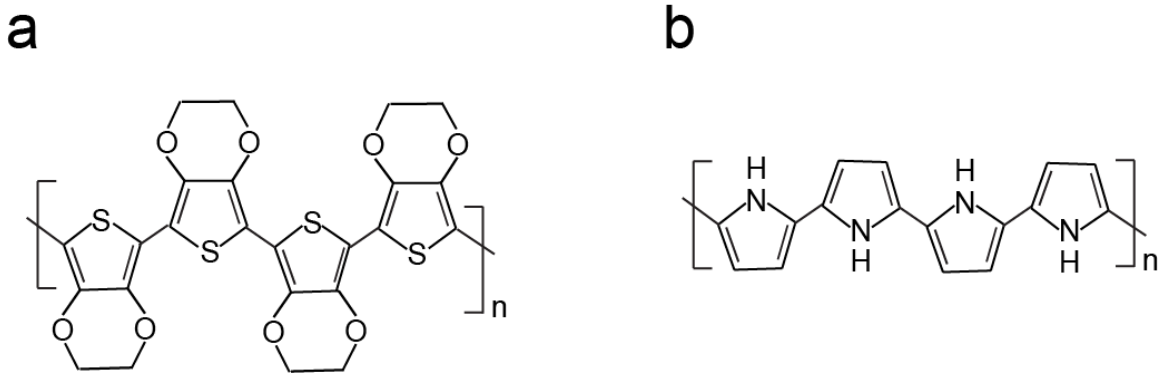

Figure 1.1. Structure of CPs (a) PEDOT and (b) PPy. Both have the characteristic conjugated π backbone that is partially responsible for the conductivity of the polymers.

1.2.1 Synthesis

One of the attractive properties of CPs is their inexpensive and facile processing, which can be carried out either chemically or electrochemically. The polymerization reaction is induced by oxidation of the monomers in solution and then proceeds by free radical polymerization to create insoluble polymer precipitates [20]. Chemical polymerization utilizes strong oxidizing agents,

such as ammonium peroxydisulfate, permanganate ions, or hydrogen peroxide, that are either added in bulk to a solution of monomer to create a CP suspension, or coated onto a surface to induce the formation of a thin CP film [21]. In general, chemical polymerization of CPs is beneficial for applications in which large quantities of polymer are desired because of the scalability of the reaction; however, poor control over the uniformity of the final CP product limits the use of this method for applications requiring thin films. On the other hand, electrochemical polymerization of CPs is a highly controllable reaction and is more widely used for creating thin films of polymer. In this method, an oxidizing current or voltage is passed through an electrode immersed in an electrolyte solution of monomer to initiate free radical polymerization, and the synthesized CP deposits preferentially at the electrode surface to create a thin film. All of the work described in this dissertation utilizes electrochemical synthesis of thin CP films at the surface of electrodes and, as such, will be the focus here.

The benefit of electrochemical polymerization lies in the ability to finely control the type of electrical stimulation applied through the electrode, which will ultimately lead to a high level of control over the properties of the synthesized polymer film. In general, there are three methods of electrochemical deposition: potentiodynamic, potentiostatic, and galvanostatic [22]. In the potentiodynamic method, the electrode potential is cycled through a wide range that includes the oxidation potential of the monomer. When the electrode potential surpasses the oxidation potential, polymer is synthesized and deposited at the electrode surface, and when the potential is swept back below that potential, deposition ceases, resulting in a thin layer of polymer. As the deposition continues, additional thin layers are deposited onto the surface of the previous layer, enabling control over the final thickness of the CP film. However, the repeated

cycling allows solvent molecules to be entrapped between layers of the CPs, creating a disordered structure in the final CP film.

Alternately, the potentiostatic and galvanostatic methods hold the electrode potential or current, respectively, at a point above the oxidation potential of the monomer during the entire duration of the synthesis. In these methods, CP is continuously deposited onto the surface of the electrode and the thickness and morphology of the final film is controlled by the total length of the deposition and the magnitude of applied electrical stimulation [14, 23]. The polymerization reaction can be described by the following equation:

$$(n+2)HMH \rightarrow HM(M_n)MH^{(nx)+} + (2n+2)H^+ + (2n+2+nx)e^- \qquad (1)$$

where HMH is the starting species, and *x* is the doping level of the specific CP, which generally falls between 0.25 and 0.4 [22]. According to Equation (1), the amount of polymer formed during the reaction is directly related to the number of electrons consumed during the reaction. As such, controlling the current during CP deposition by using the galvanostatic method provides the most reliable means of controlling the CP film growth because the current is fixed at a particular magnitude for the duration of the reaction. On the other hand, with the potentiostatic method, the current can fluctuate throughout the course of the deposition reaction, resulting in inconsistencies in the total amount of charge passed during a particular time period and a decrease in the repeatability of the reaction. While the galvanostatic method has the benefit of repeatability, the potentiostatic method has been demonstrated to produce CP films that exhibit higher conductivity and lower impedance that possibly results from a larger surface area created during the non-uniform deposition [24]. Each of the deposition techniques exhibit benefits and

drawbacks, but ultimately, the electrochemical synthesis methods provide a huge level of control over the final film properties, allowing the CPs to be tailored to a wider array of potential applications.

1.2.2 Electrical Properties

CPs are unique among polymeric materials because they exhibit intrinsic conductivity, while most other polymers are insulating in nature. The excellent ability of CPs to conduct electrical current was first explored in the 1970s with the characterization of polysulfur nitride and polyacetylene. These early studies found that these polymer materials could behave like metals, and their conductivity could be increased by orders of magnitude after oxidation into their polymeric cation form [25-27]. The conductivity of CPs arises from 1) their conjugated backbone, and 2) the formation of polarons and bipolarons in their structure as the ionized backbone is neutralized by ionic dopant molecules.

The conjugated structure consists of alternating single and double bonds between the carbon atoms in their backbone. The double bonds in the structure contain delocalized π-bonds that overlap and can share electrons, creating a continuous supramolecular orbital though which the electrons freely move [28]. In parallel to the conjugated structure, the doping process of the CP improves its conductivity. During synthesis by electrochemical oxidation, the CP is produced in its ionized form, with net positive charges accumulating on its backbone. Any negatively charged species present in the aqueous polymerization environment moves into the growing CP to neutralize the charge and stabilize the CP structure. This dopant molecule then creates holes in the electronic structure of the CP and creating polarons and bipolarons, mobile charge carriers consisting of loosely localized electrons surrounded by lattice distortions [29]. When an

electrical voltage is applied to the CP film, the polarons and bipolarons move, leading to the passage of current through the polymer. The conductivity of CPs can vary hugely, and is largely dependent on the type of dopant molecule or synthesis method used [22, 24, 30, 31].

1.2.3 Redox Properties

A unique property of CPs is their ability to switch between their oxidized and reduced forms in response to electrical stimulation. After synthesis *via* galvanostatic or potentiostatic methods, the CP exists in its oxidized state, carrying positive charges on its backbone that are balanced by negatively charged dopant molecules. With the application of a reducing voltage potential, the CP will switch to its reduced state and small, mobile anionic dopants will exit the film as the backbone neutralizes [28]. In the case where CP has been doped with large, immobile dopants that are sterically restricted from moving out of the film, cations will instead move into the film to neutralize the immobile dopant during CP reduction. The reversible redox properties of CPs have been used as a method to achieve controllable release of various drug molecules for applications in biomedicine [32-37].

1.2.4 CP Bioapplications

The type of dopant molecule used in CP systems can have a huge impact on both the electrical and physiochemical properties of the CP film. A wide range of different dopants have been investigated for CP applications, from small ions such as chloride or phosphate, to large polymers such as poly(styrenesulfonate) (PSS), and bioactive molecules such as hyaluronic acid and nerve growth factor [38-44]. Because of the versatility of potential dopant molecules and the

consequent ability to control the electrical, morphological, and chemical properties of the resultant film, CPs have been widely investigated as customizable substrates for a variety of biomedical applications [10, 13, 34, 45-47].

In the past decade, CPs have generated excitement within the field of neural engineering because their unique electroactivity opens the possibility of interfacing with the electrically excitable cells of the CNS [16]. Neural electrodes coated with CPs exhibit a much rougher surface morphology that creates a larger effective surface area and can lead to improved electrical properties. Ideal neural electrodes have a very small size profile that will enable single cell interfacing and reduce damage that occurs during insertion into tissue [5]; however, as their size decreases, their electrochemical impedance increases, reflecting the smaller surface area that will result in low signal-to-noise ratios [4, 48]. Electrochemical impedance spectroscopy, a common method of measuring the charge transfer that occurs at an electrode surface, indicates how well a particular electrode will perform and is often used as a method to evaluate neural electrodes. After being coated with CP, electrodes can exhibit decreases in impedance by an order of magnitude or more, reflecting the potential of these modifications to create improved interfaces for neural recording [14, 15, 17, 19, 41, 49]. A common problem faced during chronic neural recordings *in vivo* is the inflammatory tissue response that ultimately leads to the failure of the implanted electrode [5]. However, CPs can be doped with bioactive molecules that combat this reaction and have the potential to improve the lifespan of implanted electrodes [16, 38, 40, 42, 50]. In sum, the ability to create high surface area interfaces with favorable electrical properties, along with their ease of customization, have rendered CPs a popular material for uses in neural interfacing.

1.3 GRAPHENE AND GRAPHENE OXIDE

Carbon nanomaterials and graphene family materials, in particular, have been widely investigated in recent years for a variety of applications in electronics, optics, and medicine because of the unique properties that arise from their nanostructures. Graphene (G) is the basic unit of all carbon materials and is composed of a tightly packed honeycomb carbon lattice that is exciting because of its 2-dimensional structure. First synthesized in 2004, true G measures a single atom in thickness (ca. 0.3 nm), leading to its quantum behavior that creates exceptional conductivity, mechanical strength and optical properties [51]. To produce G, several methods have been used, with chemical exfoliation of graphite becoming popular because of its low cost and scalability, and because it creates an opportunity for chemical modification that allows for a wider range of applications [52]. In reality, the chemical method of synthesis creates a product that is not true, pristine G because it contains residual oxygen functional groups, but it exhibits similar properties and can be processed as a colloidal solution, which improves the ease of handling. The chemical exfoliation method is carried out by oxidizing graphite platelets with strong oxidizing agents, such as sulfuric acid and potassium permanganate, to create graphite oxide [53, 54]. The oxidation reaction creates multiple oxygen containing functional groups on the graphite oxide layers, and results in a stacked structure of hydrophilic graphene oxide (GO) nanosheets that are intercalated by water molecules and can be easily mechanically exfoliated with sonication treatment into few-layer or single nanosheets measuring from hundreds of nanometers to a few microns in diameter (Figure 1.2). By itself, GO is an insulating material because the ballistic electron transport that is observed in G is interrupted by defects in the lattice structure formed during the addition of oxygen functional groups. However, GO can be further processed into reduced GO (RGO) through chemical, thermal or electrochemical reduction to

produce a final product that has similar properties to G. While this chemical synthesis method was originally intended to create the final conductive RGO product as an analog to G, much attention has been focused on the intermediate GO after the observation of its interesting chemical properties and ease of functionalization.

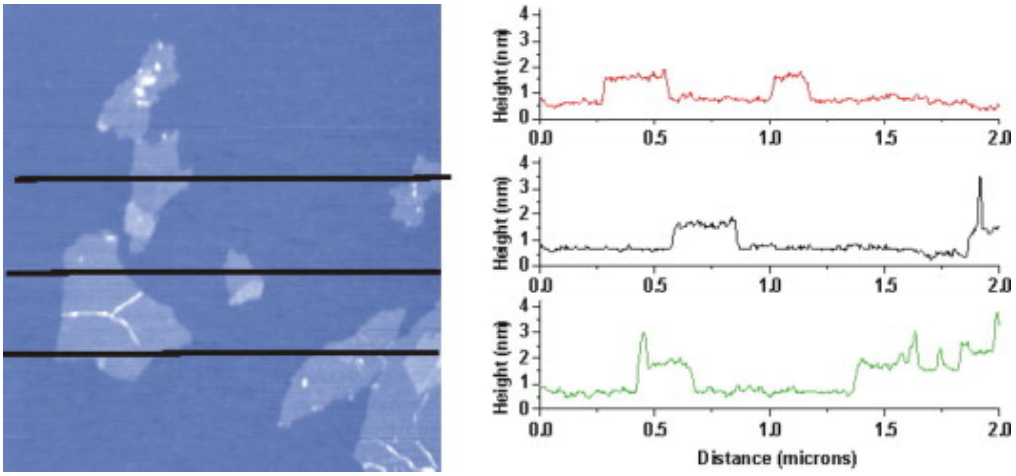

Figure 1.2. GO is a Single-Layered Nanosheet. Atomic force microscopy image of exfoliated GO sheets and corresponding height profiles showing the sheet-like structure of the nanomaterial and its single atomic layer thickness (ca. 1 nm). Image reproduced with permission from [55] © 2007 Elsevier.

1.3.1 GO Structural and Chemical Properties

While the structure of GO is still under debate, it is generally accepted that during the oxidation from G, several types of oxygen functional groups are added to the structure, creating mixed domains of sp^2- and sp^3-bonded carbon (Figure 1.3) [53, 56]. The most widely accepted structural model of GO is the Lerf-Klinowski model that includes hydroxyl (C-OH) and epoxide (C-O-C) functional groups, with a lesser amount of carboxyl (C-O-OH) functional groups

localized to the edge of the sheets [57], though other models have recently emerged to include lactol rings and tertiary alcohols [58]. The oxygen content of GO can vary considerably depending on the method of oxidation and may be a contributing factor to the dissension over its structure [53].

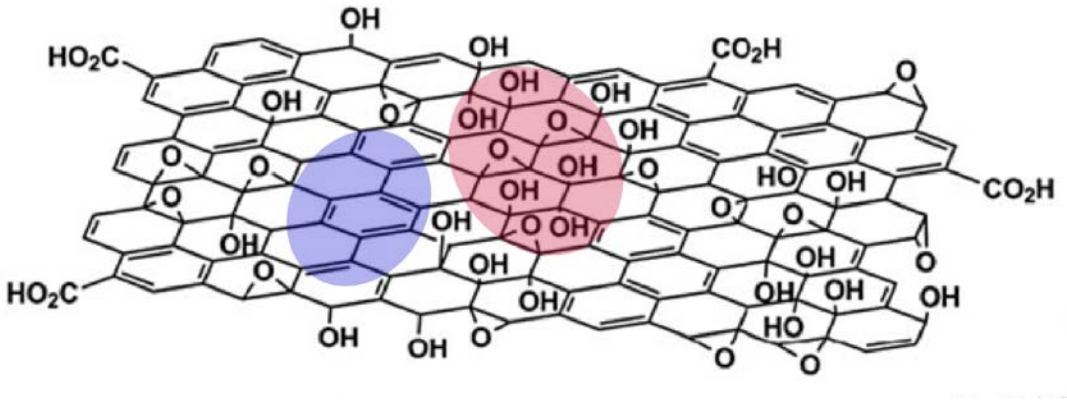

Figure 1.3. Structure of GO Based on a Variation of the Lerf-Klinowski Model. The honeycomb carbon structure exhibits domains of sp^2-bonded carbon (blue) interspersed with sp^3 carbon bonded with oxygen (red). GO contains carboxyl, epoxide and hydroxyl functional groups that endow the nanomaterial with a high level of chemical reactivity. Image adapted with permission from [53] © 2010 The Royal Society of Chemistry.

The functional groups on the GO structure have the benefit of adding chemical reactivity to the nanomaterial, which renders it suitable for a variety of applications, especially in the field of chemistry and bioscience. With its highly reactive structure, GO has been explored for use as a metal-free catalyst in synthetic reactions and electrochemistry [59, 60]. The "carbocatalyst" demonstrates catalytic oxidation of alcohols and alkenes, hydration of alkynes, and ring opening of epoxides [61, 62]. Along with its catalytic activity, the unique chemistry of GO can

additionally be used as a method to functionalize the nanomaterial to create biohybrids for medical applications. Both the carboxyl group and the epoxide group are amenable to simple reactions that can be utilized to introduce small molecules or polymers onto the structure of GO [53, 63, 64]. The existing sp^2 domains on the GO structure not interrupted by functional groups during oxidation can participate in non-covalent interactions such as π-π stacking or van der Waals interactions and have been utilized as additional methods of functionalizing the nanomaterial. By taking advantage of the ease of covalent and non-covalent modifications, GO nanosheets have been functionalized with a variety of molecules, for example, polyethylene glycol (PEG) and other polymers to improve dispersibility and biocompatibility, folic acid or magnetic particles for targeted drug delivery, fluorescent probes for cellular imaging, and aptamers, enzymes or DNA for biosensor applications [63-65].

1.3.2 Neural Engineering Applications

Within the field of neural engineering, much recent work has focused on adapting the exciting electrical and chemical properties G and GO to create functional neural electrodes or to drive the behavior of neurons and NSCs. There has been interest in fabricating G-based neural recording electrodes because of the exceptional conductivity of the material that arises from the entirely sp^2-bonded carbon structure, which creates a delocalized π-electron orbital that extends over the entire nanomaterial allowing for the ballistic transport of electrons [66]. Additionally, RGO can be formed into flexible, freestanding conductive ribbons, which could be of use in *in vivo* neural recording applications where compliant electrode designs are being pursued in order to reduce inflammatory tissue reaction [67, 68]. A flexible G electrode incased in insulating polydimethylsiloxane (PDMS) has demonstrated the ability to record electrical signals from both

cardiac and neural cells with a high signal-to-noise ratio [69]. Alternately, metal neural recording electrodes were modified with layers of G and exhibited lowered impedance and increased conductivity that suggests the modified electrode would perform well in neural recording applications [70]. Conductive G and RGO substrates have additionally been used as substrates for neuron growth and have demonstrated biocompability [71-74], the potential for patterned cell growth [75], and the ability to improve neuron cell-cell interactions with the application of weak electric fields [76]. A recent intriguing study found that NSCs differentiated on the surface of G electrodes exhibited not only an improved amount of differentiation to the neuronal lineage, but also improved functional maturation into electrically active neurons [77]. This work indicates that the conductive substrate may provide cues to the developing cells that reinforce their electrical connections and may have implications for neural tissue engineering and regeneration applications.

While the potential of G and RGO has been investigated for tissue engineering, very few studies have evaluated the use of GO for this application. Neurons growing on the surface of GO modified with amine groups [78] or choline-like units [79] exhibited healthy morphology and neurite extensions without reduced viability, indicating that these modifications create biocompatible scaffolds based on GO nanomaterials and these studies demonstrate their potential for neural tissue engineering.

1.4 DISSERTATION ORGANIZATION

The work described in this dissertation explores a GO/CP nanocomposite as a material for communicating with cells in the nervous system. While CPs have been extensively studied as

neural interfacing materials over the past decade, and several recent studies have evaluated the use of G/GO nanomaterials for neural tissue engineering, few have evaluated the potential of GO/CP nanocomposites for interacting with the nervous system. By creating a composite of these two materials, the chemical functional groups present on the GO that can be utilized for functionalization or chemical catalysis are combined with the unique electrical and redox properties of the CP, and the result is a highly versatile neural interfacing material that has multiple applications.

In *Chapter 2* and *Chapter 3*, neurons and NSCs are seeded on the surface of a GO/PEDOT nanocomposite to evaluate its potential as a scaffolding material for neural tissue engineering. These chapters additionally demonstrate a simple, yet effective, method of immobilizing bioactive cues onto the surface of the nanocomposite film using carbodiimide chemistry. The results of the experiments indicate that the GO/PEDOT nanocomposite has potential as a scaffolding material for both neurons and NSCs. This work has implications in tissue engineering applications where controlled cell growth or differentiation is necessary to achieve a desired therapeutic effect. The work described in *Chapter 2* was published in [80] and is reproduced by permission of The Royal Society of Chemistry.

Chapter 4 demonstrates that conventional CP drug release systems can be significantly improved with the addition of GO nanosheets as co-dopants in the drug-loaded CP film synthesis reaction. The unique structure of the GO nanosheets enables an increase in the amount of drug loaded into the film, and creates a means to fine tune the release properties of the drug delivery platform. These results have implications in clinical applications where precise, temporally controlled drug delivery can minimize systemic side effects and maximize drug effectiveness.

The work in this chapter was published in [81] and is reproduced by permission of the American Chemical Society.

In *Chapter 5*, the GO/PEDOT nanocomposite was evaluated for its potential as a dopamine (DA) sensor. Glassy carbon electrodes modified with the nanocomposite detected DA with a higher level of sensitivity and reduced the amount of interference from a competing analyte. The unique structure of the GO nanosheets created a chemical environment at the electrode surface that resulted in the improved detection properties. The promising results of this work suggest that the GO/PEDOT composite may be applied to *in vivo* chemical detection applications, were current devices suffer from poor sensitivity to the low physiological levels of DA present in the brain.

Finally, *Chapter 6* characterizes an *in vitro* model of neuronal injury and regeneration that integrates electrophysiological recordings to monitor the changes in neuronal firing patterns in response to injury. Preliminary work suggests that the injury model has potential use as a lab-on-a-chip method for testing pharmaceuticals and cell therapies, or as a platform to gain basic knowledge about cellular processes that occur following brain injury. This work provides the foundation for the development of a multifunctional device consisting of a multielectrode array (MEA) with GO/PEDOT-modified electrodes capable of simultaneous electrical and chemical recordings, drug delivery, and surface patterning.

The work presented in this dissertation demonstrates the huge amount of versatility the GO/CP nanocomposite embodies, with applications in cell scaffolding, drug delivery and chemical sensing, among others. While the work here focuses solely on the potential of the nanocomposite in neural interfacing applications, its uses are not limited to the CNS, but span all

systems in the body and, as a result of its extremely unique chemical and electrical properties, extend to fields outside biomedicine.

2.0 PURE GRAPHENE OXIDE DOPED CONDUCTING POLYMER NANOCOMPOSITE FOR BIO-INTERFACING

2.1 INTRODUCTION

With advances in the preparation and characterization of graphene (G) and graphene oxide (GO), there has been exponentially growing interest in these materials because of their outstanding electrical, physical and chemical properties [82-84]. The application of G [85-90] and GO [91-94] for interacting with biological systems has only recently been explored, though it has demonstrated great potential for fields such as biosensing, tissue engineering, and drug delivery [64, 65]. To date, studies evaluating the biocompatibility of G and GO have been inconclusive, with some reports demonstrating severe dose-dependent toxicity [95, 96], while others indicate that G nanomaterials may enhance cell growth [93, 97]. These conflicting results suggest that the biocompatibility of G and GO depends heavily on their specific chemical and physical states as well as their preparation methods, and further investigation is warranted [98, 99].

Another class of conductive organic material, conducting polymers (CPs), has been extensively studied in biological and biomedical fields such as biosensors, neural tissue engineering and neural electrodes [17, 46, 49, 100, 101]. In these applications, it is desired to immobilize biomolecules to the polymer in order to impart functionalities specific for interfacing with the biological systems. Such modification often requires the substrate material to have at

least one derivatizable functional group, which many of the CPs, such as polyethylenedioxythiophene (PEDOT), lack. In order to add functional groups to PEDOT, generally two strategies have been adopted. One is the direct addition of functional groups to the monomer 3,4-ethylenedioxythiophene (EDOT), followed by polymerization of the modified EDOT monomer [102-108]. This method requires tedious synthesis and purification procedures for the modified EDOT monomers, and the added functional groups may pose electronic and steric limitations during polymerization [109]. The other strategy is the copolymerization of EDOT with other monomers or molecules that possess functional groups [110-112]. Although considerably simple, this method is still unsatisfactory because the existence of these molecules may impair the conductivity and stability of the resultant PEDOT. Another method of imparting bioactive function to PEDOT is to dope the polymer with the bioactive molecules directly. Peptides, drugs and proteins have been directly incorporated in PEDOT for neural interfacing or controlled drug delivery [38, 101, 113, 114]. However, only negatively charged biomolecules can be used as dopants and most of them are poor dopants because of their weak charge and large size. Poor dopants lead to difficulty in electropolymerization and low conductivity of the resulting polymer. Furthermore, the biomolecules are entrapped throughout the film, limiting the exposure of the functional domain at the surface.

GO possesses many oxygen containing functional groups, such as carboxyl, hydroxyl and epoxide, rendering it hydrophilic and dispersible in aqueous solutions [53, 115, 116]. This property, along with its abundance of negatively charged carboxyl groups, makes it an excellent dopant for the electropolymerization of conducting polymers. Additionally, GO has recently been shown to act as a promoter of neuronal growth and maturation, making it an interesting candidate as a neural interfacing material [73, 117, 118]. CP/GO nanocomposites have exhibited

favorable electrical properties, energy storage and stability [90, 119]; however, the performance of GO/PEDOT nanocomposites as biomaterials has yet to be substantially characterized. In this work, we report the straightforward electrochemical synthesis of a PEDOT material doped exclusively with GO and demonstrate its *in vitro* compatibility with neuronal cells. The GO sheets are partially entrapped by PEDOT on the surface of the nanocomposite and many of the carboxyl functional groups of GO on the surface are exposed freely, enabling biomolecule decoration on the GO/PEDOT film surface via carbodiimide conjugation. We achieve successful covalent immobilization of peptide RNIAEIIKDI (p20), the functional neurite outgrowth domain of extracellular matrix protein, laminin [44, 50, 120, 121], and this immobilization procedure may be universally applied to bioactive proteins and peptides for a variety of bio-interfacing applications.

2.2 MATERIALS AND METHODS

2.2.1 Materials

Graphite powder was purchased from Bay Carbon Inc. (SP-1, Bay City). 3,4-Ethylenedioxythiophene (EDOT), poly(sodium-4-styrenesulfonate) (PSS, M_W ~ 70,000), phosphate buffered saline (PBS, pH 7.4, 10 mM sodium phosphate and 0.9% NaCl), glutaraldehyde (25% in H_2O), osmium tetroxide (OsO_4, 4 wt.% in H_2O), hexamethyldisilazane (HMDS), 1-Ethyl-3-(3-dimethylaminopropyl)carbodiimide (EDC), and *N*-Hydroxysuccinimide (NHS) were purchased from Sigma-Aldrich. The peptide RNIAEIIKDI (p20) was synthesized at

the University of Pittsburgh Peptide Synthesis Facility. All other chemicals were of analytical grade, and Milli-Q water from a Millipore Q water purification system was used throughout.

2.2.2 Electrodeposition

GO was synthesized through the oxidization of graphite powder according to the modified Hummers method [54, 122], and characterized using transmission electron spectroscopy (TEM) (JEOL JEM-2100F). GO/PEDOT films were electrodeposited onto platinum/iridium (Pt/Ir) microelectrodes (standard tip, diameter: 2-3 μm, MicroProbes, Gaithersburg, MD) for electrochemical characterization or gold sputtered plastic microscope coverslips (macroelectrode area: 0.38 cm^2) for surface characterization and cell culture using a Gamry Potentiostat, FAS2/Femtostat (Gamry Instruments, Warminster, PA) with Gamry Framework software. A conventional three-electrode system with the Pt/Ir or gold electrode acting as the working electrode, a platinum foil as the counter electrode, and a silver/silver chloride (Ag/AgCl) reference electrode (CH Instruments, Austin, TX) was used. The GO/PEDOT was electropolymerized from an aqueous solution containing 0.02 M EDOT and 10 mg mL^{-1} GO. PEDOT/PSS films were synthesized from an electropolymerization solution containing 0.02 M EDOT and 0.1 M PSS. A constant potential of 1.0 V was applied to achieve a charge density of 200 nC total for microelectrodes or 100 mC cm^{-2} for macroelectrodes.

2.2.3 Modification of GO/PEDOT with p20

The peptide p20 was covalently immobilized on the surface of the GO/PEDOT coated electrodes through an amine reaction between carboxyl groups on the GO and amine groups on the peptide.

The GO/PEDOT electrodes were incubated in a solution of 0.2 mg mL^{-1} p20, 0.2 M EDC and 0.2 M NHS in sterile H_2O for 3 h at room temperature, and then thoroughly washed with sterile PBS to remove any free p20, EDC or NHS. In another set of samples, GO/PEDOT films were incubated with p20 in the absence of EDC/NHS as a control for physical adsorption. The amount of p20 on the surface of the covalently modified GO/PEDOT film was quantified using amino acid hydrolysis followed by high performance liquid chromatography as previously described [44].

2.2.4 Electrochemical Impedance Spectroscopy

The electrochemical impedance spectroscopy (EIS) was measured with an Autolab potentiostat/galvanostat, PGSTAT128N (Metrohm Autolab) with Nova 1.8 software using a three-electrode system with a platinum foil counter electrode and Ag/AgCl reference electrode. The EIS was measured in PBS in the frequency range from 10 Hz to 100 kHz using an alternating current sinusoid of 20 mV in amplitude with the direct current potential set to 0 V.

2.2.5 GO/PEDOT Film Surface Analysis

The surface of PEDOT/GO films was characterized using Fourier transform infrared (FTIR) spectroscopy, scanning electron microscopy (SEM) and x-ray photoelectron spectroscopy (XPS). FTIR measurements were carried out using a Bruker Vertex 70 spectrometer equipped with a Hyperion 2000 microscope. A 20x attenuated total reflectance **(**ATR) objective was employed to record the spectra of deposited thin films. The ATR spectra were converted to transmittance spectra via the standard method within the spectrometer operation software package, OPUS 6.5.

The surface morphologies and microstructures of the GO/PEDOT films were examined with an XL30 SEM (FEI Company) operated at 10 kV. Samples with neurons growing on the surface were analyzed with the same SEM, but at a lower operating potential of 5 kV. Samples with cells were treated with 2.5% glutaraldehyde and 1% OsO4, both for one hour in sequence, followed by dehydration. The dehydration was performed by soaking the samples in 30% and 50% ethanol in PBS, 70% and 90% ethanol in water, and 100% ethanol in sequence for 15 min each, followed by immersion in HMDS for 15 min.

XPS analysis of GO/PEDOT films after treatment with p20 in the presence or absence of EDC/NHS was performed with a K-Alpha XPS system (Thermo Scientific) equipped with a monochromated Al K_α source (1486.68 eV). High resolution scans of the C1s and N1s regions were taken at two locations on each sample.

2.2.6 Primary Neuron Culture

GO/PEDOT coated macroelectrodes were fixed to the surface of 24-well culture plates with Kwik-Sil (World Precision Instruments) and sterilized with exposure to UV light for 15 min. Following sterilization, the polymer surfaces were washed with sterile PBS. Cortical tissue was isolated from E18 Sprague-Dawley rat embryos and treated with 0.025% Trypsin in a digestion buffer containing 137 mM NaCl, 5 mM KCl, 7 mM Na_2HPO_4, and 25 mM HEPES. Neurons were dissociated with gentle tritruation and maintained in Neurobasal medium (Invitrogen, 21103-049) supplemented with B27 (Invitrogen, 17504-044), GlutaMax (Invitrogen, 35050-061) and Antibiotic-Antimycotic (Invitrogen 15240-062). For neuron growth assays, cells were seeded on GO/PEDOT and PEDOT/PSS surfaces at a density of 100k cells per electrode and grown for 3 days. For neuron viability and death assays, polymer samples were cut to fit into 96-

well plates and seeded with neurons at a density of 10k per well. For the cell cultures intended to assess the p20 functionalization on GO/PEDOT films, similar procedures were followed. In order to measure the neurite length easily by preventing the formation of very long and interconnected neurites, neurons were seeded on the GO/PEDOT surfaces at a density of 100k cells per electrode and grown for only 24 h before fixation and immunocytochemical analysis.

2.2.7 Immunofluorescence Staining and Quantification

Neurons growing on the polymer surfaces were fixed in 4% paraformaldehyde in PBS for 15 min and washed several times with PBS. The cells were immersed in a blocking buffer (5% goat serum/0.2% triton-X in PBS) for 20 min followed by incubation in mouse monoclonal antibody against β-III-tubulin (TuJ1, 1:1000, Sigma) for 1 h. After washing in PBS, the cells were incubated in goat anti-mouse Alexa Fluor 488 (1:1000, Invitrogen) secondary antibody for 1 h, washed in PBS and counterstained for nuclei using Hoechst 33342 (Invitrogen).

TuJ1-immunoreactive cells were imaged using a fluorescence microscope. For each experimental group, 10 random 10x images were collected from each sample (n = 3). Neuron density was quantified by counting the number of TuJ1-immunoreactive cells that extended at least one neurite that measured longer than the width of the cell body. Neurite analysis was performed using the NeuronJ plugin for ImageJ (http://rsbweb.nih.gov/ij/). Neurites extending from each TuJ1+ cell body were traced and measured, and the average neurite length was calculated.

2.2.8 Neuron Viability and Toxicity Assay

The viability of neurons growing on the GO/PEDOT composite and PEDOT/PSS films, as indicated by their mitochondrial activity, was assessed with the MTT Cell Proliferation Assay Kit (Molecular Probes). The ratio of absorbance signal at 570 nm to 630 nm (reference wavelength) was used to assess metabolic activity. All polymer samples were normalized to a blank containing the polymer sample with no cells, and compared to a positive control containing cells growing on the tissue culture polystyrene (TCP) well surface.

Percentage of cell death was assessed using the propidium iodide (PI) assay. PI fluoresces after binding to the nuclear material of dead cells, while the plasma membrane of healthy cells excludes the dye. Polymer samples were prepared and neuron culture performed as in the MTT assay. Fluorescence was evaluated in a spectrometer with an excitation at 530 nm and emission at 618 nm. Polymer samples were normalized to controls containing the same polymer with 100% dead cells, and compared to cells growing on the TCP control surface.

2.2.9 Statistical Analysis

All statistical analyses were carried out in SPSS software. Student's t-tests were utilized for comparisons of two experimental groups and one-way analysis of variance (ANOVA) tests followed by Bonferroni's post hoc analysis were utilized for comparisons of more than two experimental groups. Statistical significance was considered for $p < 0.05$ (*) and $p < 0.01$ (**). All data is presented as the mean (± SEM).

2.3 RESULTS AND DISCUSSION

2.3.1 Synthesis and Characterization of GO/PEDOT Film

GO was synthesized using the modified Hummers method and its microsheet morphology was confirmed with transmission electron microscopy (TEM) (Figure 2.1). For GO/PEDOT film synthesis, electropolymerization of EDOT was carried out in aqueous solution containing only EDOT and GO.

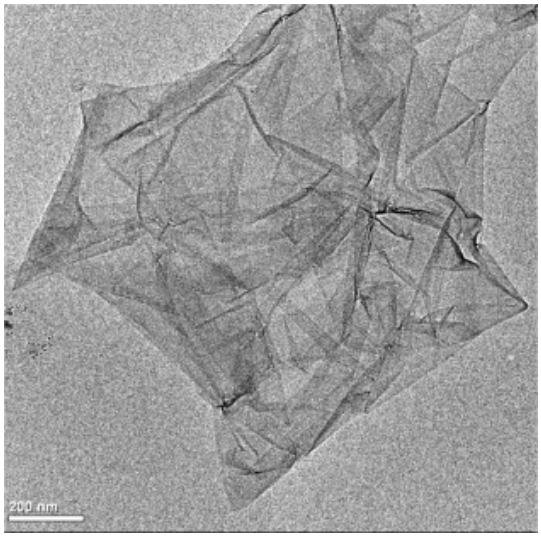

Figure 2.1. TEM Micrograph of the Prepared GO.

No additional electrolyte was used in order to avoid the involvement of any dopant other than GO. In the presence of the negatively charged GO, EDOT could be successfully electropolymerized on the electrode surface, indicating that GO, itself, acts to sufficiently dope the polymer film. To maintain a conductive polymerization solution, a GO concentration of 10 mg mL^{-1} was utilized. Because solutions containing lower amounts of GO resulted in slower or

less charge passage during the polymerization reaction, a high concentration of GO was selected to ensure adequate film growth. The resulting film is uniform, and the incorporated GO created a network-like surface morphology (Figure 2.2).

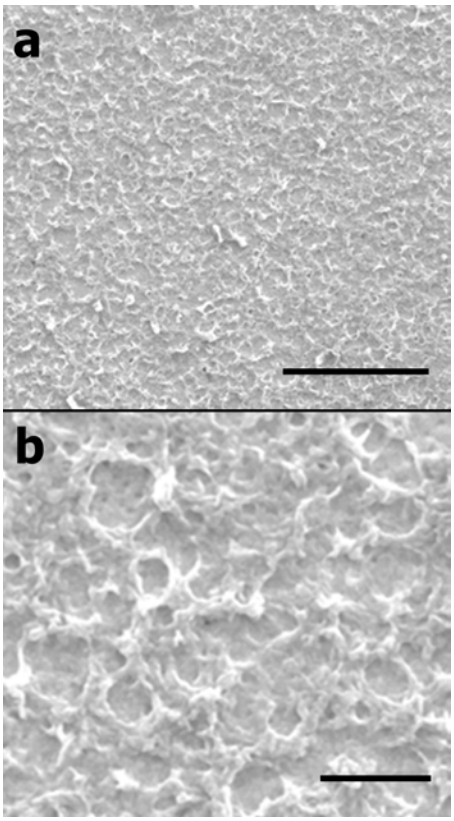

Figure 2.2. SEM images of the Electrodeposited PEDOT/GO. Images illustrate the rough, network-like morphology of the surface. The film was electropolymerized at 1.0 V for 600 s in 0.02 M EDOT solution containing 10 mg mL^{-1} GO. Scale bar in (a) is 5 μm. Scale bar in (b) is 1 μm.

FTIR analysis of the synthesized GO sheets and the GO/PEDOT films verified successful incorporation of GO into the film (Figure 2.3). Pure GO exhibits peaks at 3396 cm^{-1}, 1726 cm^{-1}, 1404 cm^{-1}, 1283 cm^{-1}, and 1058 cm^{-1} that represent carboxylic O-H stretching and vibration, carboxylic C=O stretching and vibration, O-H deformation, epoxy C-O stretching and vibration,

and alkoxy C-O stretching and vibration, respectively [90, 123]. The spectrum of the electrodeposited GO/PEDOT nanocomposite contains the characteristic peaks for C=O stretching and vibration of carboxyl groups at 1744 cm^{-1} and O-H deformation at 1410 cm^{-1}. The PEDOT polymer does not contain either carboxyl or hydroxyl functional groups, so these must be attributed to GO, the sole dopant in the polymerization solution, indicating that the GO sheets have been successfully incorporated into the polymer film. Notably, the presence of the carboxylic carbonyl peak indicates that the film contains carboxylic acid functional groups provided by the GO sheets that can be utilized for biomolecule immobilization with carbodiimide cross-linking. The carboxylic O-H stretching and vibration band that should be apparent around 3400 cm^{-1} is absent in the GO/PEDOT spectrum, and is likely obscured by the tail of the ~ 1 eV bipolaron absorption band, a typical attribute of conductive polymers [41].

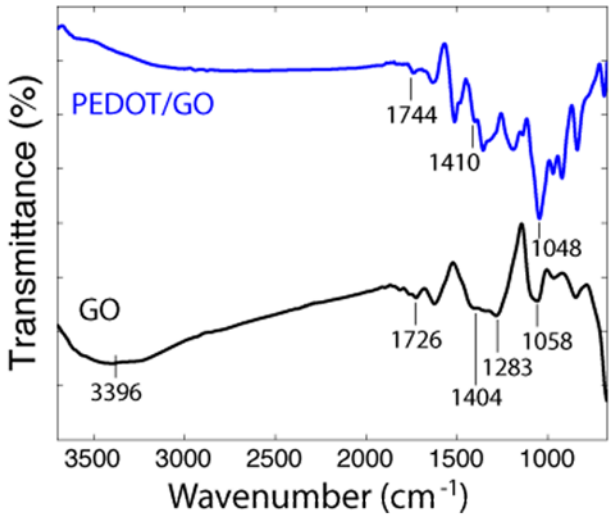

Figure 2.3. FTIR Spectra of GO and GO/PEDOT Nanocomposite.

2.3.2 Cytotoxicity of GO/PEDOT Nanocomposite

Although PEDOT doped with various molecules, such as heparin [124], poly(styrene sulfonate), (PSS) [18] and adhesive peptides [125] has been shown to be non-cytotoxic, and soluble GO has demonstrated inconsistent toxicity effects [93, 96, 99], the biocompatibility of GO incorporated in conducting polymers has not previously been studied. To explore the cytocompatibility of the GO doped conducting polymer film, the viability and death of neurons growing on the GO/PEDOT surface after 24 h were evaluated with the MTT viability and propidium iodide (PI) exclusion assays and compared to PEDOT films containing the commonly and extensively studied dopant PSS. To isolate the effects of the polymer surface directly on the cell viability/death, the surfaces were not coated with laminin, an extracellular matrix protein widely used to promote neuron attachment and growth on various surfaces [126, 127]. There was no significant difference in viability between the GO/PEDOT and PEDOT/PSS films, with each group exhibiting greater than 96% of the metabolic activity of neurons growing on a control TCP surface (Figure 2.4a). Neurons growing on the GO/PEDOT surface did not undergo a higher percentage of death than the cells on the PEDOT/PSS surface (GO: 12.79 ± 5.0; PSS: 20.61 ± 3.78, Figure 2.4b).

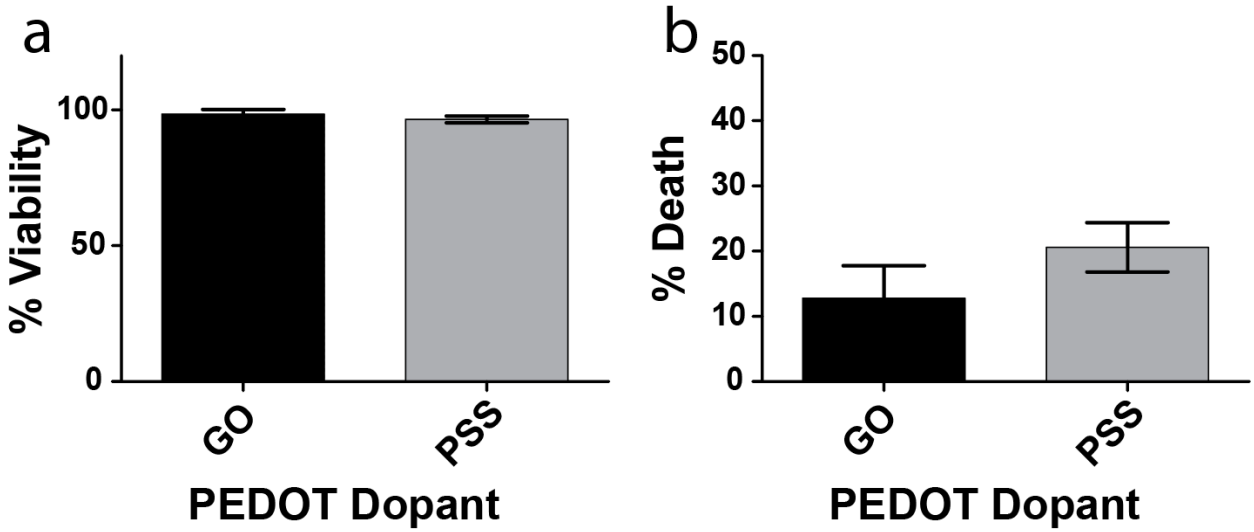

Figure 2.4. Cytotoxicity Assessment of PEDOT Films. (a) Viability and (b) death of neurons growing on PEDOT films doped with GO or PSS at 24 h in culture. GO/PEDOT films perform similarly to control PEDOT/PSS films, exhibiting no loss of viability and minimal cell death. Error bar represents SEM (*n* = 5).

The mechanism of soluble GO cytotoxicity shown in previous reports remains unclear, but multiple processes have been suggested, including uptake into the cell or adsorption onto the cellular membrane and consequent apoptosis or death, disruption of membrane integrity and cellular exchange, interference with cell adhesion, or induction of oxidative stress [95, 96, 128, 129]. The absence of significant cytotoxicity caused by GO/PEDOT films in the current study may arise from the entrapment of the GO sheets within the film, hindering their ability to diffuse within the culture media and interact freely with the neurons. Cells growing on the surface of the film are largely contacting the PEDOT polymer, which has demonstrated biocompatibility with neuronal cells [18]. The minimal toxicity of GO/PEDOT films indicates that the nanocomposite has potential as a neural interfacing material. However, long-term toxicity studies must be performed to determine the full cytocompatibility of the material.

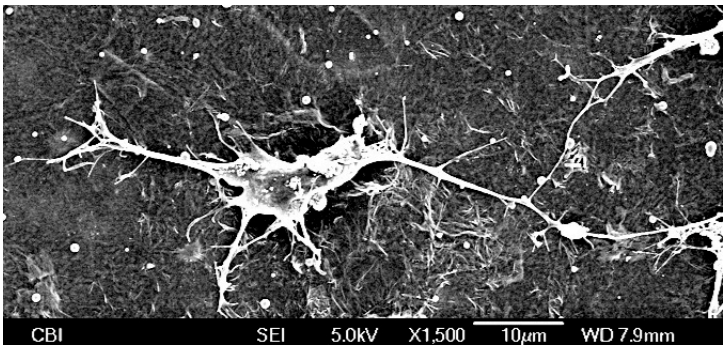

Figure 2.5. SEM Image of a Neuron Growing on the GO/PEDOT Surface at 1 d in Culture. The cell exhibits extensive neurite branching and forms contacts with other cells, demonstrating the biocompatibility of the GO/PEDOT film.

2.3.3 Neuron Growth on the GO/PEDOT Nanocomposite

To evaluate the neural biocompatibility of the GO/PEDOT composite, films were electrochemically deposited on gold sputtered coverslips, and the resulting GO/PEDOT coated coverslips were used as substrates to grow primary neuron cultures. SEM imaging revealed that neurons exhibited healthy growth on the surface of nanocomposite films in the absence of laminin treatment (Figure 2.5). Cells spread and flattened on the composite surface and interconnected with other neurons, demonstrating that the surface supported neural attachment and maturation. Due to the specific network-like microstructure of the GO/PEDOT film, some of the smaller processes of neurons intimately grew along or around the partially exposed GO ridges on the surface of the film, potentially using the film morphology as a guidance cue for neurite outgrowth. Representative fluorescent images show neuron attachment and growth on GO/PEDOT and PEDOT/PSS films after 3 d in culture (Figure 2.6a, b). The neurons grew on the surface of the GO/PEDOT film at a density comparable to that of PEDOT/PSS, indicating that the GO is not specifically contributing any obstruction to the attachment of cells (Figure 2.6c).

While previous GO biocompatibility studies have indicated that GO initiates downregulation of adhesion proteins, such as laminin, fibronectin, and focal adhesion kinase-1, leading to a decrease in cellular adhesion [96], our data suggest that GO entrapped in the polymer matrix may not have such adverse effects on neuron attachment. This agrees with a proposed mechanism for decreased cell adhesion that attributes altered gene expression to the activation of intracellular pathways after GO nanoparticles adhere to the cell membrane [96]. GO sheets embedded in the PEDOT polymer matrix may be restricted from interacting with the cell membrane in a way that would initiate changes in gene expression, rendering the GO/PEDOT film a favorable surface for cell attachment and growth.

Neurons growing on the GO/PEDOT film exhibited significantly longer neurites than cells growing on the PEDOT/PSS film (Figure 2.6d, GO: 36.4 ± 2.0 μm; PSS: 22.5 ± 1.8 μm, $p < 0.01$). This finding is supported by previous work demonstrating that pure GO surfaces promote neurite outgrowth in hippocampal neurons [73], and soluble GO can enhance neurite outgrowth in SH-SY5Y neuroblastoma cells by potentially shuttling adsorbed proteins into the cell body during uptake [118]. Although the GO from the GO/PEDOT film is likely not being taken into the neuron cell body due to its entrapment within the polymer matrix, its ability to strongly physically adsorb proteins, a consequence of the huge surface area of its single-layer carbon structure, may attract components of the cell media to the surface of the polymer film, enhancing growth cone outgrowth. Additionally, neurons have been shown to be extremely responsive to a variety of topographical cues, and in particular, surface roughness has been shown to promote neurite extension [128, 129]. The rough, network-like surface morphology of the GO/PEDOT film (Figures 2.2 and 2.5), compared to the smooth and featureless surface of PEDOT/PSS at the same scale (previously reported in [50]) may contribute to the longer neurite outgrowth in

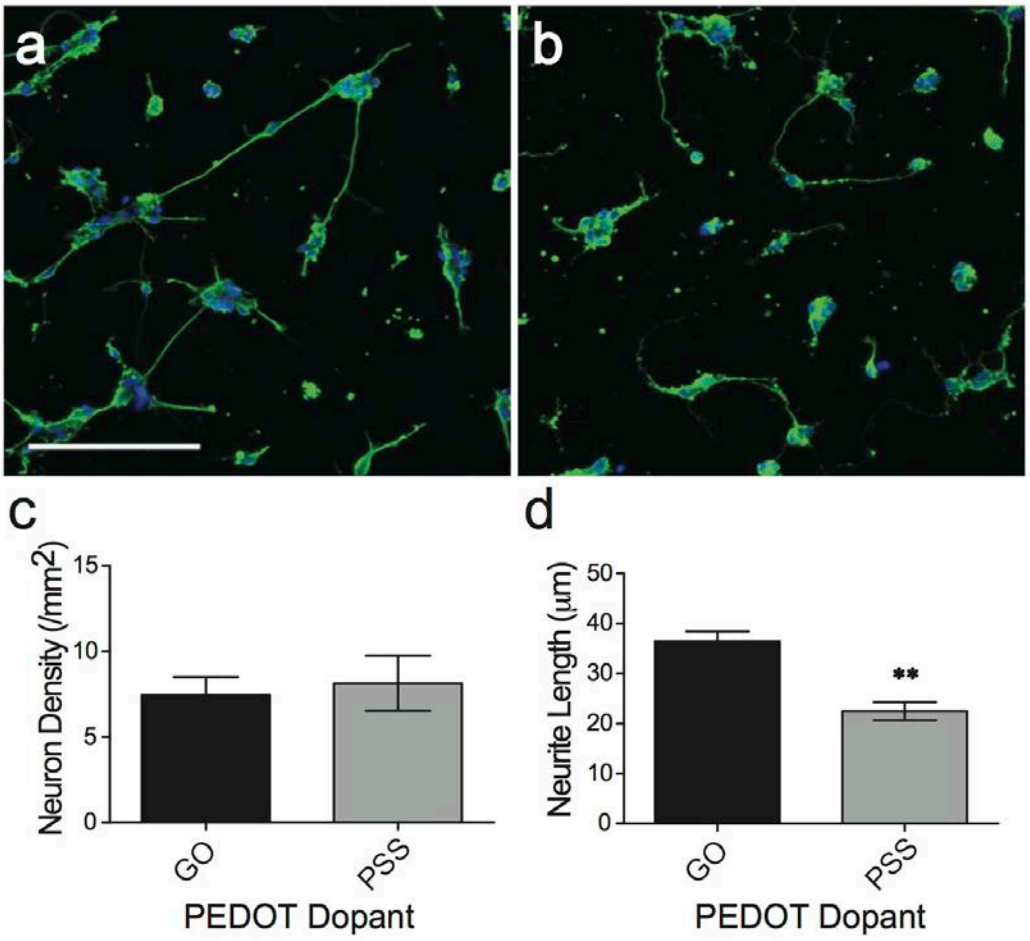

Figure 2.6. Neuron growth on PEDOT surfaces doped with GO and PSS at 3 d. Representative 20x fluorescent images of β-III-tubulin immunofluorescent reactivity (green) of neurons growing on (a) GO and (b) PSS doped PEDOT. Blue color is Hoechst nuclear counterstain. Scale bar represents 100 μm. (c) Neuron density and (d) average neurite length (± SEM; *n* = 3) of cells growing on the polymer surfaces. GO doped PEDOT films support neurons with longer neurite extensions than PSS doped PEDOT films ($p < 0.01$).**

GO/PEDOT as compared to PEDOT/PSS. Regardless of the mechanism, the desirable effect on neurite outgrowth demonstrates that GO/PEDOT films are an amenable material for supporting neuronal growth and maturation, and may be useful substrates for neural tissue interfacing applications.

2.3.4 Bioconjugation of GO/PEDOT Films with p20 Peptide

The GO sheets on the top layer of the GO/PEDOT films are partially embedded, as demonstrated by the network-like morphology of the film (Figure 2.2), and the exposed portions of the GO, rich in carboxyl groups (Figure 2.3), provide the GO/PEDOT films with many free functional groups. Utilizing carbodiimide conjugation to modify these functional groups, we demonstrate a novel method of biomolecule patterning on conducting polymer films. A laminin fragment peptide, p20, which is reported to promote neurite outgrowth [50, 120], was conjugated to the electrodeposited film. The peptide was covalently attached to the GO/PEDOT film through the formation of amide bonds between the carboxyl groups on the surface of GO/PEDOT and the amine groups of the p20, with the assistance of cross-linkers EDC and NHS. The presence of p20 on the film after carbodiimide modification was verified by hydrolysis and amino acid quantification (5.37 pmol-mm^{-1}).

XPS analysis of the GO/PEDOT film evaluated the surface chemistry of the film after p20 immobilization with EDC/NHS (Figure 2.7). The deconvoluted C1s region (Figure 2.7a) consists of four peaks in addition to the main C-C peak located at 284.8 eV, including a C-O/C-S peak at 285.6 eV, an epoxy C-O-C peak at 286.9 eV, a N-C=O peak at 288.2 eV and an O-C=O peak at 288.8 eV [130, 131]. The PEDOT contributes to the C-S and C-O-C peaks, the GO

sheets contribute to the C-O, C-O-C, and O-C=O peaks, and the peptide contributes to the O-C=O and N-C=O peaks. Analysis of the C1s region of the PEDOT/GO film treated with p20 in the absence of EDC/NHS resulted in a similar deconvolution. During the amide bond formation in the presence of EDC/NHS, a carboxylic acid provided by the GO reacts with an amine on the peptide, resulting in a net gain of one amide bond and a net loss of one carboxylic acid bond. However, since both the GO and peptide contain carboxylic acids, a comparison of the ratio of amide to carboxylic acid between the experimental groups cannot be used to verify the formation of covalent amide bonds between the peptide and the film with the addition of EDC/NHS. The carboxylic acid signal of the GO sheets is likely variable across the film depending on the proportion of GO exposed to the surface versus embedded within the polymer matrix, so the ratio of amide to carboxyl will not reflect the amount of covalently attached peptide. A more appropriate method of evaluating the amide formation is to monitor the ratio of amine to amide bonds. During the covalent reaction, one amine in the peptide p20 reacts with a carboxylic acid group to form an amide bond, so there will be more amide and less amine after the covalent treatment, as compared to the physical adsorption treatment. A high-resolution scan of the N1s region of the film treated with p20 and EDC/NHS revealed a peak centered at 388.9 eV, corresponding to the nitrogen in the peptide (Figure 2.7b). Deconvolution of the N1s peak resulted in a C-N (amine) peak at 399.7 eV, a N-C=O (amide) peak at 400.3 eV, and a protonated amine peak at 401.8 eV [130, 132]. The amide/amine ratio is 0.58, compared to 0.19 in the absence of EDC/NHS crosslinking, indicating that the EDC/NHS treatment produced covalent linkages between the peptide and the GO/PEDOT film.

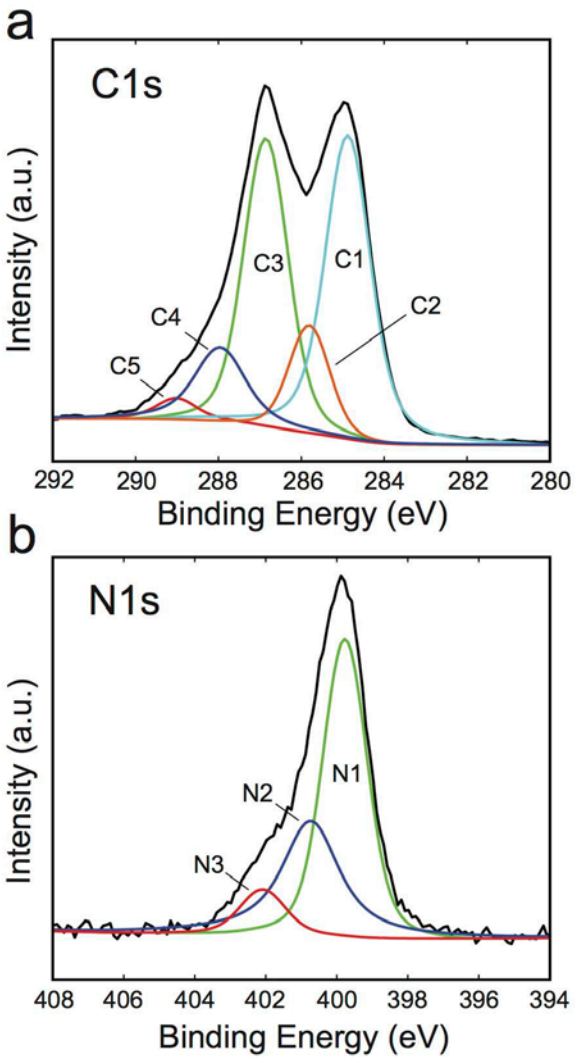

Figure 2.7. High-Resolution XPS Spectra of the GO/PEDOT Surface after Treatment with p20 in Conjugation with EDC/NHS. Deconvoluted peaks of the (a) C1s region (C1: C-C; C2: C-O/C-S; C3: C-O-C; C4: N-C=O; C5: O-C=O) and (b) N1s region (N1: C-N; N2: N-C=O; N3: protonated amine).

The electrical properties of the electrodeposited GO/PEDOT films before and after p20 immobilization were studied using EIS. As shown in Figure 2.8a, coating the electrode with the GO/PEDOT film resulted in decreased impedance across all frequencies measured. This significant impedance decrease may be attributed to an increase in the effective surface area of the electrode due to the network-like surface microstructure of the nanocomposite polymer film

[14]. Longer deposition times resulted in a progressive decrease in impedance, demonstrating the film properties can be tuned as desired by controlling deposition parameters (Figure 2.9). At 1 kHz, a frequency relevant to single unit neural recording, the impedance is decreased by an order of magnitude after the GO/PEDOT deposition, indicating that the film may be a beneficial microelectrode coating to improve the recording and stimulation capability of neural electrodes [133]. The Nyquist plot of the impedance (Figure 2.8b) demonstrates that the bare metal has mostly capacitive behavior, as indicated by its steep linear curve. The electrodes coated with GO/PEDOT films exhibit a knee that separates capacitive behavior at low frequencies and diffusive behavior, characterized by a more gradual slope, at higher frequencies [90, 134]. The emergence of diffusion-dominated behavior may be attributed to the creation of a diffusion barrier by the conducting polymer film. After immobilization of p20 at the surface of the polymer film, the impedance increases slightly, a possible result of the creation of a nonconductive peptide layer at the electrode surface; however, the impedance remains significantly lower than that of the bare metal electrode.

The bioactivity of the immobilized p20 was assessed with primary neuron culture on the functionalized GO/PEDOT films. After 24 h in culture, neuron attachment and average neurite length were quantified and compared among GO/PEDOT films unmodified with peptide (bare), and films modified with p20 via physical adsorption or covalent immobilization. Representative fluorescent images illustrating β-III-tubulin immunoreactivity and neurite outgrowth on each film are shown in Figure 2.8a-c. While there are no differences in the density of neurons attached to each film (Figure 2.10d), the average neurite length (Figure 2.10e) of the neurons grown on the GO/PEDOT films covalently modified with p20 is significantly longer than that on the other

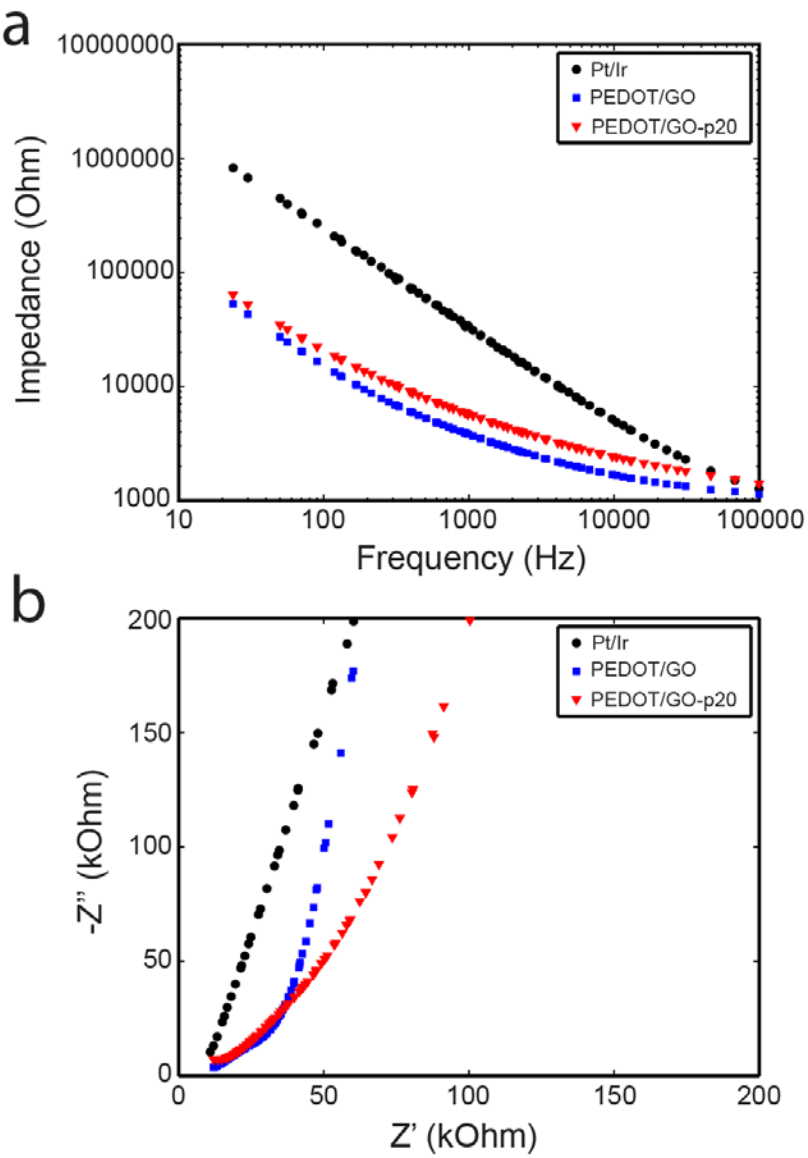

Figure 2.8. Electrochemical Impedance Spectroscopy of p20-Modified GO/PEDOT Films. (a) Bode and (b) Nyquist plots of the electrochemical impedance behavior of platinum iridium microwires uncoated (black circles), coated with GO/PEDOT (blue squares), and coated with GO/PEDOT covalently modified with p20 (red triangles).

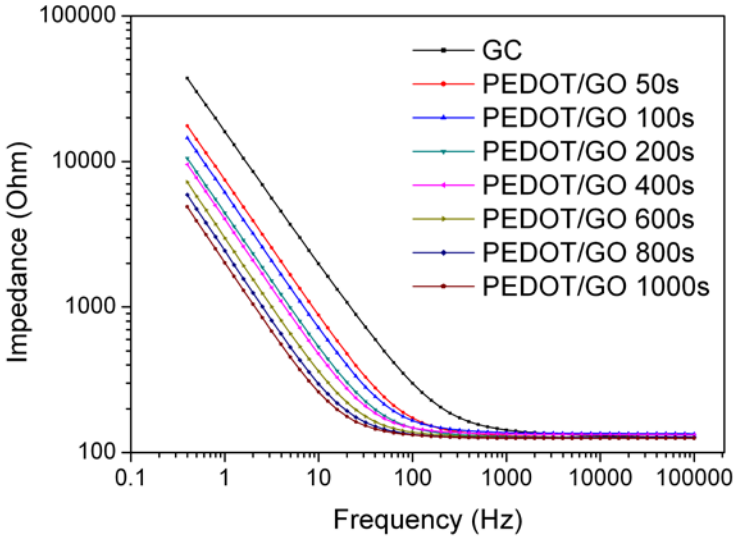

Figure 2.9. Electrochemical Impedance Spectroscopy Comparison of Glassy Carbon Electrodes Without and With GO/PEDOT Coatings of Different Electrodeposition Times. Longer deposition times result in decreased impedance values.

two films (bare: 14.29 ± 0.63 μm; adsorption: 14.59 ± 1.72 μm; covalent immobilization: 20.48 ± 1.45 μm, $p < 0.05$). This observation can be ascribed to the effect of p20, which is the neurite outgrowth domain of laminin protein, and has been shown to enhance neurite outgrowth when incorporated into conducting polymer films as a dopant [44, 50]. There was no discernable effect of p20 when physically adsorbed on the GO/PEDOT film (Figure 2.10). It is possible that the peptide does not retain its bioactivity, potentially due to conformational changes as a consequence of the physical adsorption onto the film that may obstruct laminin receptors on the neurons from binding to the peptide. Covalent anchoring of p20 to the GO/PEDOT film leaves most of the peptide free to interact with the cell, preserving the bioactivity of the peptide. It is also possible that the physically adsorbed peptide desorbs over the course of the cell culture experiment, resulting in less neurite outgrowth. The covalently conjugated p20 is very stable and

continues to support neurite outgrowth after presoaking in PBS at 37°C for 3 d prior to neuron culture (data not shown). This simple method of functionalizing GO doped PEDOT films with biomolecules and its superior effectiveness over traditional biomolecule adsorption clearly demonstrates the potential of the nanocomposite as a bio-interfacing material.

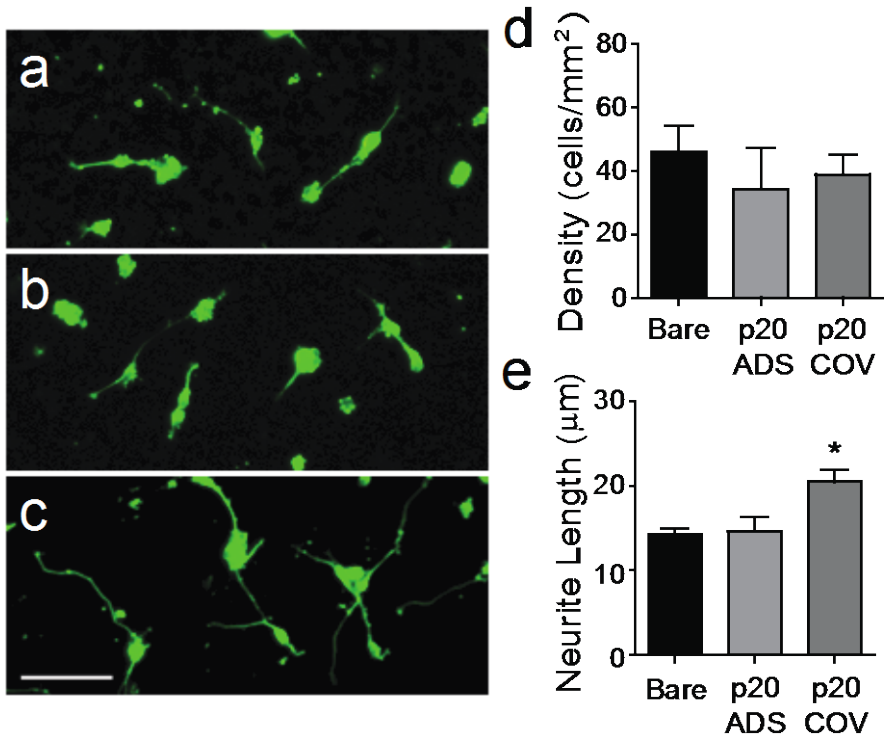

Figure 2.10. Neuron Attachment and Neurite Outgrowth on GO/PEDOT Surfaces Modified with p20 Peptide at 24 h in Culture. Representative 20x fluorescent images of β-III-tubulin immunofluorescent reactivity of neurons cultured on (a) bare, (b) physically adsorbed p20 (p20 ADS) and (c) covalently immobilized p20 (p20 COV) GO/PEDOT surfaces. Scale bar represents 50 μm. (d) Neuron density (± SEM; *n* = 3) growing on the p20 modified GO/PEDOT surfaces. Modification with p20 did not result in a change in cell density. (e) Average neurite length (± SEM; *n* = 3) of neurons growing on the p20 modified GO/PEDOT surfaces (p* < 0.05). Covalent immobilization, but not physical adsorption of p20 on the film surface enhanced neurite outgrowth.**

2.4 CONCLUSIONS

We have successfully prepared a conducting polymer PEDOT material doped solely with GO. The electrodeposited GO/PEDOT films showed good conductivity, and they can significantly lower the impedance of the coated electrodes. The GO/PEDOT films possess a network-like surface structure due to the presence of partially embedded GO sheets, and they supported the growth of neurons with minimal toxicity. Most interestingly, the partially exposed GO pieces on the surface of the GO/PEDOT films are rich in free carboxyl groups, which offer the GO/PEDOT films active functional groups for surface modification. Functional laminin peptide, p20, was successfully bioconjugated to the surface of the GO/PEDOT film through a simple cross-linking reaction that may be universally applied to a multitude of biomolecules. It is expected that this biocompatible GO/PEDOT material with excellent modifiability will find important biological and biomedical applications, such as neural interfacing and biosensing.

3.0 DIRECTED NEURAL STEM CELL DIFFERENTIATION WITH A FUNCTIONALIZED GRAPHENE OXIDE NANOCOMPOSITE

3.1 INTRODUCTION

Neural stem cells (NSCs) are multipotent cells with the potential to generate neurons, astrocytes, and oligodendrocytes, the main components of the central nervous system (CNS). In the mature brain, NSCs reside primarily in areas of neurogenesis, the subventricular zone of the lateral ventricle and the subgranular zone of the hippocampus, where they proliferate and give rise to new neurons throughout the lifetime of an animal [135, 136]. In adult neurogenesis, newborn neurons respond to a series of environmental cues by migrating to specific locations, sprouting axons and dendrites to exhibit mature neural morphologies, and eventually integrate into existing circuitry by forming active synapses with local neurons [137-139]. The ability of NSCs to generate functionally mature neurons capable of joining existing populations of cells makes NSCs, derived from either adult or embryonic tissues, appealing candidates to potentially restore function to damaged brain tissue by rewiring broken connections. A major challenge in utilizing NSCs for regenerative therapies is the poor control over the survival, differentiation, maturation and functional integration of the transplanted cell population [140-143]. Tools that can control the behavior of NSCs, both for basic research purposes and therapeutic applications, are needed to address the challenges faced along this continuum.

NSCs are not intrinsically wired for differentiation to a particular CNS cell type, but instead are influenced by extrinsic factors such as growth factors, extracellular matrix components, paracrine and juxtacrine signaling from other cells within their niche, as well as electrical or mechanical cues from their microenvironment [144-149]. By taking advantage of the responsiveness of NSCs, biomimetic scaffolding materials can be engineered to manipulate NSC proliferation, differentiation, and maturation pathways to improve their effectiveness in cell replacement therapies. One method used to provide functional cues to NSCs is conjugation of extracellular matrix proteins or bioactive peptides onto the surface of scaffolding materials to drive NSC attachment and preferential differentiation [146, 150-154].

Conductive substrates that have the ability to stimulate cells with electrical current have also been investigated as scaffolding materials because NSCs and CNS progenitor cells are exposed to electrical signaling during development that influences their organization and maturation into adult tissue [155-157]. Conducting polymers (CPs) such as poly(pyrrole) and poly(3,4-ethylenedioxythiophene) (PEDOT) are intrinsically conductive materials that have been used to electrically interface with the nervous system and neural stem cells [47, 158-160]. CPs are simple to process, biocompatible, and have versatile physical and electrical properties by means of their synthesis method, making them attractive materials for cell scaffolding [18, 29-31, 43]. During their polymerization, anionic molecules are incorporated into the bulk of the CP film as dopants, providing a method to incorporate bioactive molecules such as growth factors, extracellular matrix proteins, and functional peptides, that can then influence cell attachment and growth [38, 40, 42, 44, 50]. However, this method can interrupt the conductivity and mechanical stability of the CP or mask the active sites of the biomolecules because they are located within

the polymer matrix [42]. For this reason, methods to covalently immobilize biomolecules on the surface of CP films are desirable.

While traditional CPs do not contain free functional groups that can be utilized in covalent cross-linking reactions, graphene oxide (GO) nanosheets have been used as dopants in order to introduce functional groups to the CP substrates [80]. GO is a two-dimensional honeycomb carbon material rich in functional groups such as hydroxyl, epoxide, and carboxylic acid [53]. Because of the presence of carboxylic acid groups in its structure, GO nanosheets are negatively charged and can therefore be incorporated into the CP films as dopants during their synthesis. GO nanocomposite CP films have demonstrated favorable electrical properties, biocompatibility, and potential for electrical interfacing with neuronal tissue [80, 90, 117, 161, 162]. In this work, we investigate the ability of GO/PEDOT nanocomposite films to act as a NSC scaffold. The viability, attachment, and differentiation of NSCs on the GO/PEDOT nanocomposite surface was compared to NSC behavior on conventional PEDOT films doped with poly(sodium-4-styrenesulfonate) (PSS). Additionally, we demonstrate that the surface of the nanocomposite can be easily modified with bioactive molecules to selectively drive NSC differentiation towards either neuronal or oligodendrocyte lineage.

3.2 MATERIALS AND METHODS

3.2.1 PEDOT Film Synthesis

The GO/PEDOT nanocomposite films were electrochemically deposited onto the surface of gold sputtered plastic coverslips from an aqueous solution using a Gamry poteniostat, FAS2 femtostat

(Gamry Instruments) and a three-electrode setup with a platinum foil counter electrode and a silver/silver chloride reference electrode (CH Instruments). The deposition solution contained 3,4-ethylenedioxythiophene (0.02 M; Sigma-Aldrich) and either GO (10 mg ml^{-1}) or poly(sodium-4-styrenesulfonate) (PSS) (0.1 M; Sigma-Aldrich). GO was synthesized using the modified Hummer's method as previously described and sonicated for 20 min prior to electrodeposition into the polymer to ensure nanosheet exfoliation [80, 81]. The films were electrodeposited using chronocoulometry at 1 V until a charge density of 100 mC cm^2 was reached. The synthesized films were washed in dH_2O for 3 d prior to cell culture to ensure the removal of any loosely adsorbed monomer or dopant.

3.2.2 Modification of GO/PEDOT Nanocomposite Films with Biomolecules

GO/PEDOT nanocomposite films were modified using carbodiimide chemistry to create an amine bond between the biomolecule and the GO sheets at the surface of the film. The nanocomposites were immersed for 3 h in a solution containing either interferon-γ (IFNγ, Sigma-Aldrich) or platelet-derived growth factor AA (PDGF-AA, Sigma-Aldrich) at a concentration of 2.5 μg mL^{-1} with 1-Ethyl-3-(3-dimethylaminopropyl)carbodiimide (EDC; 0.2 M; Sigma-Aldrich) and *N*-Hydroxysuccinimide (NHS; 0.2 M; Sigma-Aldrich) in sterile dH_2O. As a physical adsorption control, the nanocomposite films were incubated in either IFNγ or PDGF-AA, as above, but in the absence of EDC and NHS. All prepared samples were washed repeatedly with sterile phosphate buffered saline (PBS) after the modification procedure. Samples for cell culture were stored in PBS until use, and samples for characterization were stored dry.

3.2.3 GO/PEDOT Characterization

The morphology of the electrodeposited GO/PEDOT and PEDOT/PSS films were evaluated using scanning electron microscopy (SEM, JEOL JSM6510) with an operating potential of 3 kV. Roughness analysis was carried out with a scanning probe microscope in tapping atomic force microscopy (AFM) mode (Veeco Dimension V). Root mean square roughness (R_q) was calculated using Nanoscope Analysis software (Bruker).

Fourier-transform IR (FTIR) spectroscopy was used to evaluate the surface of the nanocomposite following carbodiimide crosslinking with IFNγ and PDGF-AA. The analysis was carried out with a Bruker Vertex 70 spectrometer with a Hyperion 2000 microscope at a 20x attenuated total reflectance (ATR) objective.

3.2.4 NSC Isolation and Culture

NSCs were isolated from the cortical tissue of E18 Sprague-Dawley rat embryos. Briefly, the tissue was triturated in a solution of Hank's Balanced Salt Solution (HBSS, Sigma-Aldrich) containing Glutamax (1%, Invitrogen) and Penicillin-Streptomycin (Pen-Strep; 1%, Invitrogen). The tissue was allowed to settle and the supernatant was centrifuged to pellet the cortical cells. After resuspension in NeuroCult NS-A proliferation medium (StemCell Technologies) supplemented with recombinant human epidermal growth factor (EGF; 20 ng mL^{-1}, Invitrogen), recombinant human basic fibroblast growth factor (bFGF; 10 ng mL^{-1}, Invitrogen), Heparin (2 mg mL^{-1}; StemCell Technologies), and Pen-Strep (1%), the cortical cells were maintained at 37°C for 3 d or until the formation of neurospheres, at which point they underwent passage. The cells were passaged as necessary every 3-4 d and were used for assays within passages 2 to 4.

For all NSC culture experiments, the neurospheres were passaged to obtain a single-cell suspension and seeded on culture surfaces at a density of 150,000 cells cm^{-2}. The seeded cells were maintained at 37°C in NeuroCult NS-A Differentiation medium (StemCell Technologies) supplemented with Pen-Strep (1%) in the absence of growth factors to induce differentiation. The culture medium was exchanged every 3 to 4 d as necessary.

3.2.5 Viability Assays

The viability of differentiating NSCs after exposure to soluble GO nanosheets was assessed with the MTT Cell Proliferation Assay. Cells were seeded on the surface of 96-well plates that were treated with poly-L-ornithine (PLO, 20 μg ml^{-1} in PBS, 1 h incubation) and after 24 h were treated with GO nanosheets at concentrations of 10, 25, 50, 100, and 200 μg mL^{-1}. The treated cells were assayed at 1 d, 3 d or 7 d (n = 5 for each group). The ratio of absorbance signal at 570 nm to 630 nm was quantified using a spectrophotometer. The experimental groups were normalized to controls that contained GO nanosheets without cells, and all data is presented as the percent viability compared to positive controls consisting of cells not exposed to the GO nanosheets. The viability of NSCs growing on the surface of the GO/PEDOT and PEDOT/PSS films was assessed similarly. The cells were assayed at 3 d and 7 d (n = 3 for each group), normalized to controls that contained the PEDOT films without cells, and compared to positive controls that consisted of cells growing on tissue culture plastic.

3.2.6 NSC Attachment and Differentiation on GO/PEDOT Substrates

NSCs were seeded on the surface of the PEDOT films that were treated with PLO (20 μg ml^{-1}in PBS, 1 h incubation) and fixed with paraformaldehyde (4%) at 30 min to evaluate the initial cell attachment, or at 7 d to assess differentiation. The samples were immunostained with markers for immature neurons (mouse monoclonal anti-β-III-tubulin, TuJ1; 1:500; Sigma-Aldrich), astrocytes (rabbit polyclonal anti-glial fibrillary acidic protein, GFAP; 1:500; DAKO) or oligodendrocyte precursors (mouse monoclonal anti-O4; 1:500; R&D Systems). Briefly, the cells were treated in blocking buffer (5% goat serum in PBS alone for O4 or with Triton-X, 0.02%, for TuJ1 and GFAP) for 20 min, then incubated in primary antibody for 2 h at room temperature followed by fluorescent secondary antibody (Alexa Fluor 488 anti-mouse or Alexa Fluor 594 anti-rabbit; Molecular Probes) for 45 min at room temperature. The cells were counterstained for nuclei using Hoechst 33342 (Invitrogen).

TuJ1-immunoreactive (ir) cells or O4-ir cells were quantified to determine the extent of neuronal and oligodendrocyte differentiation on each culture substrate (n = 3 for each). Each sample was imaged using a 20x objective and 10 random images were taken and used for quantification. Values were reported as the percent of differentiation by dividing the number of TuJ1-ir or O4-ir cells by the total number of nuclei present in the image. The NeuronJ plugin for ImageJ (http://rsbweb.nih.gov/ij/) was used to evaluate neurite growth from neurons. The average neurite length was quantified by tracing each neurite extending from each TuJ1-ir cell and averaging to obtain the mean length per cell. The total oligodendrocyte area was quantified using the ImageJ threshold and measure functions to define the O4-ir area for each cell.

3.2.7 Statistical Analysis

All statistical analyses were performed using GraphPad Prism software. Student's t tests were used to compare two experimental groups, one-way ANOVAs were used to compare three experimental groups, and two-way ANOVA was used to compare three experiment groups across multiple measures. All data is presented as the mean ± SEM.

3.3 RESULTS AND DISCUSSION

3.3.1 Morphological Characterization of GO/PEDOT Nanocomposite Film

The GO/PEDOT nanocomposite was deposited onto gold macroelectrodes by electrochemical polymerization from an aqueous solution containing the EDOT monomer and GO nanosheets. The synthesized film exhibited a characteristic surface morphology that included both sub-micron sheet-like features arising from smaller GO nanosheets engulfed in the polymer and larger wrinkle features that are likely the edges of larger GO nanosheets protruding from the nanocomposite surface (Figure 3.1a) [163]. The GO/PEDOT morphology differs significantly from that of PEDOT films doped with PSS, which exhibit uniform, compact features at the film surface (Figure 3.1b). This difference in morphology has implications for its ability to interface with cells.

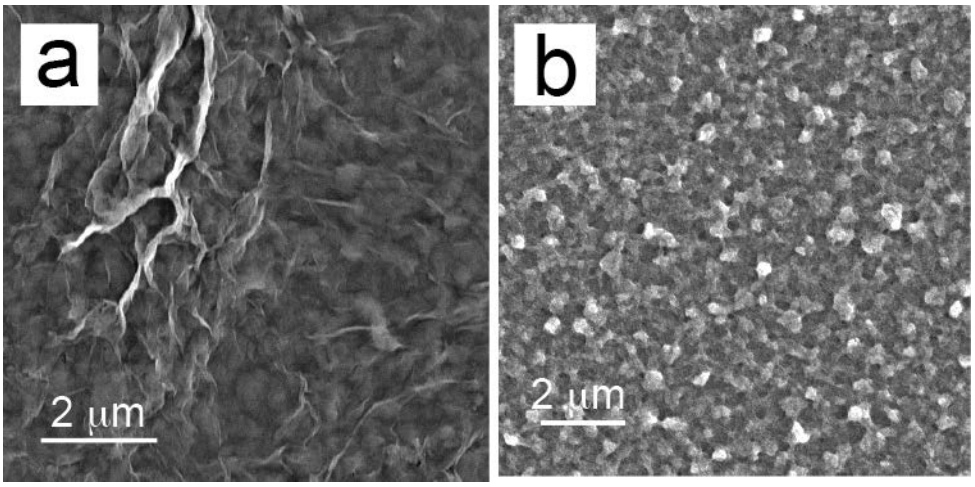

Figure 3.1. Surface Morphology of PEDOT Films. SEM images of PEDOT doped with (a) GO nanosheets or (b) PSS illustrating the dopant-dependent surface morphologies of CP films.

Neurons and NSCs have been shown to be highly responsive to various material properties such as surface morphology, stiffness, and roughness [128, 146, 164, 165]. This responsiveness indicates that creating cell-scaffolding materials with alterable physical properties will provide a means to control cell behavior to learn about their physiology or to produce appropriate cell behaviors for regenerative therapies. CPs demonstrate a wide array of morphological properties depending on their dopants, as demonstrated in Figure 3.1 and in work by others [30, 43], or by their synthesis method [14, 15, 23]. To further characterize the morphology of the GO/PEDOT nanocomposite, the surface roughness was evaluated with AFM. As expected, the GO/PEDOT nanocomposite exhibited a much rougher surface than that of the PSS-doped PEDOT film, as a result of the larger peaks and valleys created on the film surface by the larger GO nanosheets (Figure 3.2).

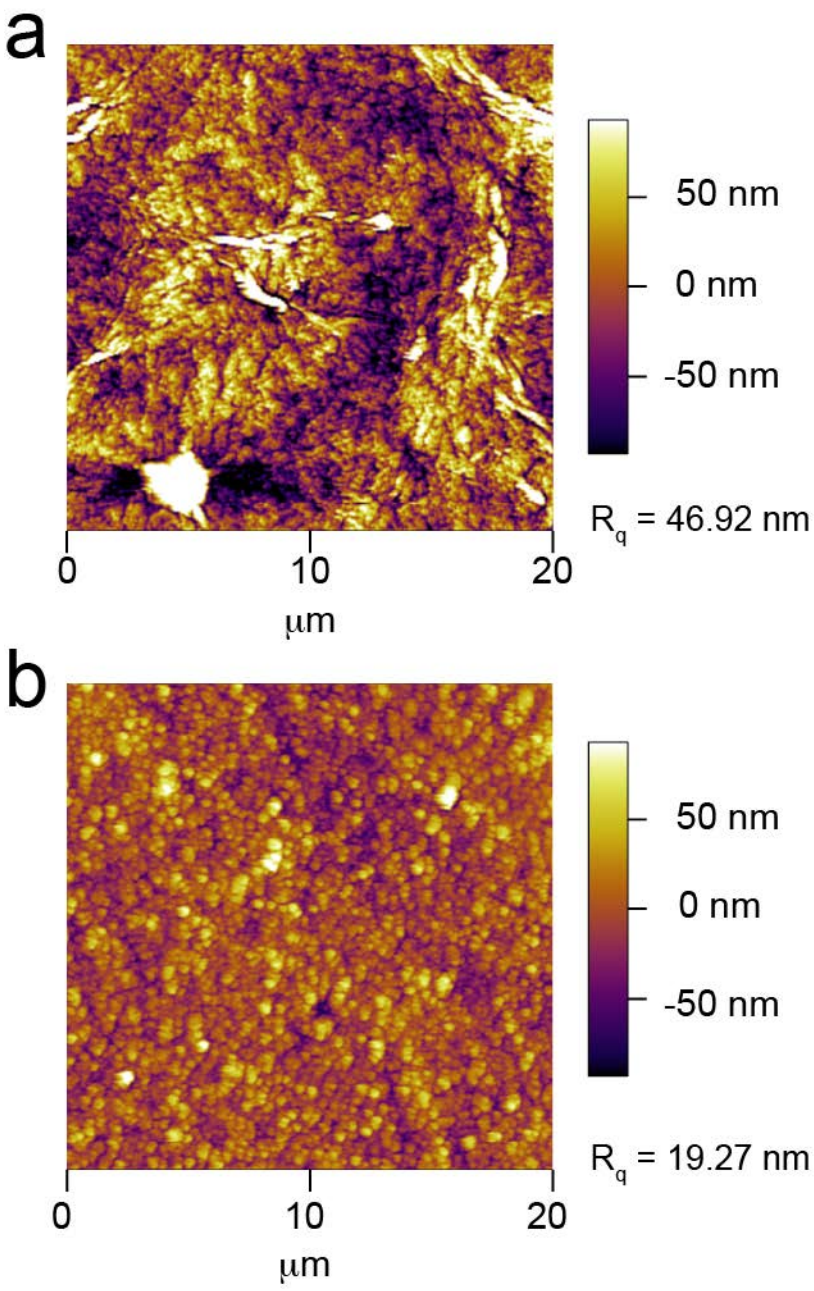

Figure 3.2. Surface Roughness Characterization of PEDOT Films. Representative AFM images of PEDOT doped with (a) GO or (b) PSS demonstrating the higher root mean square (R_q) surface roughness of GO/PEDOT nanocomposite films.

3.3.2 Toxicity Assessment of GO/PEDOT Nanocomposite

The cytotoxicity of nanoparticles has been under scrutiny in recent years with the increasing number of nanomaterials investigated for applications in biology and medicine [166-168]. The results of GO toxicity testing have been varied, likely as a result of the inconsistent methods used during the synthesis of the nanosheets and the variety of different cell types used for the assays [93, 169]. In light of these conflicting toxicity reports, we evaluated the effect of soluble GO nanosheets applied at varying concentrations to rat embryonic-derived NSCs. The GO nanosheets exhibited both time- and dose-dependent toxicity effects on the NSCs, with exposure to concentrations under 25 $\mu g\ ml^{-1}$ for 1 d creating no reduction in viability as measured by mitochondrial activity (Figure 3.3a). At doses higher than 25 $\mu g\ ml^{-1}$, the NSCs exhibited a large decrease in viability after only 1 d, and all doses elicited a decrease in viability after a 3 d or 7 d exposure. The mechanism of GO toxicity is still under investigation, though studies have shown that the nanoparticles can be endocytosed into the cell to alter gene expression, increase the production of reactive oxygen species, and elicit cell apoptosis [96, 167, 170, 171].

While the safety of soluble GO nanosheets remains questionable, work has demonstrated that when GO is contained within a polymer substrate or deposited onto a surface, there are no adverse effects on cell viability [73, 80, 172, 173]. The viability of NSCs cultured on the surface of the GO/PEDOT nanocomposite film for 3 d and 7 d was assessed and compared to that of NSCs growing on the surface of PEDOT doped with PSS, which has demonstrated good biocompatibility [18, 105]. At both time points, NSCs growing on the GO/PEDOT nanocomposite exhibited no decrease in their viability, similar to cells growing on the PSS-doped PEDOT substrate (Figure 3.3b).

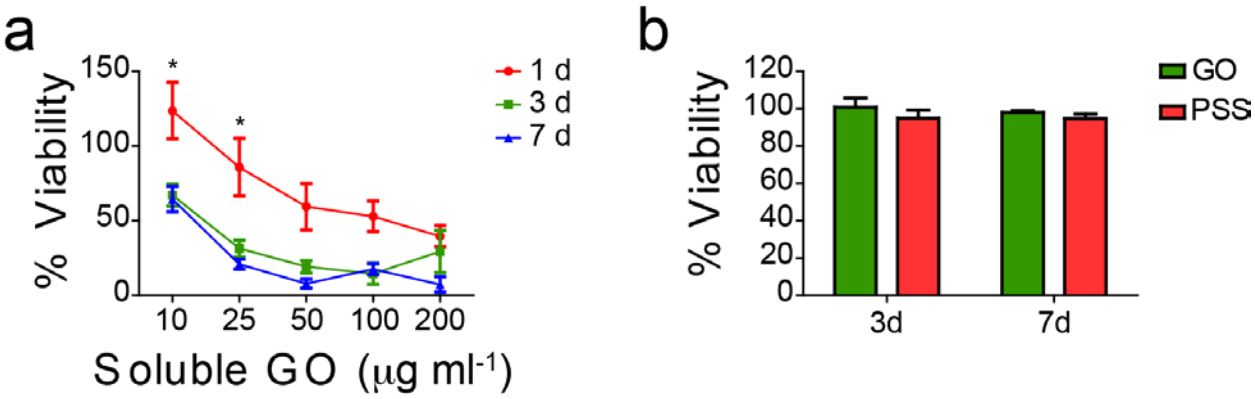

Figure 3.3. Toxicity Assessment of Soluble GO Nanosheets and GO/PEDOT Nanocomposite Film. (a) Viability of NSCs exposed to GO nanosheets for 1, 3, or 7 d at various concentrations. GO exhibits both a time- and dose- dependent toxicity effect on the cells (* $p < 0.05$; $n = 6$). (b) Viability of NSCs cultured on the surface of GO/PEDOT nanocomposite films or PEDOT doped with PSS for 3 d or 7 d. Cells exhibited no decrease in viability at either time point on either surface ($n = 3$).

3.3.3 NSC Attachment and Differentiation on GO/PEDOT Substrates

The attachment and growth of NSCs on the surface of the GO/PEDOT nanocomposite was evaluated to determine its performance as a cell scaffold. NSCs were seeded on the surface of PLO-coated substrates and cultured in differentiation media for either 30 min to evaluate attachment onto the substrate or 7 d to evaluate differentiation into neuronal lineages. At the 30 min time-point, the density of NSCs attached to GO/PEDOT did not differ from the density on the surface of the PEDOT doped with PSS, suggesting that initial attachment to the two surfaces was similar (Figure 3.4a). However, by 7 d in culture, NSC density on the GO/PEDOT nanocomposite surface surpassed that of the PEDOT doped with PSS (Figure 3.4b). Adhesion plays an essential role in stem cell maintenance, proliferation and differentiation, and on artificial substrates is mediated by a number of factors including surface charge, wettability and nanotopography [146, 174]. Because cell density differences occur at the 7 d time point, it is

possible that the initial adhesions formed were more stable on the GO/PEDOT nanocomposite surface, allowing for better growth during the longer culture. One possible explanation for the improved attachment may be that the PLO adsorbed more readily at the GO/PEDOT nanocomposite surface. PLO modification is commonly used to create a more hydrophilic substrate for improved cell attachment [175]. PLO is positively charged as a result of its multiple amine groups, and it might electrostatically interact with the negative carboxylic acid groups contributed by the GO at the surface of the nanocomposite. A second possibility for the improved cell density at later time points is that extracellular matrix (ECM) proteins secreted by the cells may have adsorbed on the GO/PEDOT nanocomposite surface more favorably than at the PEDOT doped with PSS surface. Again, electrostatic interactions might play a role, but additionally, π-stacking interactions can also occur between aromatic structures in the proteins and the benzene rings contained in the GO nanosheets [95, 97]. Proliferation may also play a role in the improved density present at the GO/PEDOT surface at 7 d. Compared to the density of cells growing on the GO/PEDOT surface at 30 min there is approximately a 7x increase at the 7 d time point. The NSCs were maintained in differentiation media without growth factors so the cells should not continue to proliferate. However, it is possible that the surface of the GO provides a mitogenic cue that encourages the NSCs to remain in their proliferative state and continue dividing, even in the absence of growth factors. Future work to investigate the effect on NSC proliferation will assist in characterizing the influence of the GO/PEDOT nanocomposite on NSC behavior.

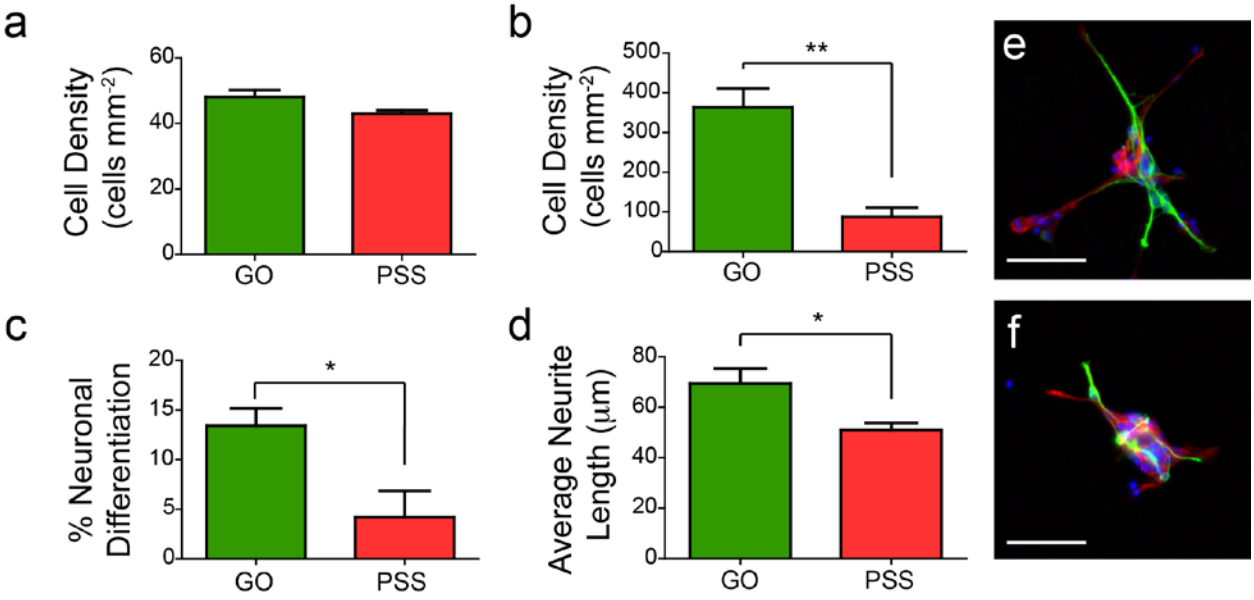

Figure 3.4. NSC Attachment and Differentiation on PEDOT Scaffolds. Total cell density present on PEDOT films doped with GO or PSS at (a) 30 min and (b) 7 d in culture in differentiation media. There are no differences between the groups during the initial attachment, but a significantly higher density of cells is present on the GO/PEDOT nanocomposite at 7 d ($p < 0.01$; $n = 3$). (c) Percent of neuronal differentiation and (d) average length of neurite outgrowth from differentiated neurons on PEDOT films after 7 d. The GO/PEDOT film supports a higher yield of differentiated neurons and a longer average neurite length (* $p < 0.05$; $n = 3$). Representative fluorescent images of differentiated NSCs growing on the (e) GO/PEDOT nanocomposite and the (f) PEDOT/PSS substrate. Cells were immunolabeled for neuron-specific TuJ1 (green), astrocyte-specific GFAP (red) and nuclei (blue). Scale bar measures 50 μm in (e) and (f).**

For regenerative therapies in the central nervous system, neurons are often the therapeutic target population because the normal functioning of these cells drives all behaviors and cognition [141, 176]. The dysfunction of neurons and neural circuitry commonly underlies the morbidity of neuropsychiatric disorders, neurodegenerative diseases and traumatic brain injury. For this reason, engineered scaffold materials that can drive neuronal differentiation and maturation are of great interest to improve the therapeutic ability of NSC populations. The differentiation

behavior of NSCs growing on the surface of the materials was evaluated at 7 d to determine the suitability of the GO/PEDOT nanocomposite as a scaffolding material. The GO/PEDOT nanocomposite supported significantly more neuronal differentiation than the PEDOT doped with PSS (Figure 3.4c, e, f) and those differentiated neurons extended longer neurites on the GO/PEDOT nanocomposite surface (Figure 3.4d, e, f). Improved neuronal differentiation on the surface of the nanocomposite may arise from biophysical cues from the rough nanotopography, chemical cues provided by the substrate itself or adsorbed ECM proteins secreted from the differentiating cells.

Neural stem cells have demonstrated high sensitivity to nanostructured substrates, with nanoscale roughness affecting cell differentiation pathways [146, 164, 177]. NSCs selectively differentiate into neurons when seeded on nanoscale fibrous substrates, a morphology that may imitate the fibrous ECM structure *in vivo* [177]. The wrinkle-like morphology of the PEDOT/GO nancomposite film may mirror this fibrous morphology (Figure 3.1) and be the driving factor behind the improved neuronal differentiation observed on its surface. Additionally, neuronal precursor cells are also sensitive to nanoscale features during development, indicating that the surface roughness may also contribute to the improved neurite growth exhibited by the cells growing on the GO/PEDOT nanocomposite [128]. In addition to the influential surface topography of the GO/PEDOT nanocomposite, it is possible that its chemical content may play a role in the increased neuronal differentiation. It has been demonstrated that chemical functional groups present on a substrate can have a significant impact on NSC growth and differentiation [178]. Amine and carboxylic acid groups support neuronal differentiation, while sulfonic acid groups will not. On both substrates explored here, the surfaces have been treated with PLO that contains amine groups that would promote neuronal differentiation. However, the surface of the

GO/PEDOT nanocomposite likely contains free carboxylic acid functional groups that could be synergistically contributing to the neuronal differentiation, while the PEDOT doped with PSS would have many sulfonic acid groups that are present on the PSS molecules that would be non-permissive to neuronal differentiation.

3.3.4 Directed NSC Differentiation on Functionalized GO/PEDOT

A successful method of engineering scaffolding materials is surface patterning with bioactive peptides and proteins to provide cues to seeded cells [179]. In their microenvironment, stem cells are exposed to a multitude of soluble and immobilized cues that influence all aspects of their behavior [180], creating a need for highly customizable scaffolding materials that can present a variety of cues to recapitulate the *in vivo* environment and enable fine control over NSCs for particular therapeutic applications. To explore the potential of the GO/PEDOT nanocomposite film as an adjustable scaffold to drive NSC behavior, the surface of the nancomposite was modified with either pro-neuronal or pro-oligodendrocyte biomolecules. GO has been noted as a highly modifiable material, a property that arises from the plentiful functional groups in its structure [53, 64]. The GO nanosheets in the nanocomposite contain multiple carboxylic acid groups at their edges, some of which may be accessible at the surface of film, as indicated by the wrinkle-like structures in the film morphology that are created by the edges of the nanosheets protruding from the polymer surface (Figure 3.1). Previous work described in *Chapter 2* has shown that these free carboxylic acid groups can be utilized to cross-link a functional peptide onto the surface of the nanocomposite to influence neuron growth [80]. Extending these studies, the efficacy of cross-linking larger molecules like IFNγ and PDGF-AA using carbodiimide chemistry was investigated. IFNγ is a cytokine that is secreted by infiltrating immune cells

following brain injury, and has been shown to promote neuronal differentiation [181] while PDGF signaling increases oligodendrocyte precursor proliferation and differentiation [182]. Both IFNγ and PDGF-AA act on cell surface receptors and do not need to be internalized to initiate the intracellular pathways that result in the changes in cell behavior, which suggests that the covalent immobilization technique will not interfere with the bioactivity of the molecules. These were chosen as model biomolecules to demonstrate the versatility of the GO/PEDOT nanocomposite as a NSC scaffold.

Biomolecules were attached to the surface of the GO/PEDOT nanocomposite using carbodiimide crosslinking that creates amide bonds between the carboxylic acid groups of the GO nanosheets and the amine groups on the proteins. To verify the presence of biomolecules after the crosslinking procedure, the surfaces were analyzed using FTIR (Figure 3.5). The unmodified GO/PEDOT nanocomposite film exhibited a spectrum that included characteristic GO peaks including carboxylic C=O (1742 cm^{-1}), O-H (1418 cm^{-1}), C-OH (1367 cm^{-1}), epoxide (1209 cm^{-1}) and alkoxy C-O (1067 cm^{-1}), as well as characteristic PEDOT peaks including thiophene (1520 cm^{-1}, 1487 cm^{-1}, and 1240 cm^{-1}), ethylenedioxy (1142 cm^{-1}, 1093 cm^{-1}, and 930 cm^{-1}), and C-S (981 cm^{-1} and 845 cm^{-1}) [161, 183]. The biomolecule-modified surfaces both exhibit strong amide I bands around 1650 cm^{-1} that arise from C=O stretching of the amide bonds in their protein structure, and the IFNγ spectrum exhibited an amide III band at 1298 cm^{-1} that arises from CN stretching and NH bending [184]. Additionally, on both biomolecule modified spectra, the carboxylic C=O shifts to the right, suggesting that the source may no longer be the free carboxylic acid groups from the GO nanosheets, which would have been consumed during the formation of the amide bond between the biomolecules and the

nancomposite surface, but rather the C=O signal from the proteins on the nanocomposite surface [185].

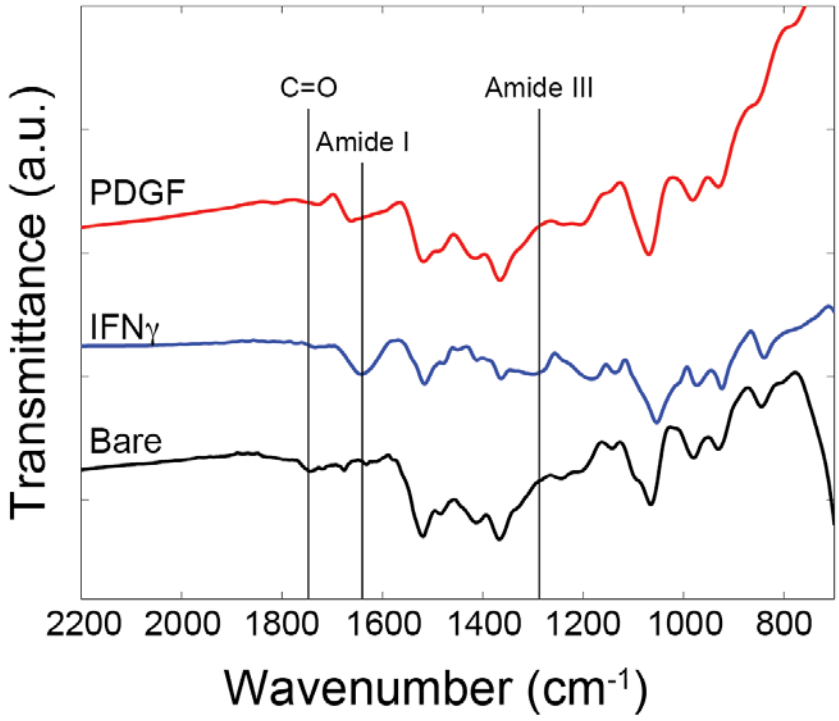

Figure 3.5. Characterization of Immobilized Biomolecules at the Surface of the GO/PEDOT Nanocomposite. Representative FTIR spectra of bare, unmodified GO/PEDOT (black), and GO/PEDOT modified via carbodiimide chemistry with IFNγ (blue) and PDGF-AA (red). Amide bands appear on the protein-modified film spectra, confirming their presence on the film. The carboxylic C=O signal present on the bare film shifts to the left, suggesting that the free carboxylic acids bound to the ring structure of the GO nanosheets have been consumed during the reaction and the new signal arises from carboxylic acids present in the proteins.

The differentiation behavior of NSCs growing on the surface of the modified nanocomposite films was evaluated after 7 d in differentiation medium. The surface of the nanocomposites was not treated with PLO to ensure that any effect on cell density or differentiation was due to the IFNγ or PDGF modification, rather than non-specifically adsorbed

PLO. NSCs growing on the film covalently modified with IFNγ through carbodiimide chemistry (IFNγ-CM) exhibited significantly more neuronal differentiation than cells growing on an unmodified nanocomposite film (bare) or a nanocomposite film modified with IFNγ via nonspecific physical adsorption (IFNγ-PA) (Figure 3.6). There was no difference between the groups in cell density or length of neurite extension (data not shown). The differentiated neurons growing on the surface of the IFNγ-PA and the bare nanocomposite mostly existed within large cell clusters containing astrocytes (Figure 3.6a, b), while the differentiated neurons on the IFNγ-CM surface often localized outside of the cell clusters, indicating a higher affinity for the substrate.

Oligodendrocytes, which produce myelin that insulates neuron axons, are a promising cell population for cellular therapies targeted at demyelinating diseases of the nervous system such as multiple sclerosis. *In vitro*, the rate of oligodendrocyte differentiation from NSCs is very low, making the development of therapies relying on oligodendrocyte transplantation difficult. To address this need, we modified the GO/PEDOT with oligodendrocyte mitogen PDGF-AA to assess its ability to drive the NSCs toward the oligodendrocyte lineage. Differentiation was evaluated at the surface of PDGF-CM, PDGF-PA, and bare GO/PEDOT nanocomposite substrates after 7 d in differentiation medium. As hypothesized, the PDGF-CM surface significantly improved the amount of oligodendrocyte differentiation compared to the bare nanocomposite surface (Figure 3.7d). Notably, the extent of oligodendrocyte process outgrowth, quantified by total cell area, was significantly higher on the PDGF-CM substrates as compared to the PDGF-PA and bare substrates (Figure 3.7a, b, c, e). The higher level of process outgrowth indicates that the cells have matured further down their differentiation pathway and confirms that the cross-linking procedure preserved the bioactivity of the protein.

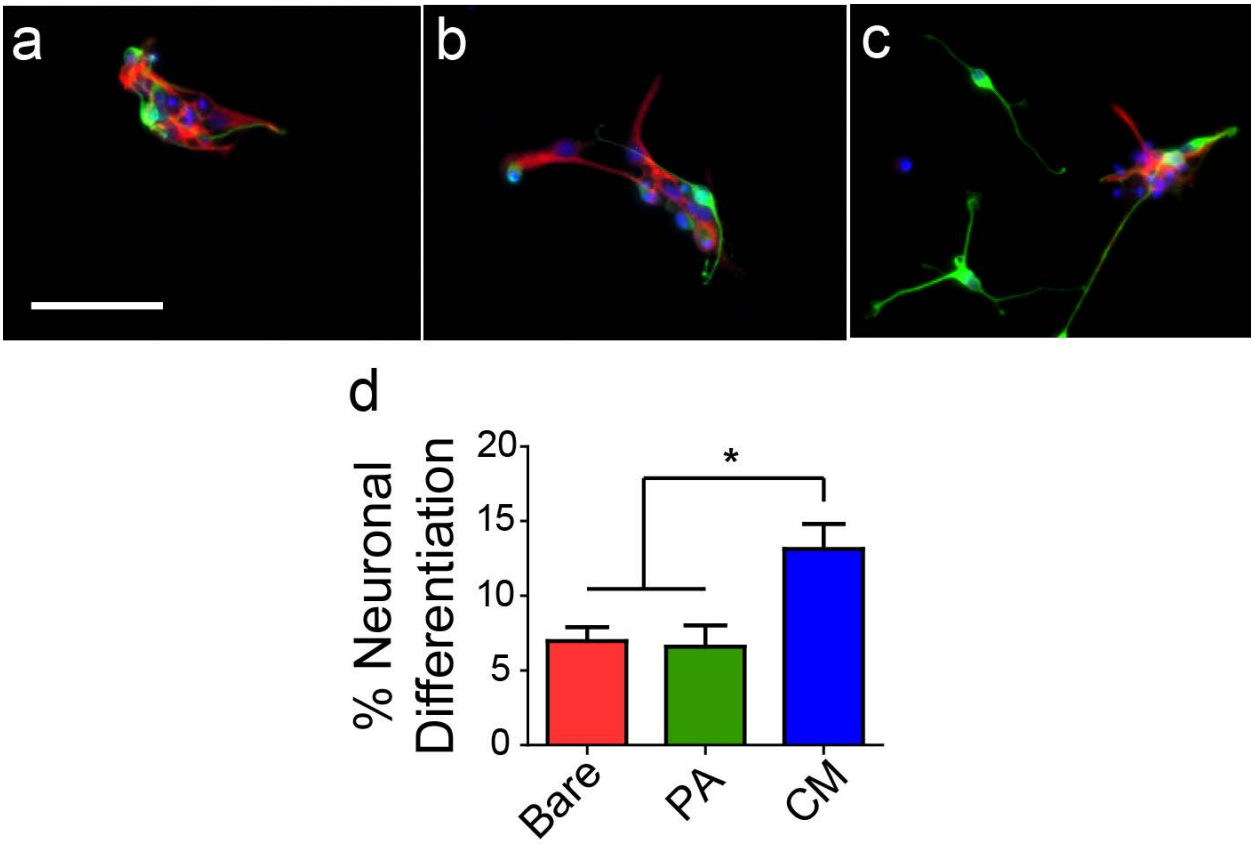

Figure 3.6. Differentiation of NSCs on the IFNγ-Modified GO/PEDOT Nanocomposite. Representative fluorescent images of NSCs differentiated for 7 d on the surface of the (a) bare GO/PEDOT nanocomposite, or the GO/PEDOT nanocomposite modified with IFNγ by (b) nonspecific physical adsorption (PA) or (c) covalent carbodiimide cross-linking (CM). Cells were immunolabeled for neuron-specific TuJ1 (green), astrocyte-specific GFAP (red) and nuclei (blue). Scale bar measures 50 μm. (d) Percent of neuronal differentiation on each surface demonstrating the efficacy of the IFNγ-CM (* $p < 0.05$; $n = 3$).

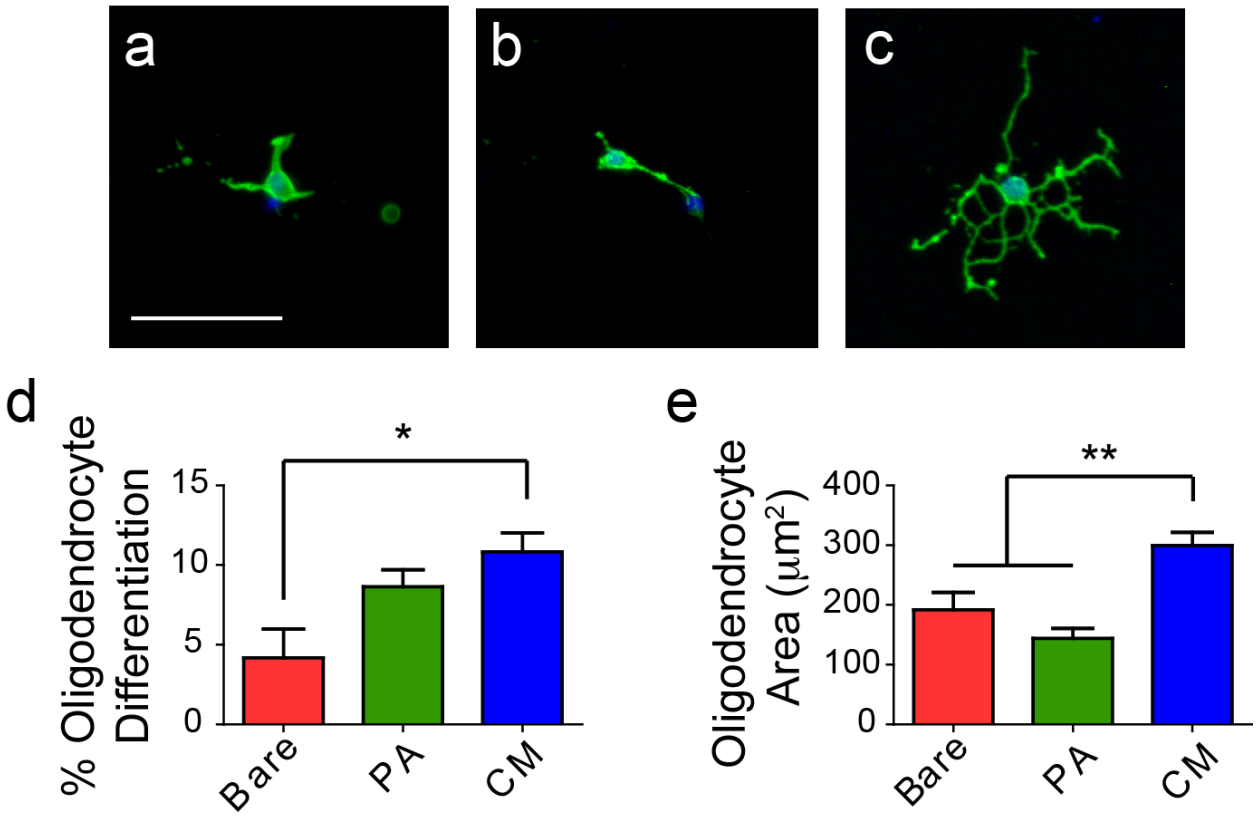

Figure 3.7. Differentiation of NSCs on the PDGF-modified GO/PEDOT Nanocomposite. **Representative fluorescent images of NSCs differentiated for 7 d on the surface of the (a) bare GO/PEDOT nanocomposite, or the GO/PEDOT nanocomposite modified with PDGF by (b) nonspecific physical adsorption (PA) or (c) covalent carbodiimide cross-linking (CM). Cells were immunolabeled for oligodendrocyte precursor cell marker O4 and counterstained for nuclei (blue). Scale bar measures 50 μm. (d) Percent of oligodendrocyte differentiation on each surface demonstrating the efficacy of the PDGF-CM (* $p < 0.05$; $n = 3$). (e) Average spreading area of differentiated oligodendrocytes on each surface showing the improved process outgrowth on the PDGF-CM surfaces (** $p < 0.01$; $n = 3$).**

In both cases, the CM biomolecule performed better than the PA biomolecule. This demonstrates the superiority of the covalent crosslinking procedure and its ability to present the molecules to the cells in a way in which they can still interact with their receptors. Carbodiimide cross-linking activates the amine groups present on the arginine, lysine, asparagine, and glutamine amino acid residues of the protein for the covalent interaction with the carboxylic acid groups at the GO/PEDOT nanocomposite surface. There are multiple potential cross-linking sites on both IFNγ (47 residues) and PDGF (25 residues), increasing chances that the cross-linking will occur at a site that does not interfere with receptor binding. Although the biomolecules that were nonspecifically physically adsorbed were present at the nanocomposite surface after repeated washing prior to the start of the cell culture (FTIR data not shown), they did not significantly affect NSC differentiation, indicating that the proteins either desorbed over the course of the culture period, were denatured as a consequence of adsorption, or the receptor binding sites were masked.

3.4 CONCLUSIONS

While NSC therapies hold tremendous potential for the treatment of various CNS injuries and disorders, shortcomings related to the control of cell differentiation into specific lineages must be addressed. We explored the potential of a GO/PEDOT nanocomposite film as a scaffolding material to influence the behavior of cultured NSCs *in vitro*. The unmodified GO/PEDOT composite supported higher cell densities and improved neuronal differentiation as compared to conventional PEDOT films doped with PSS. By utilizing free carboxylic acid groups donated by GO at the surface of the nanocomposite, biomolecules were covalently immobilized at the film

surface to preferentially promote either neuronal or oligodendrocyte lineage differentiation. The conductive nature of the GO/PEDOT nanocomposite will enable future investigations of the influence of electrical stimulation on NSC biology and its potential synergy with the presentation of chemical cues. The GO/PEDOT nanocomposite has potential for applications in *in vitro* processing of NSCs for transplantation, exploratory *in vitro* experimentation to elucidate the biology of NSC differentiation and maturation, and *in vivo* applications in which chemically decorated, conductive scaffolding materials can be utilized to explore activation of endogenous NSC populations or to improve the transplantation efficacy of exogenous cells.

4.0 ELECTRICALLY CONTROLLED DRUG DELIVERY FROM GRAPHENE OXIDE NANOCOMPOSITE FILMS

4.1 INTRODUCTION

On-demand release of drug molecules from biomedical devices enables precise, targeted dosing that can be temporally tuned to meet requirements for a variety of therapeutic applications [186-188]. Recent advances have facilitated the use of various cues, such as UV- and visible-wavelength light, NIR radiation, magnetic field, ultrasound and electrical stimulation to trigger drug release *in vivo* from implanted smart materials [186, 189, 190]. These techniques enable greater control over drug delivery, compared to traditional *in vivo* drug-release systems that rely on passive delivery that is programmed prior to implantation and cannot be modified in response to changing therapeutic needs. To achieve precise, controlled drug delivery, nanomaterial drug carriers are increasingly investigated because of their unique structures and tunable properties [168, 191]. For example, the large surface area and sp^2 carbon lattice associated with carbon nanomaterials, such as carbon nanotubes, graphene, and graphene oxide (GO), enable highly efficient drug loading, while their capacity for modification provides multiple routes for targeted and controlled drug delivery [192, 193].

GO is a two-dimensional nanomaterial composed of a honeycomb carbon lattice structure with hydroxyl, carboxyl and epoxide functional groups [53]. It is known for its exceptional

electrical, chemical, and mechanical properties and has been investigated recently as a material for a variety of biomedical applications [64, 80, 193-196]. Of these applications, targeted drug delivery has been particularly interesting. The presence of reactive functional groups at the basal plane and edges of GO nanosheets creates an opportunity to covalently modify the particles for use in targeted drug delivery, while the abundance of localized π-electrons at the nanosheet surface enables π-π interactions with aromatic drug compounds [197, 198]. Targeted drug delivery has been achieved by covalently modifying drug-loaded GO with cancer cell–targeting antibodies and molecules or by functionalization with paramagnetic particles for magnetically directed delivery [199-203]. However, once at the targeted location, these methods rely on desorption of the drug molecules from the GO nanosheets through either passive or pH/redox-controlled mechanisms, which limits the ability to control the drug dosage in real time [198, 201]. A drug-loaded hydrogel composed of reduced GO and poly(vinyl alcohol) enabled on-demand control of dosing *via* modulation of drug release rate with the application of an external electric field [204]. However, this system required the use of large voltages that could be damaging to biological tissues, and drug passively diffused from the bulk of the polymer in the absence of stimulation because of the porous morphology of the hydrogel.

In this work, we describe an electrically controlled drug delivery system based on GO nanosheets incorporated into a conducting polymer (CP) film. CP-mediated drug delivery systems, composed of an electrode coated with a drug-loaded CP thin film, yield highly flexible release profiles that are favorable for addressing dosing needs that may change over the course of treatment [34]. Drug-loaded CP films release drug molecules in response to electrical stimulation, with the amount and duration of release controlled by the type of stimulation applied to the film [32, 35, 205]. A major limitation of CP-mediated drug release is the finite amount of

drug that can be loaded into and released from the thin films. We address this shortcoming in CP-mediated release systems by developing a CP nanocomposite film composed of poly(pyrrole) (PPy) doped with graphene oxide (GO) nanosheets for controlled delivery of anti-inflammatory drug.

Nanocomposite films consisting of GO nanosheets and CPs have recently generated interest as materials for bioapplications, such as cell scaffolding or chemical sensing, as a result of their favorable electrical properties, good stability, neuronal biocompatibility and ease of surface modification with bioactive molecules [80, 90, 162, 206, 207]. We demonstrate that, when incorporated into PPy along with the anti-inflammatory drug dexamethasone (DEX), the GO nanosheets create a highly stable nanocomposite film that releases the drug molecules on-demand in response to electrical stimulation, without passive diffusion. The CP matrix provides a conductive scaffold through which electrical stimulation can be applied in order to elicit drug release from the nanocomposite, while the GO nanosheets act as nanocarriers that improve the amount of drug loaded into and released from the nanocomposite film. Furthermore, altering the thickness and size of the GO nanosheets by utilizing its unique response to sonication treatment changes the physical properties and release profile of the nanocomposite, suggesting that the system can be tuned to the needs of various applications, making it a valuable tool for both therapeutics and research within the field of biomedicine.

4.2 MATERIALS AND METHODS

4.2.1 Electrochemical Apparatus

All electrochemical experiments were performed with a Gamry Potentiostat, FAS2/Femtostat (Gamry Instruments), using a three-electrode set-up with glassy carbon working electrodes (3 mm diameter, CH Instruments), a platinum wire counter electrode, and a silver/silver chloride reference electrode (CH Instruments).

4.2.2 GO Synthesis

GO was synthesized from graphite powder (SP-1, Bay Carbon Inc., Bay City). A pre-oxidation step was performed to increase the extent of oxidation of the final product, followed by oxidation by the modified Hummer's method [54, 208]. In brief, a solution of 50 mL H_2SO_4, 10 g $K_2S_2O_8$ and 10 g P_2O_5 was heated to 80°C. Graphite powder (12 g) was added and reacted for 6 h at 80°C. The solution was diluted with 2 L dH_2O, filtered through a glass filter (pore size: 2.5 – 4.5 μm), and air-dried overnight. The pretreated graphite (688.5 mg) was added to 23 mL H_2SO_4 chilled to 0°C, and 3 g $KMnO_4$ was added while the temperature was controlled below 10°C. The solution was reacted for 2 h at 35°C, and then 46 mL dH_2O was added while the temperature was controlled below 50°C. The solution was reacted for an additional 2 h at 35°C and then was diluted with 140 mL dH_2O. A 2.5-mL volume of H_2O_2 (30%) was added, and the mixture was allowed to settle overnight. After decanting the supernatant, the GO was washed by ultracentrifugation with 500 mL HCl, followed by washing with copious dH_2O until the wash

solution reached a neutral pH value. The GO was dialyzed for 4 d and then stored in H_2O until use.

4.2.3 Nanocomposite Film Synthesis

GO/PPy-DEX nanocomposite films were electrochemically synthesized on the glassy carbon electrodes from an aqueous solution containing pyrrole (0.2 M, Sigma-Aldrich), dexamethasone 21-phosphate disodium salt (10 mg ml^{-1}, Sigma-Aldrich) and GO nanosheets (5 mg ml^{-1}). The GO suspension was ultrasonicated for 30 min or 60 min immediately prior to electropolymerization. A constant potential of 0.8 V *vs*. a silver/silver chloride reference electrode was applied until the charge density reached 400 mC cm^{-1}. Conventional PPy-DEX films were electrochemically synthesized under the same conditions, with the exclusion of the GO nanosheets from the aqueous polymerization solution.

4.2.4 Electrochemical Measurements

Electrochemical impedance spectra of prepared films were collected in PBS, in the frequency range of 1 to 100 kHz, using an alternating current sinusoid of 5 mV. CV analysis was performed in PBS by sweeping the potential from -0.9 V to 0.5 V at 100 mV s^{-1}.

4.2.5 Nanosheet and Film Characterization

GO nanosheet thickness and size was evaluated with atomic force microscopy (Bruker Dimension V SPM). Nanosheet suspensions were drop coated on mica surfaces, and the height

profile was analyzed in tapping mode. Nanoscope Analysis software (Bruker) was used to calculate the histograms of sheet thicknesses and mean nanosheet diameter after 30-min or 60-min sonication treatments. The surface morphology and microstructure of the nanocomposite film were evaluated with scanning electron microscopy (JEOL JSM6510). Film surface chemistry was evaluated with attenuated total reflectance Fourier transform IR (Bruker Vertex 70), and elemental analysis was performed by energy-dispersive X-ray spectroscopy (Oxford INCA EDS).

4.2.6 Electrically Controlled Drug Release

For all drug release experiments, modified electrodes were immersed in PBS and submitted to release stimulation. The PBS solutions containing the released drug were analyzed with UV spectroscopy at a wavelength of 242 nm to quantify the amount of DEX released. To compare the amount of DEX released from conventional PPy-DEX films and the GO/PPy-DEX nanocomposite, a square-wave, biphasic voltage pulse (-2 V for 5 s, followed by 0 V for 5 s) was applied for 1000 cycles, and the cumulative amount of DEX release was quantified. To determine total amount of releasable drug from the GO/PPy-DEX nanocomposite, films underwent aggressive voltage pulses (-2 V for 5 s, followed by 0 V for 5 s) until cumulative drug release reached a plateau. The plateau value was considered the total amount of releasable drug contained in the nanocomposite. To evaluate the release profile in response to repeated stimulus application, films were submitted to square-wave, biphasic voltage pulses (-0.5 V for 5 s, followed by 0.5 V for 5 s). The amount of drug release was reported as the percentage of total drug release (the plateau value) determined using the aggressive voltage stimulation. The

negative phase of the stimulus was varied from -2 V to -0.25 V to evaluate the stimulus magnitude effect on drug release.

4.2.7 DEX Loading Capacity Assay

The amount of DEX loaded on GO sheets was evaluated by incubating DEX (100 μM) with GO (0.5 mg ml^{-1}) in H_2O for 2 h at room temperature. Prior to incubation with DEX, the GO suspension was sonicated for 30 min or 60 min. The mixture was centrifuged for 30 min at 14,000 RPM to pellet the DEX-loaded GO nanosheets, and the supernatant was analyzed with UV spectroscopy at 242 nm to determine the amount of DEX remaining in solution. The amount of drug loaded was calculated by subtracting the amount of free DEX in the supernatant from the amount of DEX in a sample not incubated with GO.

4.2.8 Bioactivity Assay

All animal procedures were approved by the Institutional Animal Care and Use Committee of the University of Pittsburgh. Hippocampal tissue was isolated from E18 Sprague Dawley rat embryos, treated with a digestion buffer containing 0.025% trypsin, 137 mM NaCl, 5 mM KCl, 7 mM Na_2HPO_4, and 25 mM HEPES. For astrocyte cultures, dissociated hippocampal cells were maintained in DMEM supplemented with fetal bovine serum and penicillin/streptomyocin, grown to confluence in a culture flask, trypsinized and seeded on bare glass coverslips at a density of 15k cells/cm^2. The cultures were incubated for 1 h at 37°C to allow cell attachment and then were treated with release solutions from the GO/PPy-DEX films (rDEX) or a prepared DEX solution (DEX). The DEX release solutions were obtained by applying an aggressive

voltage stimulation paradigm (-2 V for 5 s, followed by 0 V for 5 s, 1000 cycles) to the GO/PPy-DEX film. The total amount of DEX in the release solution was quantified using UV spectroscopy, and a volume was added to the culture media to create a concentration of 1 μM DEX. For neuron cultures, dissociated hippocampal cells were maintained in Neurobasal with B27, GlutaMax, horse serum and penicillin/streptomyocin. Glass coverslips were prepared for neuron culture by coating with polyethylimine (PEI) followed by laminin, and neurons were seeded on the coverslips at a density of 25k cells/cm^2. To evaluate any toxic byproduct released from the films, control films without drug underwent the same aggressive electrical stimulation parameters as the drug-loaded films, and the resulting release solutions were added to the neuronal culture at the same volumes as the treatments.

4.2.9 Immunofluorescence

After 2 d (neurons) or 4 d (astrocytes), the cultures were fixed in 4% paraformaldehyde for 30 min. The cells were blocked and permeabilized by immersion in a solution containing 5% normal goat serum and 0.2% TritonX. Neuron cultures were immunostained with mouse monoclonal anti-ß-III-tubulin (1:500, Sigma-Aldrich), and astrocyte cultures were immunostained with polyclonal rabbit anti-glial fibrillary acidic protein (GFAP, 1:500, Dako). For both culture types, the samples were incubated in the primary antibody for 2 h, washed with PBS, incubated in a goat Alexa Fluor 488 (1:1000, Invitrogen) against the appropriate species for 45 min, washed in PBS and counterstained for nuclei with Hoechst 33342 (1:1000, Invitrogen). Immunoreactive cells were imaged with a Zeiss Axioskop 2 fluorescent microscopic. Six random 10x images were collected from each sample (n = 4), and mean neuron density, average neurite length and astrocyte density were quantified.

4.2.10 Statistical Analysis

All statistical analyses were done using SPSS software (IBM). Student's t-tests or one-way analysis of variance (ANOVA), followed by Tukey's post hoc analysis, were used to compare experimental groups. All data are presented as mean (± SEM).

4.3 RESULTS AND DISCUSSION

4.3.1 GO/PPy Nanocomposite Film Synthesis and Characterization

The DEX-loaded GO/PPy (GO/PPy-DEX) films were electrodeposited onto glassy carbon electrodes from a solution containing both GO nanosheets and DEX. During CP film polymerization, negatively charged species are loaded into the polymer matrix to balance positive charges formed on the backbone of the growing polymer. The GO nanosheets are negatively charged as a consequence of carboxylic acid groups formed at their edges during the oxidation procedure, enabling them to be incorporated into the CP film as dopant molecules, along with anionic drug molecules (Figure 4.1a). During the electropolymerization reaction, the GO nanosheets compete with the free anionic DEX, as dopant molecules. Fourier-transform IR spectra of the GO/PPy-DEX film display peaks attributable to both GO and DEX, indicating that the drug molecules are successfully loaded into the film, along with the GO nanosheets (Figure A1.1). GO nanosheets have been noted for their large surface/volume ratio and sp^2-hybridized carbon structure, which enables efficient loading of aromatic drug molecules, such as DEX [97, 193]. Therefore, although some DEX molecules are directly doped into the film, a portion of the

drug molecules may adsorb on the GO nanosheets and be carried into the synthesized composite films as the nanosheets are incorporated as dopant molecules.

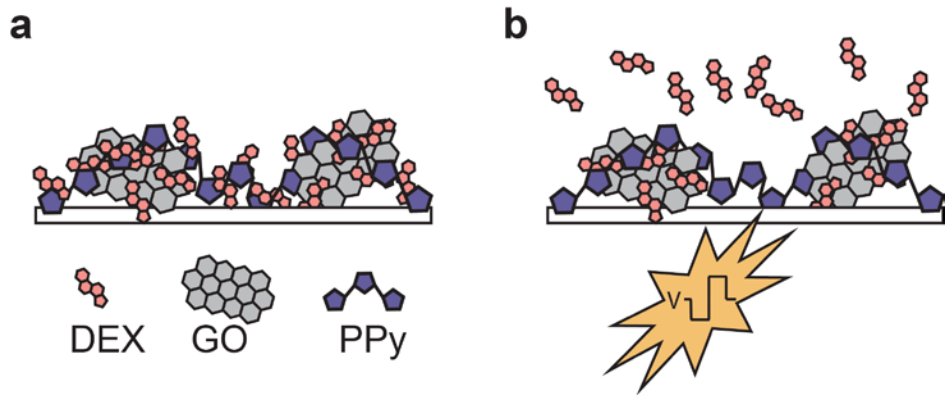

Figure 4.1. Drug Loading into and Release from the GO/PPy Nanocomposite. Schematic representation of (a) the GO/PPy-DEX nanocomposite and (b) DEX release from the GO/PPy nanocomposite in response to electrical stimulation. During synthesis, positive charges form on the growing polymer backbone and are balanced by anions, such as GO and DEX molecules, present in the deposition solution. Reduction of the nanocomposite with voltage stimulation elicits release of small, mobile drug molecules as the polymer backbone neutralizes.

The electrical properties of the GO/PPy-DEX film were explored using electrochemical impedance spectroscopy and cyclic voltammetry (CV), and compared to conventional PPy-DEX films that do not contain GO nanosheets as co-dopants. The electrode modified with GO/PPy-DEX film exhibited an impedance drop across all measured frequencies compared to both the bare electrode and the electrode modified with PPy-DEX, indicating that the nanocomposite film improves the capacitance of the electrode/electrolyte interface (Figure 4.2a). CV analysis carried out in phosphate buffered saline (PBS) showed that the electrodes modified with GO/PPy-DEX film have a higher charge-storage capacity, compared to both bare electrodes and PPy-DEX modified electrodes, as determined by comparison of the area underneath the CV curves (Figure

4.2b). The CV curve of the GO/PPy-DEX modified electrode exhibits a reduction peak at -0.52 V that occurs as anionic DEX molecules leave the film as a consequence of the negative potential sweep through the film, and an oxidation peak at -0.09 V that is associated with re-doping by small ions in the PBS or by DEX previously adsorbed on GO [209]. The GO/PPy-DEX reduction peak is much broader with a higher amount of current passed between 0 V and -0.5 V. The larger reduction peak area, which reflects the amount of drug molecules leaving the film, suggests that the GO/PPy-DEX film will release drug more effectively than the PPy-DEX film. The low impedance and high charge storage capacity of the synthesized nanocomposite reflect the excellent electrochemical properties of the nanocomposite film; as these properties decrease and increase, respectively, more current will pass through the film in response to a particular voltage pulse, enabling more efficient drug release.

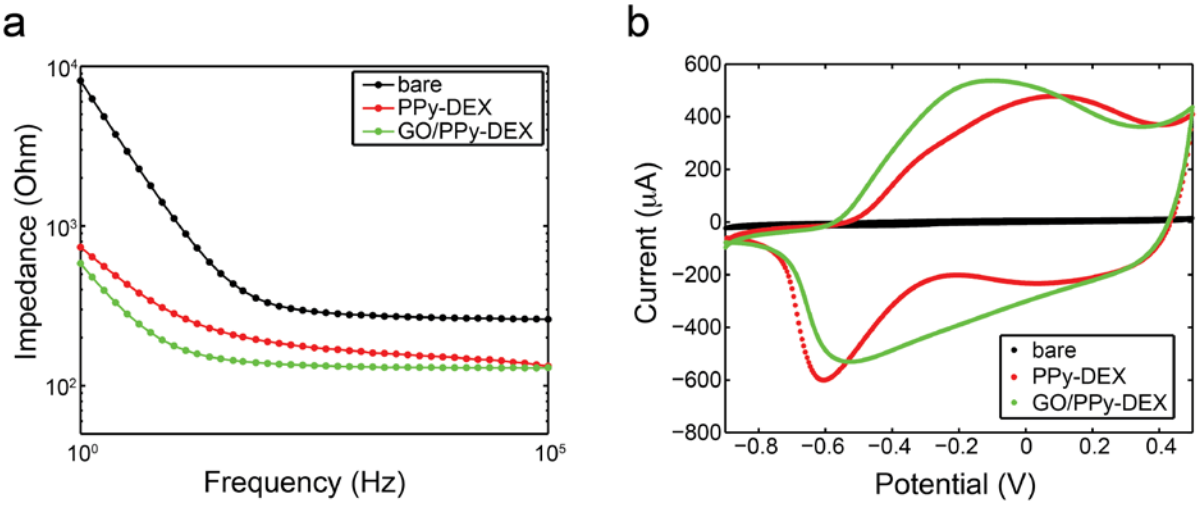

Figure 4.2. Electrical Properties of the GO/PPy-DEX Nanocomposite Film. (a) Electrochemical impedance spectra and (b) cyclic voltammograms for the bare glassy carbon electrodes, electrodes modified with a PPy-DEX film, and electrodes modified with the GO/PPy-DEX nanocomposite film. The GO/PPy-DEX modified electrodes exhibit lower impedance values and higher charge-storage capacity, indicating the electroactivity of the nanocomposite.

4.3.2 Electrically Controlled Drug Release from GO/PPy Nanocomposite

Electrically controlled release of DEX molecules can be achieved by utilizing the unique redox properties of the GO/PPy-DEX nanocomposite film. When the film is electrochemically reduced, the anionic DEX molecules previously associated with the positive charges along the PPy backbone in the oxidized form will be released as the charges on the polymer backbone are neutralized (Figure 4.1b). Since large dopant molecules are generally immobile within CP films, the GO nanosheets, which measure from hundreds of nanometers to microns in the x-/y-direction, are expected to remain within the CP during film reduction [53, 209]. To evaluate the drug-releasing performance of the GO/PPy-DEX nanocomposite film, voltage pulses were applied through the nanocomposite when immersed in PBS, and the release solution was analyzed by UV absorbance spectroscopy to quantify the amount of DEX expelled from the film. Drug release from the GO/PPy-DEX nanocomposite was compared to release from conventional PPy-DEX films that do not contain GO nanosheets as co-dopants. The films were stimulated with an aggressive, biphasic voltage pulse (-2 V for 5 s, followed by 0 V for 5 s) for 1000 cycles to evaluate the total DEX release from the films (Figure 4.3a). When the PPy films were co-doped with GO nanosheets, the aggressive release paradigm elicited 2.3x the amount of drug release of conventional PPy films without GO (209.7 μg cm^{-2} *vs.* 88.9 μg cm^{-2}, $p < 0.01$, $n = 3$). Conducting polymer mediated drug release is thought to be a surface area dependent process, with drug releasing more efficiently from the surface than the bulk of the film [33, 205]. The nanocomposite film exhibits a much rougher surface morphology than conventional PPy films without GO (Figure A1.2), and the difference in the film surface area is a possible cause of the significant improvement in drug payload.

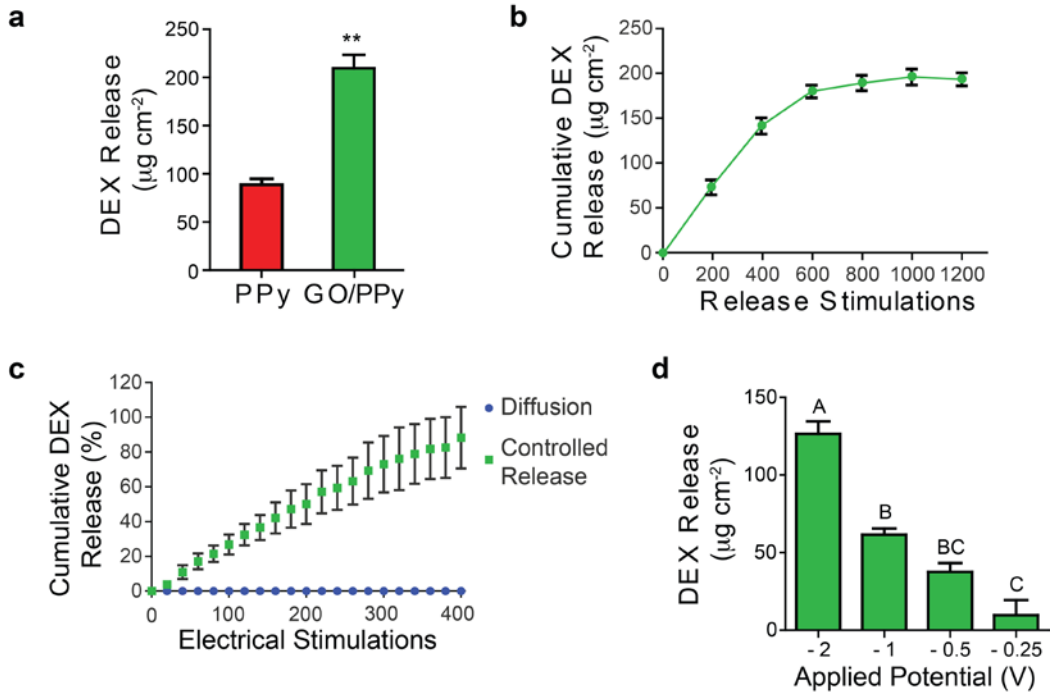

Figure 4.3. Electrically Controlled DEX Release from GO/PPy Nanocomposite Film. (a) Total DEX release from PPy films with or without GO as a co-dopant in response to an aggressive square wave, biphasic voltage stimulation (-2.0 V for 5 s, followed by 0 V for 5 s) repeated for 1000 stimulations. The GO/PPy-DEX nanocomposite release a significantly larger quantity of DEX ($p < 0.01$; $n = 3$). (b) Cumulative release profile of the GO/PPy-DEX nanocomposite in response to aggressive repeated square wave, biphasic voltage stimulation (-2.0 V for 5 s, followed by 0 V for 5 s) for 1200 stimulations ($n = 6$). The release profile reaches a plateau at 600 voltage pulses under this aggressive stimulation paradigm, indicating that all available drug has been released at this point. (c) Cumulative release profile of the GO/PPy-DEX nanocomposite in response to milder release stimulation (-0.5 V for 5 s, followed by 0.5 V for 5 s) and in the absence of electrical stimulation (passive diffusion) ($n = 3$). Electrical stimulation elicited linear release for up to 400 pulses, while no drug passively diffused from the film when no voltage stimulation was applied. (d) Effect of voltage stimulus modulation on amount of DEX released from nanocomposite films. GO/PPy-DEX nanocomposite films were submitted to 100 square wave, biphasic stimulation pulses where the negative phase was varied from -2 to -0.25 V, the positive phase was 0.5 V, and the stimulus lingered at each phase for 5 s. Bars labeled with nonmatching letters indicate a significant difference between groups ($p < 0.01$; $n = 3$).

To determine the maximum amount of drug released from the GO/PPy-DEX nanocomposite film, the cumulative release profile in response to the aggressive stimulation was evaluated. After 600 stimulations, the drug-release profile reaches a plateau, suggesting that no more drug can be released from the GO/PPy-DEX film (Figure 4.3b). Small quantities of DEX can be repeatedly released from the GO/PPy-DEX film in response to milder electrical stimulation (-0.5 V for 5 s, followed by 0.5 V for 5 s), creating a drug-release profile that is linear over 400 stimulations, while no observable amount of drug passively diffuses from the film in the absence of stimulation (Figure 4.3c). Modulation of the voltage stimulation magnitude altered the amount of drug released from the nanocomposite, demonstrating the flexibility and high level of dosage control provided by the release system (Figure 4.3d). There was no visible cracking or delamination of the GO/PPy-DEX film after 1000 release stimulations (-0.5 V for 5 s, followed by 0.5 V for 5 s), reflecting the good stability of the nanocomposite (Figure A1.3). The sustained linear release profile, responsiveness to changes in stimulation magnitude, and stability following repeated stimulation demonstrate the potential of the GO/PPy nanocomposite for applications requiring long-term and temporally precise drug dosing.

The bioactivity of the released drug was assessed by addition of solutions containing DEX released from GO/PPy films to primary astrocyte cultures and evaluation of the extent of interruption in cell proliferation. DEX is a synthetic glucocorticoid (GC) commonly used to treat inflammation and is used here as a model drug to demonstrate the efficacy of the released drug. Chronic DEX exposure has been shown to interrupt astrocyte proliferation, likely by down-regulating GC receptor expression [210]. Astrocyte cultures exposed to the release solution or a prepared DEX solution (1 μM) showed similar reductions in cell density after 4 d of culture, compared to control cultures that received no drug treatment (Figure 4.4, $p < 0.05$). The drug

release solutions were obtained using the aggressive stimulation paradigm (-2 V for 5 s, followed by 0 V for 5 s, 1000 cycles). These data indicate that the process of loading and stimulated release does not detectably alter the bioactivity of DEX molecules. However, it should be noted that within the release solution, there are drug molecules that were released during early cycles, as well as later cycles. Therefore, it is possible that if some of the drug released during the later cycles lost bioactivity as a result of repeated exposure to the voltage stimulation, the loss would be obscured by the presence of the more bioactive drug released by earlier cycles. Future work is needed to further elucidate the ability of DEX and other drug molecules to withstand chronic exposure to voltage stimulation while encapsulated in the nanocomposite film.

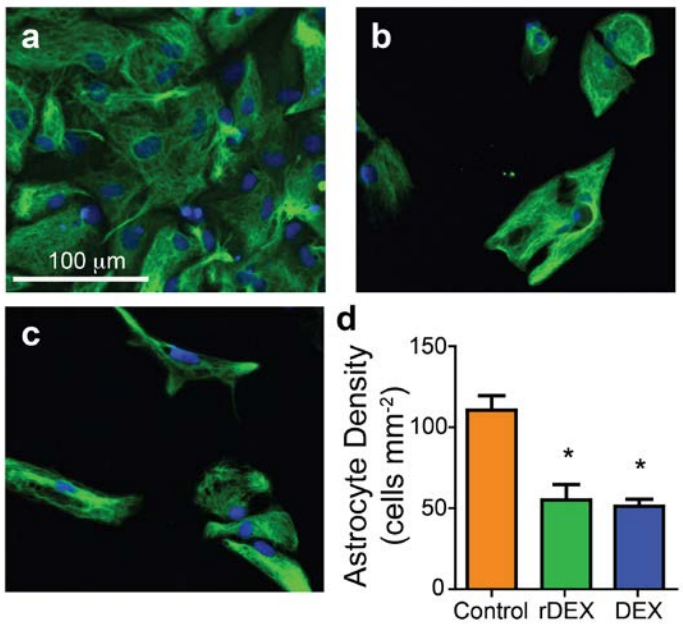

Figure 4.4. Bioactivity of DEX Released from GO/PPy Nanocomposite Film. Representative fluorescent images of astrocyte cultures exposed to (a) no drug (control), (b) DEX released from GO/PPy nanocomposite films (rDEX), and (c) prepared solutions of 1 μM DEX (DEX). GFAP (green); Hoechst 33342 (blue). (d) Density of astrocyte cultures 4 d after exposure to drug treatment. *Indicates significant difference from control ($p < 0.05$, $n = 4$).

The safety of graphene nanoparticles for use in bioapplications has been questioned as a result of a growing body of evidence indicating the potential toxicity of soluble nanomaterials [167, 169, 195]. To exclude the possibility of potential release of any toxic byproducts from the GO/PPy film, including soluble GO nanosheets, DEX release solutions were applied to primary neurons, a more sensitive cell population that does not proliferate and should be unresponsive to DEX treatment. In addition, GO/PPy films without drug loading underwent the same stimulation protocol as drug-loaded films, and the release solution was applied to neuron cultures. No effect on neuronal cell density was observed under either condition after 2 d of exposure (Figure 4.5), and the cells exhibited robust, interconnected neurite extensions indicative of healthy growth. This suggests that the interruption of astrocyte growth in response to the application of released DEX was due to specific actions of DEX, rather than non-specific cytotoxicity from components of the GO/PPy film, such as monomer or GO nanosheets, that may have delaminated from the electrode during electrical stimulation.

4.3.3 Tuning of Nanocomposite Properties

During chemical synthesis of GO, oxidized graphite sheets are commonly exfoliated with ultrasonication to obtain single- and few-layer GO (s/fGO) nanosheets. During sonication, the sheets also are reduced in the x-/y-dimension to create a smaller particle size that can measure as few as hundreds of nanometers, depending on the extent of sonication treatment [53, 211]. To investigate the effect of altering the GO nanosheet size on the properties of the nanocomposite, GO suspensions were submitted to 30 or 60 min of sonication immediately prior to incorporation into the nanocomposite film. Atomic force microscopy measurements verified that the sonication

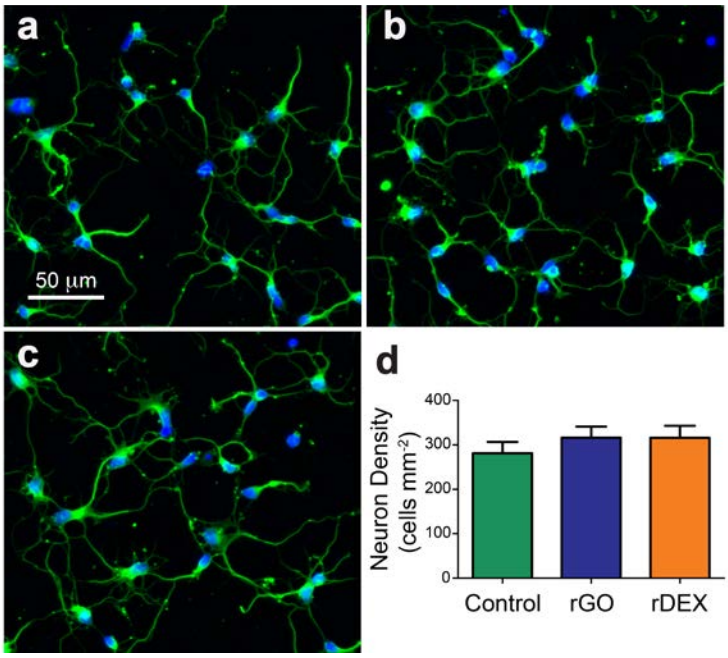

Figure 4.5. Effect of Released DEX on Neuronal Cultures. Representative fluorescent images of neurons treated with (a) no drug (control), (b) release solutions from GO/PPy films without DEX loaded (rGO), or (c) release solutions from GO/PPy-DEX films (rDEX). β-III-tubulin (green); Hoechst 33342 (blue). (d) Neuronal density after 2 d of exposure to drug treatment. The treated cultures showed no significant difference compared to control cultures (*n* = 4).

treatment successfully reduced the size and thickness of the GO nanosheets. After 60 min of sonication, the distribution of nanosheet thickness shifted to smaller values, compared to the distribution in the 30-min treatment group, indicating that the nanosheets were exfoliated into more s/fGO sheets (Figure 4.6a). As expected, the mean diameter of the GO nanosheets also decreased as the duration of sonication treatment increased (467.8 nm *vs*. 392.7 nm, $p < 0.05$), verifying that the mechanical vibrations created during sonication break the nanosheets into smaller pieces (Figure 4.6b). The size and thickness of the GO nanosheets can dictate their physiochemical properties, such as surface area, colloidal stability, and surface chemistry, all of which can affect the deposition and properties of the nanocomposite film [53, 212].

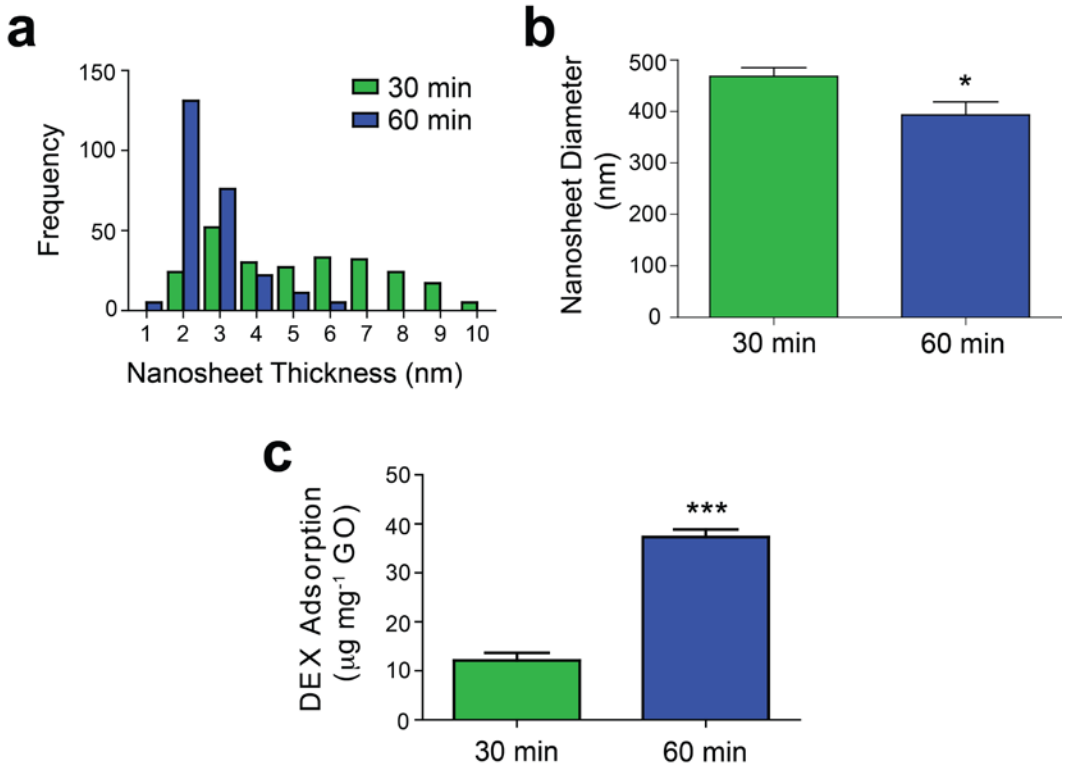

Figure 4.6. Effect of Ultrasonication on GO Nanosheet Properties. (a) Histogram of nanosheets thickness and (b) average diameter of nanosheets after 30-min and 60-min sonication (*p < 0.05; n = 6). (c) Amount of DEX adsorbed by free GO nanosheets (*p < 0.001; n = 3). Increasing duration of sonication treatment results in GO nanosheets that are thinner and smaller in diameter and that adsorb more DEX molecules.**

With longer sonication, the soluble GO nanosheets physically adsorb a larger amount of DEX molecules per unit mass (Figure 4.6c). The increase in loading capacity likely stems from the larger amount of GO surface area that is created within the suspension as multi-layer GO nanosheets are exfoliated into multiple s/fGO particles. The propensity of graphene and GO to adsorb drug molecules such as DEX arises from the abundance of 2p orbitals extending from the planar surface of the nanomaterial that will readily participate in π–π interactions with aromatic compounds [53, 198]. Therefore, it is expected that as surface area increases through exfoliation, more active locations are uncovered, and a larger quantity of drug molecules may be adsorbed.

The improved loading capacity of GO may enable the nanomaterial to act as a nanocarrier by shuttling adsorbed drug into the nanocomposite film and increasing the total drug load. The extent to which GO sonication treatment affects drug load into the nanocomposite was evaluated by elemental analysis using Energy Dispersive Spectroscopy (EDS). EDS of the DEX-loaded nanocomposite films provided a semi-quantitative summary of the amount of drug loaded into the film. Each DEX molecule contains one fluorine atom, and each subunit of PPy contains one nitrogen atom. Thus, the ratio of fluorine atoms to nitrogen atoms in the film corresponds to the amount of drug loading. As expected, nanocomposite films synthesized with GO sonicated for 60 min loaded more drug than those in the 30-min sonication group, as indicated by the F:N ratio (Figure 4.7a, $p < 0.01$). Interestingly, although increased GO sonication led to higher drug loading into the nanocomposite, the rate of DEX released from the film in response to voltage pulse stimulation was 38% higher for the nanocomposite synthesized with GO sonicated for 30 min, compared to the 60-min sonication group (Figure 4.7b, $p < 0.05$).

The schematic in Figure 4.7c depicts the proposed mechanism by which controlling GO sonication time can tune the amount of drug loaded into and released from the nanocomposite. The drug-loaded GO/PPy nanocomposite is electropolymerized from an aqueous solution containing GO sheets and DEX molecules, creating an opportunity for the drug to adsorb onto the surface of the nanosheets prior to film deposition. With longer sonication treatment, more GO sheets are present in the polymerization suspension as each multi-layer GO particle is exfoliated into several s/fGO sheets. Prior to electrodeposition, the GO sheets load some DEX molecules onto their surfaces through physical adsorption and then compete with the remaining free DEX molecules as dopants during the polymerization reaction. When GO undergoes sonication, the nanoparticle size decreases in the z-direction as each multi-layered GO exfoliates

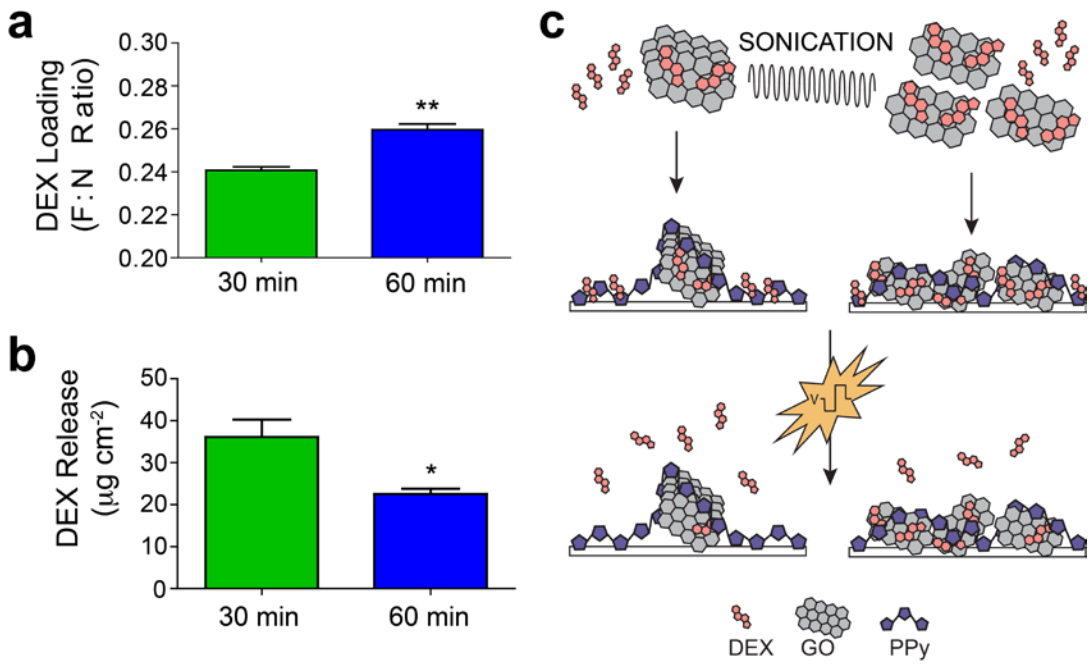

Figure 4.7. Effect of GO Sheet Sonication on GO/PPy Nanocomposite Properties. (a) Elemental analysis of GO/PPy-DEX nanocomposite film. The F:N ratio reflects the amount of drug loaded into the film. Longer sonication treatment yields a higher quantity of drug loading ($p < 0.01$; $n = 3$). (b) Amount of DEX released from nanocomposite films in response to 100 voltage pulses (-0.5 V for 5 s, followed by 0.5 V for 5 s). Less sonication results in a higher release rate (*$p < 0.05$; $n = 4$). (c) Schematic representation of the effect of GO sheet sonication on nanocomposite properties.**

into multiple s/fGO particles (Figure 4.6a) and in the x-/y-direction as each GO sheet breaks into several smaller sheets (Figure 4.6b), creating a larger number of smaller particles that would act as more-efficient dopant molecules [209]. In addition, as each multi-layered GO sheet exfoliates into multiple s/fGO particles, a larger number of reactive nanosheet edges containing negatively charged carboxylic acid groups will be present, leading to more GO nanosheets depositing into the nanocomposite film. Because each GO sheet can carry multiple drug molecules into the film, a larger total amount of DEX can be loaded as a result of increased sonication treatment.

We propose that the strong adsorption of DEX molecules onto the GO sheets is the mechanism behind the slowed drug-release rate. Because more GO nanosheets are likely to be incorporated into the nanocomposite as the amount of sonication time increases, there is likely to be less DEX directly doped into the film. Potentially, the DEX molecules adsorbed onto the surface of the GO nanosheet cannot be released from the film as easily as directly doped DEX molecules, because of the strength of the π-π interactions, limiting the amount of drug release in response to the same electrical stimulation. Potentially, as the directly doped DEX molecules exit the film upon electrical stimulation, the GO-adsorbed DEX molecules may desorb from the sheets, diffuse through the PPy matrix and replenish the doping sites. By this mechanism, the release profile of the nanocomposite would be extended. With future work to explore the GO-drug adsorption/desorption phenomenon, the unique properties of the GO/PPy nanocomposite could be utilized to create a highly tunable release system with the ability to address various dosing needs for a multitude of drug delivery applications.

Along with providing control over drug loading and release, the GO nanosheets create a unique opportunity to alter the morphological characteristics of the nanocomposite film. Sonication had a significant effect on the morphology of the GO/PPy-DEX film (Figure 4.8). With less GO sonication, the film exhibited globular, cauliflower-like features on the scale of tens of microns that are characteristic of PPy films (Figure A1.2) [34]. As the amount of GO sonication increased from 30 min to 60 min, the large globular features flattened to create a more uniform surface (Figure 4.8c). The large features are possibly a result of nucleation sites created by the multi-layer GO nanoparticles. As the nanoparticles deposit into the film, they provide a scaffold around which the growing polymer can accumulate. After a longer sonication time, the smaller s/fGO particles distribute more evenly in the film, creating a smoother surface (Figure

4.7c). At a smaller scale, small sheet-like features became more apparent at the surface of the film, suggesting that more GO sheets are incorporated into the nanocomposite (Figure 4.8d). At the 60-min sonication time point, the sheet-like features reduced in size to sub-micron dimensions, as would be expected, because increased sonication treatment fractures GO sheets into smaller particles. The ability to subtly alter the nanocomposite surface morphology at different length scales can have important implications for applications in which the film interacts with tissue or cells. Multiple cell types have demonstrated sensitivity toward mechanical and topographical cues in their environment, suggesting that the nanocomposite film morphology may be engineered to act synergistically with electrically controlled drug release to provide additional signals to the targeted cell population [213-215].

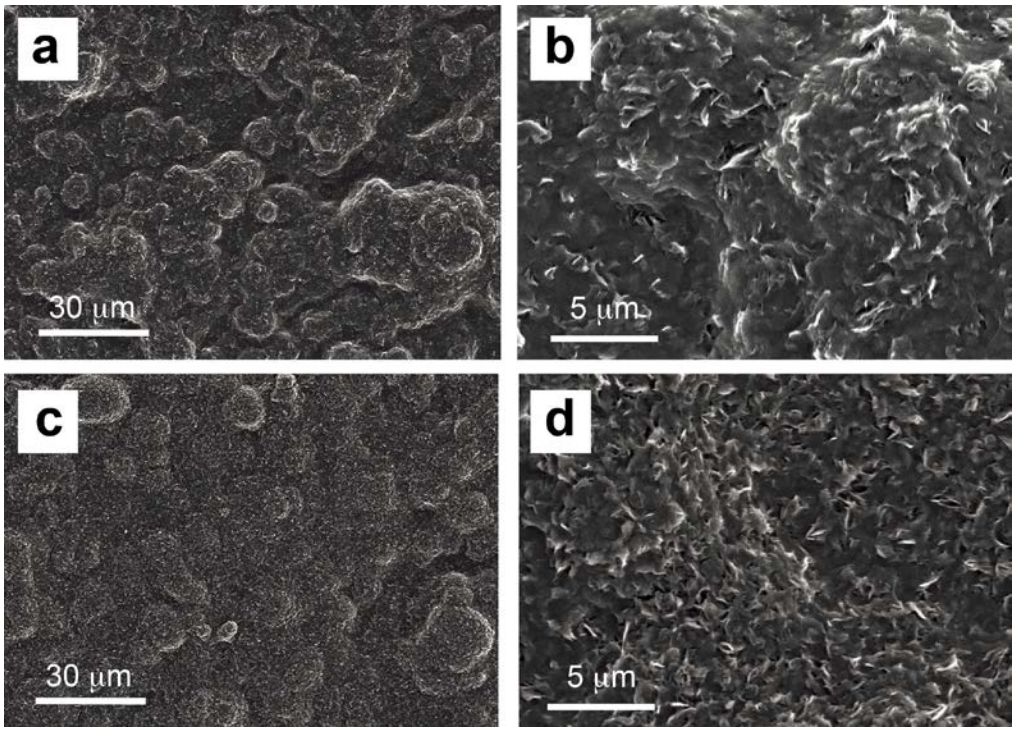

Figure 4.8. Effect of GO Sonication on GO/PPy Film Morphology. SEM images of GO/PPy-DEX films prepared with GO sonicated for (a, b) 30 min and (c, d) 60 min. Longer sonication time results in a smoother surface morphology and the emergence of more sheet-like features at the surface of the film.

4.4 CONCLUSIONS

The unique properties of GO sheets enable several degrees of customizability to the electrically controlled drug release platform. By altering the size and thickness of the nanosheets, significant changes can be made to nanocomposite film morphology, drug load, and drug release properties. As a nanocarrier, GO may enable loading of a variety of biomolecules, not limited to anionic species, into the film. Furthermore, the GO/PPy nanocomposite film exhibits a linear release profile that persists over several hundred stimulations, indicating that the release platform could be used for long-term drug release applications that require repeated dosing over time. On-demand controlled drug delivery provides more-effective therapies with less toxicity by tuning delivery directly to spatial and temporal requirements for a given application. In addition, controlled delivery may be beneficial in various *in vitro* assays, such as high-throughput drug screening or exploratory cell biology experimentation. As a result of its adjustable properties, stability, and fine control over dosing, the novel GO nanocomposite release platform described here has the potential to advance these drug delivery technologies by enabling tailored drug release profiles.

5.0 ORIGIN OF IMPROVED ELECTROCHEMICAL DOPAMINE DETECTION BY GRAPHENE OXIDE/CONDUCTING POLYMER NANOCOMPOSITE-MODIFIED ELECTRODES

5.1 INTRODUCTION

Efforts toward the development of detection methods that allow sensitive real-time monitoring of neurotransmitter signaling within the central nervous system (CNS), or point of care sampling from blood, urine or cerebrospinal fluid (CSF), have received increasing attention in recent years. The signaling of one such neurotransmitter, dopamine (DA), within the CNS orchestrates many behaviors such as learning, motivation, and motor control [216], and its dysfunction has been implicated in multiple diseases such as Parkinson's [217], schizophrenia [218], and addiction [219]. Additionally, DA has been investigated as a peripheral biomarker for the diagnosis of Parkinson's disease [220] and adrenal tumors [221]. The potential of utilizing DA signaling for both diagnostic and basic science applications motivates the development of low-cost tools for monitoring catecholamine levels in biological fluids and high-resolution *in vivo* sensors for use in the CNS [222, 223].

Traditional methods of DA detection of biological fluids include chromatography analysis, colorimetric detection, and spectroscopic analysis, among others [224-226]. These methods require complicated, expensive equipment or reagents, and have slow sample

processing times that impede their use by clinicians and makes exploratory research slow and costly. Electrochemical methods of detection have been developed that take advantage of the redox activity of DA molecules and enable simple, rapid analysis of biological samples using low-cost electrodes as sensors [222]. However, current electrochemical sensors suffer from limited sensitivity and specificity towards DA. Physiological levels of DA range from nanomolar to low micromolar, creating a need for highly sensitive tools with very low detection limits. In biological samples that contain DA, there also exist a variety of interfering molecules, such as ascorbic acid (AA) and uric acid (UA), that exhibit similar redox behavior and can obscure DA signals.

To address the shortcomings in sensor sensitivity and specificity, researchers have developed a variety of electrode modifications to improve these properties. Graphene-based materials have received much focus as biosensor materials because of their unique electrical and chemical properties [227, 228]. Reduced graphene oxide (RGO), synthesized by the chemical or electrochemical reduction of graphene oxide (GO), exhibits rapid electron transfer kinetics that enables highly sensitive detection of DA [94, 229], and composites of RGO with a variety of other materials have demonstrated the ability to selectively detect DA in the presence of interfering species [206, 230, 231]. However, little work has been done to characterize the potential of its precursor, GO, as a DA sensor. By itself, GO exhibits poor conductivity compared to its reduced form, requiring its incorporation into a conductive matrix in order to act as an effective electrode coating. Conductive polymers, such as poly(3,4-ethylenedioxythiophene) (PEDOT) and poly(pyrrole) have been utilized to create stable, conductive nanocomposites with GO, and have demonstrated potential for electrical recording and biointerfacing applications [80, 81, 90, 161-163]. In this work, we describe a GO/PEDOT

nanocomposite material and demonstrate for the first time that GO, in its unreduced form within a conductive polymer matrix, creates a sensitive and selective sensor for DA detection. The GO/PEDOT nanocomposite selectively amplifies the DA oxidation signal, but not AA or UA signals, as a result of electrostatic interactions between DA molecules and the nanocomposite surface. In addition, the nanocomposite reduces interference from AA as a result of a significant shift in its oxidation potential due to an electrocatalytic effect of the nanocomposite material on the AA oxidation reaction. The performance of the GO/PEDOT nanocomposite for selective and sensitive DA oxidation along with its electrochemical stability underlines the potential of the nanocomposite material as a novel electrode modification for the development of improved DA sensors.

5.2 MATERIALS AND METHODS

5.2.1 Materials

L-ascorbic acid (AA), 3,4-dihydroxyphenylacetic acid (DOPAC), 3,4-ethylenedioxythiphene (EDOT), 3-hydroxytyramine hydrochloride (DA), potassium chloride (KCl), sodium chloride (NaCl) and uric acid (UA) were purchased from Sigma-Aldrich. Monosodium phosphate and disodium phosphate were purchased from Fisher Scientific. Graphite powder (SP-1) was purchased from Bay Carbon, Incorporated. Phosphate buffed saline (PBS, 10x) was purchased from EMD Millipore and diluted to a 1X working concentration for all experiments (137 mM NaCl, 2.7 mM KCl, 10 mM phosphate buffer). Purified water filtered through a Milli-Q System (EMD Millipore) was used throughout all experiments.

5.2.2 Graphene Oxide Synthesis

Graphene oxide was synthesized as previously described using the modified Hummer's method, and stored in H_2O until use [54, 81]. Prior to deposition into the nanocomposite, GO nanosheets were sonicated with a probe sonicator in H_2O for 15 min, 30 min, 60 min, or 90 min to alter the thickness and x-y size of the nanoparticles.

5.2.3 Electrochemical Apparatus

A Gamry potentiostat, FAS2 femtostat (Gamry Instruments) was used for electrode pretreatment, GO/PEDOT nanocomposite film polymerization and impedance measurements. An Autolab potentiostat/galvanostat PGSTAT128N was used for all analyte detection assays. All electrochemical experiments were carried out using a three-electrode setup consisting of a glassy carbon working electrode (GC, 3 mm diameter, CH Instruments), a silver/silver chloride reference electrode (CH Instruments) and a platinum foil counter electrode.

5.2.4 Electropolymerization of GO/PEDOT Films

Glassy carbon electrodes (GCEs, 3 mm diameter, CH Instruments) were polished with 1.0 and 0.05 μm alumina slurries and cleaned by ultrasonication in 100% ethanol followed by H_2O. The GCEs were electrochemically pretreated by applying a cleaning voltage pulse (-2 V, 250 s), followed by a cyclic voltammetry sweep (0.3 V to 1.3 V, 100 mV s^{-1}, 5 cycles). Following pretreatment, GO/PEDOT nanocomposite films were electrochemically deposited onto GCEs from a polymerization solution composed of EDOT (0.2 M) and GO (5 mg ml^{-1}). GO/PEDOT

nanocomposite films were synthesized using GO nanosheets that had been sonicated for 15 min (GO15), 30 min (GO30), 60 min (GO60) or 90 min (GO90). An oxidizing current of 20 μA was applied through the GCE for 200 s to carry out the polymerization reaction. The GO/PEDOT modified GCEs were gently rinsed in H_2O to remove any adsorbed monomer or GO, and stored in H_2O until use.

5.2.5 Nanocomposite Characterization

GO/PEDOT nanocomposite surface morphology was imaged using a scanning electron microscope (SEM, JEOL JSM6510), with an operating potential of 3 kV. The atomic ratio of oxygen to sulfur was calculated as a semi-quantitative estimate of the amount of GO contained in the nanocomposite film. Elemental analysis was carried out using energy dispersive spectroscopy (EDS, Oxford INCA EDS) with an operating potential of 20 kV. For each sample (n = 4 per sonication group), the atomic percent of oxygen and sulfur were measured from three separate areas, and averaged to obtain the mean value for the sample.

The chemical bonds in the nanocomposite films were evaluated with attenuated total reflectance Fourier-transform infrared spectroscopy (ATR-FTIR) using a Bruker Vertex 70 spectrometer with a Hyperion 2000 microscope and 20x ATR objective. For each sample (n = 4 per sonication group), three separate areas were analyzed, and all spectra were averaged to obtain one spectrum per group. The areas underneath the alkoxy C-O peak (1064 cm^{-1}) and the C-S peak (845 cm^{-1}) on the averaged spectra were calculated using custom MATLAB software to evaluate changes in relative alkoxy content with increasing GO sonication treatment.

Electrochemical impedance measurements were collected in PBS using an alternating current sinusoid of 10 mV. Electrochemical stability of the nanocomposite was characterized by

collecting impedance measurements in the frequency range between 1 Hz and 100 kHz after 0, 2, and 1000 cyclic voltammetry (CV) sweeps from -0.5 V to 0.6 V at 100 mV s^{-1}. The electrochemical properties of the nanocomposite synthesized with GO treated for various sonication times were evaluated by collecting impedance measurements in the frequency range between 10 mHz and 100 kHz (n = 7 per sonication group).

5.2.6 Electrochemical Detection of DA, AA, UA, and DOPAC

All electrochemical detection assays were carried out in PBS using CV with a voltage sweep from -0.5 V to 0.6 V at a speed of 100 mV s^{-1}. Electrodes were immersed in the electrochemical cell, and known concentrations of DA, AA, UA or DOPAC were added to the PBS with a 30 s equilibration time prior to CV measurement. The oxidation peak location (E_p) was defined as the point at which the oxidation current reached its maximum. The oxidation peak current (I_p) was determined after a PBS background subtraction as the maximum current value of the oxidation peak. For assays carried out at a basic pH (9.5), PBS was prepared at the appropriate pH by altering the ratio of monosodium phosphate to disodium phosphate (3.2 mM monosodium phosphate, 2.67 M disodium phosphate), while maintaining the same phosphate buffer strength (10 mM) and ionic content (137 mM NaCl, 2.7 mM KCl) as the purchased pH 7.4 PBS.

5.2.7 Statistical Analysis

All statistical analyses were carried out in GraphPad Prism software. All data are presented as the mean ± standard error of the mean. Comparisons across two experimental groups were made with Student's t-test, and comparisons across greater than two experimental groups were made

with one-way analysis of variance followed by Tukey's post hoc analysis. Dopamine calibration curves were analyzed using linear regression.

5.3 RESULTS AND DISCUSSION

5.3.1 GO/PEDOT Stability and Electroactivity

GO/PEDOT nanocomposite films were electrodeposited onto bare GCE electrodes from an aqueous solution of monomer and GO nanosheets. During conducting polymer electrodeposition, oxidation of the monomer via electrical stimulation elicits free radical polymerization during which the polymer deposits onto the anode surface, incorporating negatively charged molecules from the polymerization solution as dopants. The GO nanosheets contain negatively charged carboxylic acid groups on their edges, enabling their incorporation into the PEDOT film [116, 162, 163, 205]. The resulting film exhibits a morphology consisting of sub-micron, fuzzy, sheetlike features that are likely GO nanosheets engulfed in the PEDOT matrix (Figure 5.1a). The nanocomposite also contains sharp wrinkles that are characteristic of pure GO films and can be observed in conducting polymer films doped with GO [117, 163]. The wrinkles may be formed by larger GO nanosheets protruding from the surface of the PEDOT matrix. The resulting nanocomposite film is a conductive, electrochemically stable electrode material. A comparison of the CV of the bare GCE electrodes and the GO/PEDOT nanocomposite-modified electrodes demonstrated that the modified electrodes exhibit a much higher charge storage capacity, as indicated by the total area inside of the curve (Figure 5.1b). This property results from an increase in surface area as the nanocomposite film deposits on the surface of the

electrode. Additionally, the electrochemical impedance of the electrode drops after modification with the nanocomposite, most notably in the lower frequency region (Figure 5.1c). In this low frequency range, impedances are influenced by the effective surface area of the electrode, with impedance value inversely correlating with surface area [232, 233]. A large effective surface area has implications for electrochemical sensing applications in which increased surface area may lead to an increased number of active sites for the targeted analyte and result in improved sensor properties.

Electrochemical detection of DA is often carried out *in vivo* by utilizing repeated CV scanning, during which the size of the DA oxidation peak is monitored over time to evaluate transient signaling in the central nervous system [222]. To evaluate its stability in response to repeated electrical stimulation, the nanocomposite-coated electrode underwent multiple CV scans and the electrochemical impedance was monitored (Figure 5.1c). After two CV cycles, the low frequency impedance values slightly increased, suggesting that there was a minimal loss of surface area from the film, likely due to loosely adsorbed oligomers or GO nanosheets delaminating from the nanocomposite surface. After 1000 CV cycles, there was no additional increase in the low frequency region, demonstrating the stability of the nanocomposite. Interestingly, there was a slight drop in impedance at the higher frequency region following multiple CV stimulations. At higher frequencies, impedance is dominated by the electrode material, rather than effective surface area, suggesting that the nanocomposite film has become more conductive, possibly as a result of small ions from the electrolyte solution moving into the polymer matrix during the stimulation [232, 233].

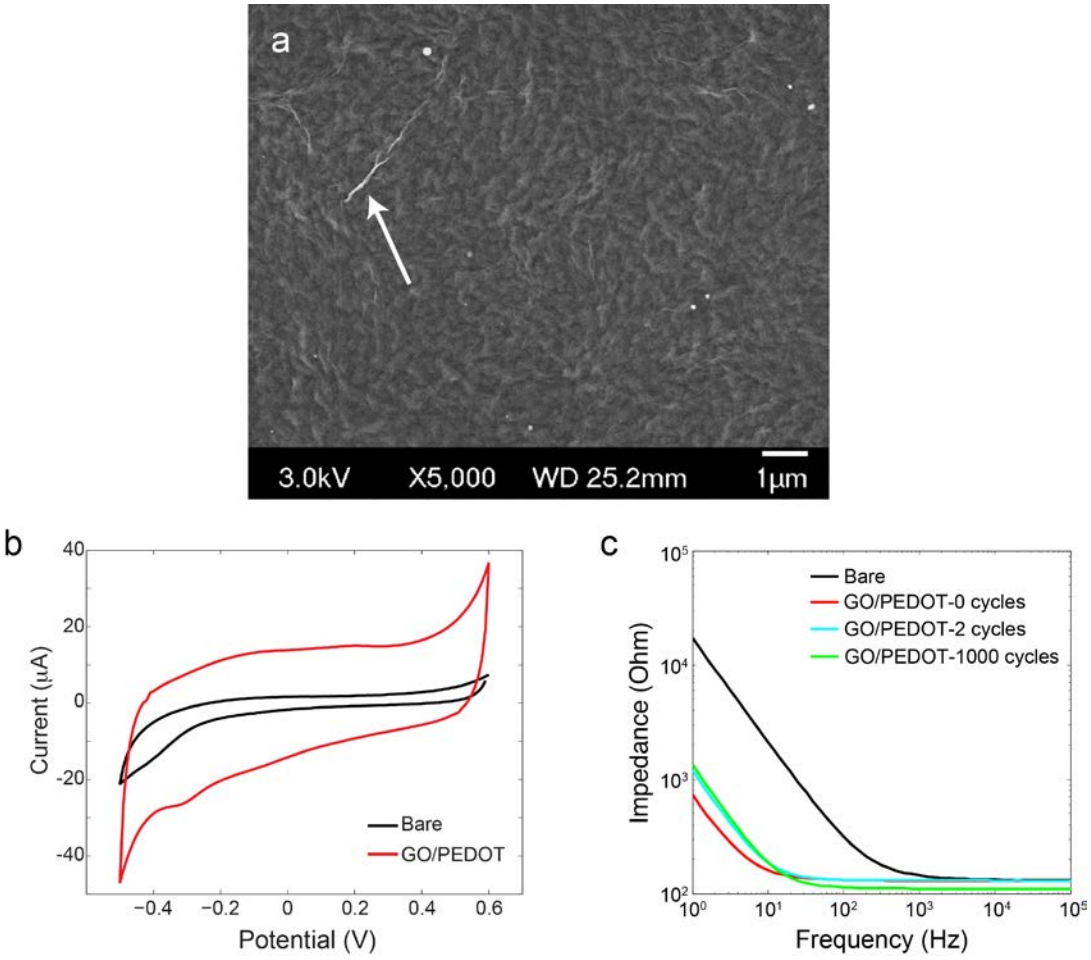

Figure 5.1. Characterization of the GO/PEDOT Nanocomposite Material. (a) Scanning electron micrograph of the GO/PEDOT nanocomposite illustrating its sheetlike morphology. The arrow points out a wrinkle feature that is likely due to the protrusion of a GO sheet from the polymer surface. (b) CV of a bare GC electrode and the GO/PEDOT-modified electrode in PBS (scan rate: 100 mV s^{-1}) demonstrating the increase in charge storage capacity after modification. (c) EIS of the bare GC electrode and the GO/PEDOT-modified electrodes after repeated CV cycling in PBS (-0.5 V to 0.6 V; 100 mV s^{-1}). The nanocomposite retains its stability after 1000 CV cycles.

5.3.2 Improved Sensitivity and Selectivity Toward DA Oxidation at the GO/PEDOT Nanocomposite

The electrochemical oxidation of DA, AA, and UA at the surface of the GO/PEDOT nanocomposite-modified electrodes was evaluated with CV and compared to the behavior of a bare GCE. Electrodes were assayed in solutions containing DA (100 μM), AA (1 mM) or UA (100 μM) separately, or in solutions containing all three analytes combined (Figure 5.2a, b). In the presence of all three analytes, the CV of the bare GCE exhibits only two distinguishable oxidation peaks, a result of the broad AA oxidation peak merging with the smaller DA oxidation peak. At the GO/PEDOT nanocomposite, DA exhibited a clear and separate oxidation peak (E_p = 147 mV) with no overlap from the interfering analyte oxidation peaks located at -28.6 mV for AA and and 287 mV for UA (Figure 5.2b). DA, AA, and UA coexist in the CNS and biological fluids such as cerebrospinal fluid and blood [222], making accurate quantification of the species difficult because of their close oxidation potentials. The GO/PEDOT-modified electrode enables more selective discrimination of DA than the bare GCE by increasing the separation between the oxidation peaks of DA and AA (Figure 5.2c). The increased separation arises from the significant leftward shift (E_p: 65.0 mV for bare GCE *vs*. -28.6 mV for GO/PEDOT, $p < 0.001$) and decreased width of the AA oxidation peak at the GO/PEDOT nanocomposite surface, that are likely a consequence of faster electron transfer to the film or improved electrocatalytic activity of the film towards AA oxidation [234, 235]. Neither the DA nor UA molecules exhibit a change in their oxidation peak location, and there is no effect on the separation between the two species at the GO/PEDOT nanocomposite surface compared to the bare GCE surface (Figure 5.2d). The absence of effect on the peak location indicates that the DA and UA oxidation

reactions are not electrocatalyzed by the GO/PEDOT film surface as is the AA oxidation reaction.

DA calibration curves of GO/PEDOT nanocomposite-modified electrodes and bare electrodes were compared to evaluate the sensitivity of the modified electrodes (Figure 5.2e). Within the range of 1 μM to 40 μM, the GO/PEDOT nanocomposite-modified electrode demonstrated a significant increase in sensitivity toward DA, indicated by the slope of the calibration curve (bare: 0.046 ± 0.005 μA μM^{-1}; GO/PEDOT: 0.151 ± 0.005 μA μM^{-1}; $p < 0.001$), with an improved accuracy, indicated by the linearity of the curve (bare: $R^2 = 0.961$; GO/PEDOT: $R^2 = 0.995$). The limit of detection, calculated assuming a signal-to-noise ratio of 3, was 83.0 nM for the GO/PEDOT electrode. This enhanced DA sensing performance may arise from a locally increased concentration of DA at the surface of the nanocomposite film as a result of interactions between the film surface and the DA molecules. Notably, there is no improvement in sensitivity toward AA or UA at the GO/PEDOT nanocomposite, suggesting the mechanism of DA interaction is not shared by these molecules (Figure 5.3).

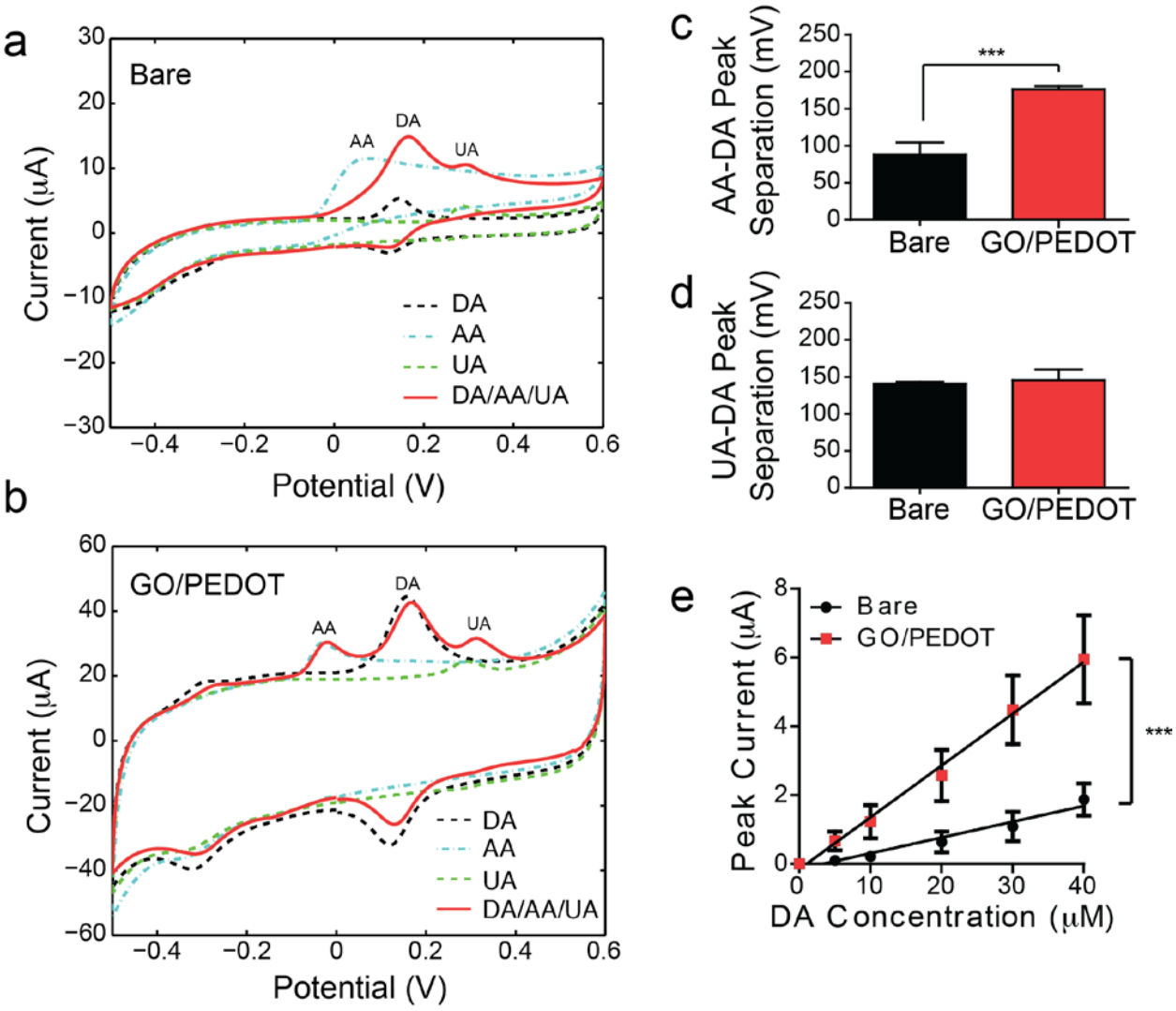

Figure 5.2. Electrochemical Oxidation of DA in the Presence of Interfering Species. CVs of the (a) bare GC electrode and (b) GO/PEDOT-modified electrode in solutions containing 100 μM DA, 1 mM AA, or 100 μM UA alone, or in combination. Three separate oxidation peaks are discernable on the CV of the GO/PEDOT-modified electrode, but not the CV of the bare GC electrode, in solutions containing all three analytes. Total separation between the (c) AA and DA oxidation peaks, and the (d) UA and DA oxidation peaks. There is a significant increase in separation between the AA and DA oxidation peaks at the GO/PEDOT nanocomposite surface (* $p < 0.001$; $n = 7$). (e) Linear DA detection curves for the bare GC and GO/PEDOT-modified electrodes, illustrating the increased sensitivity of the modified electrodes to DA (*** $p < 0.001$; $n = 7$).**

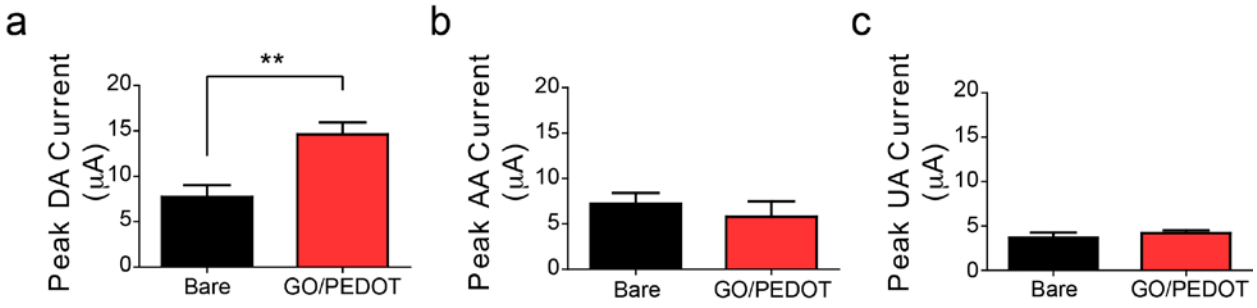

Figure 5.3. Selective Sensitivity of the GO/PEDOT Nanocomposite Towards DA. Peak oxidation current response of the bare and GO/PEDOT-modified electrodes in (a) 100 μM DA, (b) 1 mM AA, and (c) 100 μM UA measured to CV (100 mV s^{-1}). The GO/PEDOT nanocomposite selectively increases the DA oxidation current compared to the bare GC electrode, but not the AA or UA oxidation current ($p < 0.01$; $n = 7$).

At physiological pH, DA exists as a cation, while both AA and UA are anionic molecules. The difference in charge may play a role in the improved sensitivity *via* concentration of DA molecules at the nanocomposite surface through electrostatic interactions. While the bare GC electrodes contain some oxygen functional groups formed by polishing and electrochemical pretreatment that may impart a negative charge to the surface [236, 237], the GO/PEDOT nanocomposite contains a large amount of hydroxyl, carboxyl, and epoxide groups [162], with negatively-charged carboxyl groups located at the surface of the film [80]. Elemental analysis of the GO/PEDOT film with EDS gave an elemental ratio of oxygen to carbon of 0.309 (± 0.034, n = 4), which is higher than reported literature values of 0.22 for electrochemically-pretreated GC electrodes [236], indicating that there may be more negative charges at the nanocomposite surface provided by the additional oxygen functional groups. Along with electrostatic interactions between the anionic GO/PEDOT nanocomposite and the cationic DA molecules, π-π interactions may also play a role in the improved sensitivity toward DA. The DA molecule, but

neither the AA nor UA molecule, contains a phenol ring that may readily participate in noncovalent π-π stacking with the benzene rings present in GO [238, 239].

5.3.3 Mechanisms Behind Improved DA Sensitivity of the GO/PEDOT Nanocomposite

The GO nanosheets within the nanocomposite provide a unique way to subtly alter its physical properties. By changing the size and shape of the GO nanosheets prior to deposition in the nanocomposite, the physical and chemical properties can be controllably altered without grossly changing the composition of the nanocomposite. Utilizing this unique property, the mechanism by which GO nanosheets contribute to the improved sensitivity to DA can be explored. True GO nanoparticles exist as two-dimensional, single-layer nanosheets (ca. 1 nm thickness), ranging in size in the x-y-direction from hundreds of nanometers to microns, depending on the extent of oxidation. However, during synthesis from graphite *via* the modified Hummer's method, many layered GO platelets are formed as an intermediate to single-layer GO [53]. The GO platelets will persist until exfoliated by mechanical perturbation using sonication into single-layer GO, double-layer GO, and few-layer GO (3-10 nanosheet layers). With increasing sonication treatments, the distribution of sheet thicknesses shifts toward smaller values and the diameter of the sheets decreases [81, 211]. The size and thickness of the GO nanosheets can significantly alter the physical and chemical properties of the prepared GO/PEDOT nanocomposite without significantly changing its material composition, creating a unique method of probing the properties driving the electrochemical detection performance.

5.3.3.1 Effect of GO Sonication on the Nanocomposite DA Sensitivity and Chemical Properties

To investigate the effect of GO sonication on the properties of the GO/PEDOT nanocomposite, GO suspensions were sonicated for 15 min, 30 min, 60 min and 90 min prior to deposition into the nanocomposite. Electrodes modified with the sonication-treated GO/PEDOT nanocomposite were assayed for their sensitivity toward 100 μM DA using CV analysis in PBS. The magnitude of the peak DA oxidation current increased with increasing GO sonication treatment, with the 30 min, 60 min and 90 min treatment group exhibiting a significantly larger peak current than a bare, unmodified electrode (Figure 5.4a). The chemical composition of the nanocomposite films was evaluated using energy dispersive spectroscopy to investigate the source of the improved sensitivity toward DA. The oxygen to sulfur (O/S) ratio provides a semi-quantitative measure of the amount of GO incorporated into the nanocomposite film. Each PEDOT unit contains a fixed O/S ratio (2:1), and the sulfur is present only in the polymer, not the GO nanosheets. As such, any increase in the O/S ratio indicates that there are 1) more GO sheets incorporated into the film, or 2) GO sheets with higher oxygen content selectively incorporated into the film. With increasing sonication treatment, the O/S ratio of the nanocomposite film increases significantly (Figure 5.4b). It is most likely that the increased oxygen content arises from a larger number of GO nanosheets incorporating into the film. With sonication, the GO nanosheets decrease in size, and smaller molecules act as more efficient dopants in the electropolymerization reaction that creates the nanocomposite film [209].

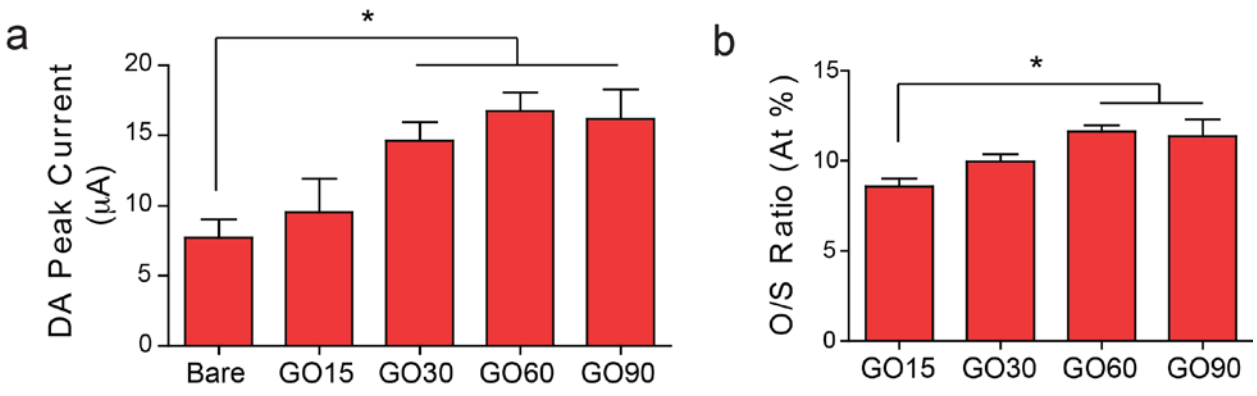

Figure 5.4. GO Sonication Improves Sensitivity of GO/PEDOT Towards DA. (a) Peak DA oxidation current at the bare GC electrodes and the GO/PEDOT nanocomposite synthesized with GO sonicated for 15 min (GO15), 30 min (GO30), 60 min (GO60), or 90 min (GO90) prior to electrodeposition into the composite (* $p < 0.05$; $n = 7$). (b) Atomic ratio of O to S in the nanocomposite synthesized from GO with varying sonication treatment prior to electrodeposition (* $p < 0.05$; $n = 5$). O/S ratio indicates the density of oxygen containing functional groups, donated by GO, in the nanocomposite film.

The increased O/S ratio positively correlates to the magnitude of the DA oxidation current ($R^2 = 0.963$, $p < 0.05$), suggesting that the increased amount of GO nanosheets within the film may produce the improved sensitivity toward DA. GO nanosheets contain negatively charged carboxylic acid groups at its edges that may electrostatically interact with DA, and benzene rings within its plane that may interact with the phenol ring of DA *via* π-π interaction. To evaluate which type of interaction causes the improved sensitivity of the GO/PEDOT nanocomposite, CV analysis of 100 μM DA was carried out in PBS at pH 9.5. At this more basic pH, the amine group on the DA molecule is deprotonated (pKa: 8.9), rendering the molecule either neutral, or slightly negative, as the hydroxyl groups become deprotonated [240]. Additionally, at this higher pH, the GO/PEDOT nanocomposite film should become more negative as the pH moves further from the pKa of the carboxylic acid groups of the GO nanosheets [241]. At these conditions, there should be much less electrostatic interaction and possibly some electrorepulsion. As

expected, the peak DA oxidation current at pH 9.5 (Figure 5.5a) is less than the current at physiological pH (Figure 5.4a) with a significant difference appearing for the nanocomposite film synthesized with GO receiving the 90-minute sonication treatment (pH 7.4: 16.18 μA; pH 9.5: 7.00 μA; $p < 0.01$). Additionally, the sonication effect present in physiological pH 7.4 conditions, in which the peak current increases with increased sonication time, is not exhibited at pH 9.5, and no differences arise between the electrode groups at the higher pH ($p = .1445$). These data support the hypothesis that the improved DA sensitivity demonstrated by the GO/PEDOT nanocomposite-modified electrodes at physiological pH is driven by electrostatic interactions between the positively charged amine group present on the DA molecules and the negatively charged carboxylic acid groups provided by the GO nanosheets in the GO/PEDOT nanocomposite. While π-interactions may exist between the benzene rings in the GO nanosheets and the phenol ring structure of the DA molecules, these interactions are clearly not the driving force behind the improved nanocomposite sensitivity that appears at higher GO sonication times because this effect completely disappears at the higher pH where the π-interactions would still persist.

To further confirm that electrostatic interactions play a role in the improved DA sensitivity of the GO/PEDOT nanocomposite, the electrochemical oxidation of DOPAC at the surface of the nanocomposite-modified electrodes was investigated with CV in PBS at physiological pH 7.4. DOPAC is a metabolite of DA and shares a similar structure to its precursor, with the exception that the amine group of DA is replaced with a carboxylic acid group to form the DOPAC molecule. At physiological pH, the DOPAC molecules exist as anions but retain the phenol ring structure. As such, electrochemical oxidation behavior of DOPAC at the surface of the GO/PEDOT nanocomposite provides valuable information regarding the

influence of electrostatic interactions *vs*. π-interactions on the sensitivity of the nanocomposite. At the surface of nanocomposite films synthesized with GO sonicated for 30 minutes or greater, the DOPAC peak oxidation current was significantly lower than the DA peak oxidation current ($p < 0.01$), demonstrating that the nanocomposite exhibits less sensitivity toward the DOPAC molecules. There is no influence of sonication treatment on the nanocomposite sensitivity toward DOPAC (Figure 5.5b), as was exhibited toward DA, suggesting that the source of interaction between DA and the nanocomposite does not exist between DOPAC and the nanocomposite. The structure of DA and DOPAC are identical with the exception of their charged functional groups, confirming that electrostatic interactions between the DA amine and the GO carboxylic acid are likely the driving force behind the nanocomposite sensitivity.

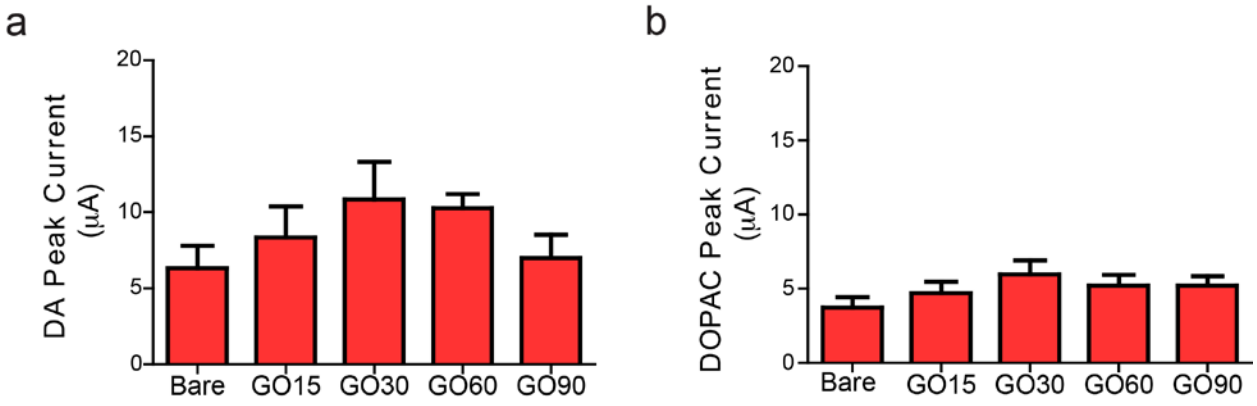

Figure 5.5. GO Sonication Does Not Effect Sensitivity of GO/PEDOT Nanocomposite Toward Neutral or Negatively Charged Analytes. (a) Peak DA oxidation current in PBS at pH 9.5 recorded at bare GC electrodes and electrodes modified with the GO/PEDOT nanocomposite synthesized with GO sonicated for 15 min (GO15), 30 min (GO30), 60 min (GO60) or 90 min (GO90) prior to electrodeposition into the nanocomposite (*n* = 7). (b) Peak DOPAC oxidation current in PBS at pH 7 recorded at bare GC electrodes and electrodes modified with the nanocomposite synthesized from GO sonicated for varying amounts of time prior to deposition (*n* = 7).

5.3.3.2 Effect of GO Sonication on the Nanocomposite Electrochemical Properties

The electrochemical properties of the GO/PEDOT nanocomposite film synthesized with sonicated GO nanosheets were evaluated with electrochemical impedance spectroscopy to further probe the mechanism behind the improved electrochemical DA detection properties. The Nyquist plots of the nanocomposite impedance demonstrate characteristic behavior of GO-doped conducting polymer nanocomposites (Figure 5.6a) [80, 90, 162]. At low frequencies, the Nyquist plots exhibit steep slopes, indicative of highly capacitive behavior, while at high frequencies (Figure 5.6a inset) the curves present a more gradual slope that reflects the diffusive behavior of the film [90, 134]. Notably, the 15-minute sonication treatment group transitions from diffusive to capacitive behavior at a lower frequency than the other treatment groups; that is, it exhibits more diffusion-dominated behavior, indicating that the shorter sonication treatment may result in a nanocomposite film with slower charge transfer kinetics. The increase in diffusive behavior of the 15-minute sonication group may arise from a larger content of few-layer GO in the nanocomposite compared to longer sonication times that would contain more single- or double-layer GO. Inherently, GO is not conductive, a result of the disruption in its π-electron network as oxygen functional groups are added to the structure during its oxidation reaction [53]. Any larger GO nanosheets contained in the nanocomposite could decrease the charge transfer of the nanocomposite film or create a diffusion barrier at the electrode/electrolyte interface that would result in the observed Nyquist behavior.

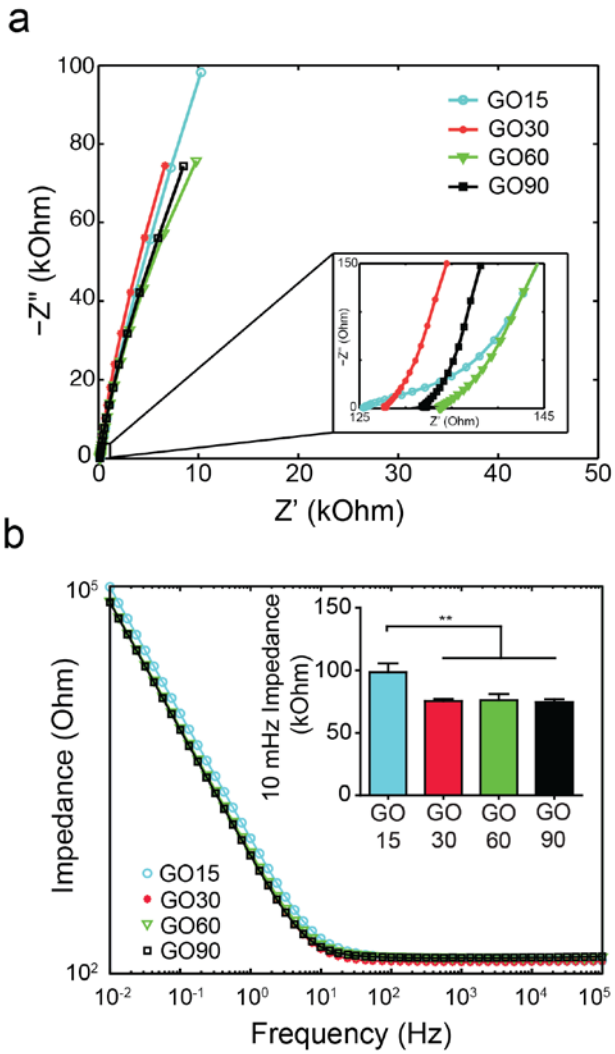

Figure 5.6. Effect of GO Sonication on the Electrochemical Impedence Spectroscopic Behavior of GO/PEDOT Nanocomposite. (a) Nyquist plots of the GO/PEDOT nanocomposites synthesized from GO sonicated for 15 min (GO15), 30 min (GO30), 60 min (GO60), or 90 min (GO90) prior to electrodeposition. Inset: High frequency range of the nyquist plot displaying the increased diffusive behavior of the GO15 nanocomposite (*n* = 7). (b) Bode plots of the GO/PEDOT nanocomposites synthesized with GO sonicated for varying amounts of time prior to electrodeposition. Inset: Comparision of the 10 mHz impedance behavior (*p* < 0.01; *n* = 7). The GO15 nanocomposite demonstrates significantly higher 10 mHz impedance, suggesting that it has a larger effective surface area.**

The impedance modulus of the nanocomposite films differs subtly as a result of GO sonication treatment (Figure 5.6b). At high frequencies, no significant changes emerge, but at impedances lower than approximately 10 Hz, the 15-minute sonication group diverges from the longer sonication groups. At the 10 mHz frequency, the impedance is significantly larger for the 15-minute sonication group than the longer sonication treatment groups ($p < 0.01$) indicating that both the capacitance and electrochemical surface area are lower (Figure 5.6b inset) [232, 233]. The decreased surface area has implications for the sensitivity of the nanocomposite towards DA electrochemical oxidation, with a lower surface area likely to produce a decreased DA sensitivity. In fact, the 15-minute sonication group does display a lower DA oxidation peak current than the longer sonication groups, with no significant improvement over the bare electrode that exists for the longer treatments (Figure 5.4a). The difference in nanocomposite surface area likely arises from the fact that the sonication treatment alters the size of the GO nanosheets, with longer sonication creating smaller, thinner sheets. Increasing GO sonication treatment prior to electrodeposition into conducting polymer films results in a rougher nanocomposite topography and the appearance of smaller features at the surface, likely due to the fact that more small GO nanosheets are preferentially incorporated into the polymer matrix as dopants [81]. A rougher surface topography would possibly provide an increased number of active sites with which the DA molecules could electrostatically interact, improving the sensitivity of the nanocomposite film towards the electrochemical oxidation of DA. The increase in surface area supports the finding that increased oxygen content in the nanocomposite correlates to a higher sensitivity towards the electrochemical oxidation DA. As more GO nanosheets are incorporated into the nanocomposite to increase its roughness and surface area, it

is expected that there would be more carboxylic acid groups provided by the GO within the nanocomposite that would interact with DA molecules to produce the boosted sensitivity.

5.3.4 Effect of GO Sonication on the Electrocatalytic Activity Towards AA

At the surface of the GO/PEDOT nanocomposite, AA exhibits a leftward shift in its oxidation potential, demonstrating the electrocatalytic effect of the nanocomposite and its potential as a material to improve the specificity of electrochemical detection methods (Figure 5.2b, c). To probe the mechanism by which the nanocomposite interacts with AA, GO/PEDOT films were synthesized using GO that underwent graded sonication treatment and the effect on electrocatalysis of AA was evaluated. The negative shift in AA oxidation potential at the nanocomposite surface, as compared to a bare electrode, was significantly less at the longest sonication time of 90 min (Figure 5.7a). GO has been noted as a highly catalytic material because of the abundance of oxygen functional groups in its structure [59, 61, 62]. The electrocatalysis of the AA oxidation reaction by GO relies on the extent of GO oxidation, with higher levels of oxygen content correlating with increased electrocatalytic activity [60]. Interestingly, the favorable electrocatalysis has been shown to disappear when GO is chemically reduced, with the AA oxidation potential moving back towards the same positive voltage exhibited by the bare electrodes [60]. This suggests that the ability of GO to electrocatalyze the AA reaction lies with its reducible oxygen functional groups, such as hydroxyl or epoxide, but not its carbonyl groups that can persist following reduction [58, 242]. To explore the role of GO oxygen functional groups, the relationship between negative potential shift and oxygen bonds in the nanocomposite films was evaluated using FTIR (Figure 5.7b). The negative potential shift significantly correlated with the alkoxy C-O content in the nanocomposite ($R^2 = 0.967$, $p < 0.05$),

but not to the other oxygen functional group content in the nanocomposite, suggesting that the electrocatalysis may arise from interactions between the AA molecule and the alkoxy functional groups present at the surface of the nanocomposite (Figure 5.7c). The AA electrochemical oxidation pathway is a two-step process with AA first directly oxidized into a dehydroascorbic acid (DHA) radical that adsorbs onto the electrode surface before further oxidation into the final product, DHA, that then desorbs from the electrode [243-245]. The formation of hydrogen bonds between the multiple hydroxyl groups on the DHA radical and the alkoxy groups of the GO nanosheets may be one way in which the nanocomposite catalyzes the oxidation reaction. The hydrogen bond interactions could coordinate the unstable DHA radical to reduce the energy barrier needed to carry out the reaction, resulting in a leftward shift in oxidation potential. At the longest sonication times, there is a reduction in available alkoxy groups, and a consequent reduction in the amount of hydrogen bond-mediated stabilization of the DHA radical would reduce the leftward shift observed in the AA oxidation potential as the reduction in the energy barrier to complete the reaction is not as large.

The origin of the decrease in alkoxy groups at the 90-min GO sonication time may be attributed to a population of smaller GO nanosheets, with a lower oxygen content per nanosheet, being incorporated into the nanocomposite. As the GO nanosheets are broken into smaller pieces with sonication treatment, only those that contain a negatively charged carboxylic acid group will be able to act as dopants in the electropolymerization reaction of the nanocomposite. Therefore, as smaller nanosheet sizes are produced at the longest sonication time, it is likely that the ratio of carboxylic acid to alkoxy in the nanocomposite would increase, and total alkoxy content would decrease, as small GO nanosheets containing only hydroxyl and epoxide groups are selectively omitted from the nanocomposite.

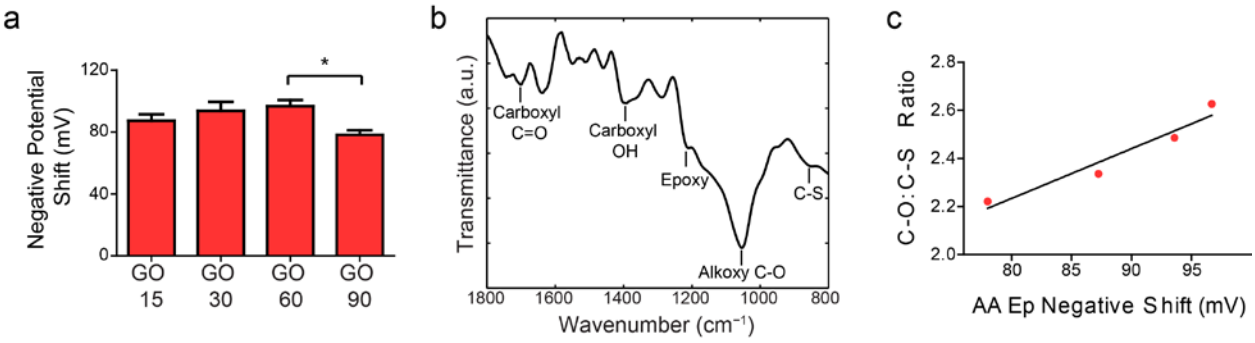

Figure 5.7. Alkoxy C-O Content in the GO/PEDOT Nanocomposite Correlates to the Shift in AA Oxidation Potential. (a) Negative shift in the AA oxidation potential, compared to a bare GC electrode, at the GO/PEDOT nanocomposite synthesized from GO sonicated for 15 min (GO15), 30 min (GO30), 60 min (GO60), or 90 min (GO90). The GO90 nanocomposite exhibits a significant decrease in the magnitude of AA oxidation potential shift ($p < 0.05$; $n = 7$). (b) Representative FTIR spectrum of the GO90 nanocomposite exhibiting peaks corresponding to oxygen containing functional groups donated by the GO and the peak corresponding to the sulfur group donated by PEDOT. (c) Linear correlation between the magnitude of the AA oxidation potential (Ep) negative shift and the ratio of alkoxy C-O to C-S peaks. The ratio is a semi-quantitative estimate of the alkoxy content in the nanocomposites.

Notably, at the nanocomposite surface there is no electrocatalysis of the DA and UA oxidation reaction, as the location of the oxidation peak does not change for either molecule (Figure 5.2). The structure of DA contains fewer hydroxyl groups than the AA structure, and the UA molecule contains no hydroxyl groups, potentially decreasing the ability of the nanocomposite to catalyze their oxidation reactions. The selective electrocatalysis of the oxidation reaction of AA, but not DA, makes the GO/PEDOT nanocomposite a promising electrode material for the selective determination of DA in biological solutions that also contain AA, such as blood, urine, or cerebral spinal fluid.

5.4 CONCLUSIONS

The electrochemical oxidation behavior of DA, AA, and UA was investigated at the surface of a GO/PEDOT nanocomposite material. The nanocomposite selectively amplified the signal of DA oxidation as a result of electrostatic interactions between the DA molecules and the negative charges at the nanocomposite surface. Interference from AA was eliminated by electrocatalysis of the AA oxidation reaction by the nanocomposite surface, shifting its oxidation potential sufficiently away from the DA oxidation potential. These data indicate that this high performance nanocomposite material will be useful for the development of more selective and sensitive biosensors that will have the potential to improve both diagnostics and exploratory science by providing a more reliable and accurate depiction of DA in biological samples and tissues.

6.0 DEVELOPMENT OF AN IN VITRO PLATFORM FOR THE STUDY OF NEURONAL INJURY AND REGENERATION

6.1 INTRODUCTION

Traumatic brain injury (TBI) presents a huge public health problem with over 2 million new cases each year, and an estimated 5.3 million Americans currently living with a TBI-related disability [246]. The challenge of treating TBI lies in the complex pathobiological cascade that occurs following injury, including processes such as induction of oxidative stress, excitotoxicity, and energy failure that ultimately lead to the activation of apoptotic pathways and widespread cell death [247, 248]. Because of the level of complexity embodying the injury response, effective clinical therapies are difficult to develop. By taking advantage of *in vitro* injury models, where experimental variables are individually isolated and probed, researchers can achieve a better understanding of the mechanisms underlying TBI and ultimately move toward the development of targeted, effective therapeutics.

Several *in vitro* models of TBI exist that can recapitulate both focal and diffuse damage occurring after injury [249, 250]. Focal injury occurs as a direct result of the initial insult, and is modeled using transection or compression injuries. Diffuse injury occurs in response to shear forces from the brain moving within the skull upon impact and has been modeled using stretch injuries. In both of these *in vitro* models, organotypic slice cultures and dissociated cultured

neuronal networks (CNNs) have been used as model systems. While they have added a great amount to the understanding of the pathology underlying TBI, most of these injury models rely on end-point molecular or genetic analyses and are limited in their ability to follow a single cell culture longitudinally after injury.

Multielectrode arrays (MEAs), consisting of grids of microelectrodes that can stimulate or record from CNNs, have been used extensively in the field of neuroscience to study the development and plasticity of electrical activity *in vitro* [251, 252]. Because of their non-invasive recording ability, the devices can collect information from a CNN over the course of several weeks, providing information about the dynamics of network activity. Recently, stretchable MEAs, composed of electrode grids on an elastomeric substrate, have been developed that can impart a stretch injury to CNNs or slice cultures to evaluate the effects of injury on electrical activity [253, 254]. However, because the electrical components and insulation materials of MEAs are easily damaged, no models have yet been developed that utilize these devices with transection or compression injuries. In this work, we describe an *in vitro* injury model based on commercially available MEAs that uses an elastomeric stamp to introduce a focal injury into a mature CNN. The injury creates dysfunctional network activity characterized by decreases in the firing rate, asynchronous firing activity and disordered burst patterns for up to 7 d following the introduction of damage. This work provides the groundwork for a platform that can be used as a tool to assess potential therapeutic interventions, such as cellular therapies, without the need of animal models.

Neural stem cells (NSCs) have the ability to differentiate into functional neurons [138] and have been implicated as a potential therapy for TBI and other brain injuries [143, 255]. However, there have been conflicting reports about their ability to survive following

transplantation and integrate into existing circuitry [140-142]. A reduced model of NSC transplantation would create a valuable platform for investigating the physiological events that occur when a population of NSCs is introduced into a damage site, and assist in providing information that could be used to improve the efficacy of current transplantation methods. Using the MEA-based model of neuronal injury, we transplanted a population of embryonic-derived NSCs into the injury site and monitored the resultant CNN activity to evaluate any therapeutic effects provided by the cells. Injured CNNs treated with NSCs did not exhibit the same activity deficits as untreated damaged CNNs, suggesting that the transplanted cells were imparting a protective effect to the damaged network. These experiments represent a first step towards creating a repeatable *in vitro* model of neuronal damage and regeneration.

6.2 MATERIALS AND METHODS

6.2.1 MEA Preparation

MEAs with 64 electrodes with a diameter of 50 μm and an inter-electrode distance of 150 μm were used for this study (AlphaMED Scientific, Osaka, Japan). The electrodes were patterned into two 32-electrode grids located at a distance of 10 mm from each other (Figure 6.1). To create a consistent cell culture area over the electrode space, a custom polydimethylsiloxane (PDMS) barrier was created to constrain the cell growth to a 15 mm x 3 mm area. The PDMS was made using a Sylgard 184 Silicone Elastomer Kit (Dow Corning, Midland, MI) at a ratio of 10:1 and cured for 48 h at room temperature, and the barrier was cut out using a stencil. The PDMS barrier and the polyacrylamide surface of the MEA were activated with a 30 s treatment

with a plasma cleaner (PDC-001, HarrickPlasma) operated with ambient air. A drop of methanol was added to the surface of the MEA to aid in the placement of the barrier, then the barrier was positioned and bonded to the surface at 37°C for 30 min. Prior to cell culture, the MEA culture surface was washed in sterile dH_2O and exposed to UV light for 10 min. The culture surface within the PDMS barrier was treated with polyethylenimine (PEI, 0.05% in borate buffered saline) for 1 h, washed with sterile dH_2O, then treated with laminin (20 μg ml^{-1} in Neurobasal medium) overnight at 37°C, washed with sterile phosphate buffered saline (PBS) and stored in PBS until culture.

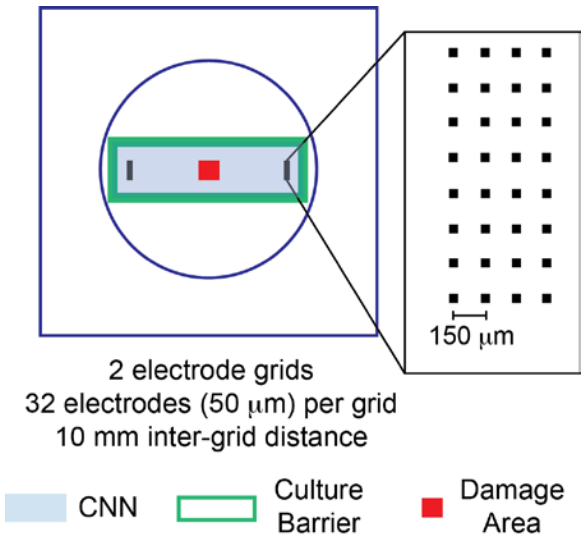

Figure 6.1. Schematic Representation of CNN Damage Platform. The device consists of a commercially available MEA that contains two grids of 32 electrodes (50 μm diameter, 150 μm inter-electrode distance) separated by a space of 10 mm. A culture barrier made of PDMS was fixed to the surface to constrain the culture area to 45 mm^2. A CNN was grown inside of the culture barrier for 22 d prior to the introduction of a focal injury using a PDMS stamp that ablated all cells within the damage area.

6.2.2 Cell Culture

Primary hippocampal neurons were isolated from Sprague-Dawley rat E18 embryos as described previously [256]. Neurons were seeded within the PDMS culture barrier at a density of approximately 11k cells per mm^2 and maintained in Neurobasal media supplemented with 2% B27 (Invitrogen), 1% Glutamax (Invitrogen), 10% horse serum (Sigma-Aldrich), and 1% penicillin-streptomycin (Pen-Strep; Invitrogen). The medium was exchanged every 2 to 3 d, as necessary. In experimental groups C2, D2, and D2-tx (Table 1), the neuron media was additionally supplemented with cytosine arabinoside (AraC; 5 μM; Sigma-Aldrich) after 8 days *in vitro* (DIV) to restrict glial growth. The AraC treatment was removed at 18 DIV in preparation for NSC transplantation.

Table 6.1. Experimental CNN Groups

Experimental Group	*Injury*	*AraC*	*NSC-Tx*	*Sample Size*
C1	none	-	-	$n = 3$
D1	9 mm^2	-	-	$n = 2$
C2	none	+	-	$n = 2$
D2	1 mm^2	+	-	$n = 2$
D2-tx	1 mm^2	+	+	$n = 2$

Embryonic NSCs were isolated from the cortices of Sprague-Dawley rat E18 embryos. Cortices were triturated in Hank's Buffered Salt Solution (HBSS, Sigma-Aldrich) supplemented with 1% GlutaMax (Invitrogen) and 1% Pen-Strep. The suspension was allowed to settle for 5

min and the supernatant was collected, centrifuged, and transferred into NeuroCult NS-A Proliferation Medium (StemCell Technologies) supplemented with recombinant human epidermal growth factor (EGF; 20 ng mL^{-1}, Invitrogen), recombinant human basic fibroblast growth factor (bFGF; 10 ng mL^{-1}, Invitrogen), heparin (2 mg mL^{-1}; StemCell Technologies), and Pen-Strep (1%). The cells were maintained at 37°C and passaged every 3 to 4 d, as necessary. NSCs were used at passages 2 or 3 for cell transplantation.

6.2.3 CNN Damage and NSC Transplantation

The neuronal injury was introduced to the cultures at 22 DIV by applying a focal injury to the center of the culture area using a PDMS stamp (9 mm^2 or 1 mm^2). The stamp was lowered into the CNN using a micromanipulator until it made contact with the underlying culture surface and removed after 30 s. Visual assessment confirmed that the cells underneath the stamp were completely ablated. After 30 min the damaged cultures underwent a partial medium exchange to alleviate some of the damage-induced chemical cascade [257]. At 3 h after injury, NSCs were added to cultures to model cell transplantation. In an effort to restrict the NSC localization to the CNN area, all media outside of the PDMS culture barrier was removed from the dish, so that approximately 50 μL of media remained, covering only the CNN growth area. NSCs were switched from their proliferation media into Neurobasal media, then 50k cells were added to the inside of the PDMS culture barrier and allowed to attach for 30 min. After the cell attachment phase, Neurobasal media was added to fill the entire MEA culture area.

6.2.4 Recording

Spontaneous extracellular network activity was recorded from the CNNs growing on the MEAs using a MED64 system with Conductor Software (AlphaMED, Osaka, Japan). The spontaneous activity was recorded from each CNN during 5-minute sessions, 3x per recording day. Each channel was recorded from simultaneously and was sampled at a rate of 20 kHz. Prior to recording, the CNNs were briefly transferred from the incubator to a sterile culture hood in order to place them into the MED64 Connector that interfaces the MEA with the amplifier. The CNNs were then placed back in the incubator and recordings took place at 37°C. Prior to starting the recording, CNNs were allowed to equilibrate for 10 min to reduce any artificial increase in cell firing activity that can occur in response to mechanical perturbations during movement [252].

Activity was monitored weekly during the first three weeks *in vitro* to ensure the development of healthy network activity. CNNs that did not develop strong synchronous bursting activity by the third week in culture were excluded from these experiments. Starting at 21 DIV, the day prior to damage/NSC-tx, activity recordings were taken daily until 7 d post injury (DPI). Control CNNs that received no treatment were recorded from daily during 21 DIV through 29 DIV, which corresponded 7 DPI in the damaged cultures, to ensure that the all comparisons across CNN groups were at similar points developmentally.

6.2.5 Data Analysis

6.2.5.1 Spike Detection

Neural recording segments were analyzed offline to determine the number of neurons recorded, noise levels, and signal amplitudes using custom automated MATLAB (Mathworks Inc., MA)

software, as described elsewhere [258, 259]. As an overview, the wide-band recordings were filtered in software to isolate the spike data (300–5000 Hz). To identify single- and multi- units, the threshold for the high-frequency data was established by using a window set at 3.5 standard deviations below the mean of the data. For each peak exceeding the threshold window, timestamps recorded and plotted as a raster plot.

6.2.5.2 Burst Detection and Analysis

The bursting activity of the CNNs is defined as a period of increased firing activity that occurred followed by a brief period of silence. Activity was considered a burst if it met the minimum requirement of at least 10 spikes occurring in sequence with an interspike interval (ISI) of less than 100 ms [260]. The following measures were used to describe the bursting behavior of the CNNs:

Burst rate (BR): defined as the frequency of bursting events, in bursts per second, occurring at an electrode during the 5-minute recording

Burst duration (BD): defined as the average length in seconds of bursts occurring at an electrode during the 5-minute recording

Intra-burst Frequency (IBF): defined as the average firing rate within bursting events occurring at an electrode during the 5-minute recording

6.2.5.3 Cross-Correlation

As a metric to quantify the connectivity of the CNN, the cross-correlation, $C_{xy}(\tau)$, between electrodes in the dish was calculated as described previously [260, 261]. In brief, the spike trains recorded from two electrodes, *x* and *y*, in the CNN were compared. For each spike on *x*, the number of spikes occurring within ± 150 ms on *y* were summed and separated into 30 ms bins so that each cross-correlation vector contained 10 elements. The $C_{xy}(\tau)$ was normalized to spikes s^{-1} by dividing each element by the total number of spikes in the *x* train and the bin size. The cross-correlation coefficient, $C_{xy}(0)$, for each electrode pair was calculated as the total number of spikes occurring within the 30 ms bin centered at $t = 0$. To obtain information about the connectivity between the two electrode grids, *X* and *Y*, the cross-grid correlation coefficient, $C_{XY}(0)$ was calculated by averaging the $C_{xy}(0)$ between each electrode on grid X and each electrode on grid Y.

6.2.5.4 Statistical Analysis

For each day, the values obtained from the 3 recordings were averaged together to decrease any within network variability. To compare changes that happened after the damage or NSC-tx, all metrics were normalized to the mean values of 21 and 22 DIV. All statistical analysis was carried out using GraphPad Prism software and presented as the mean ± SEM. For comparisons between two experimental groups, Student's t-tests were used. For comparisons across the three experimental groups over the 7 d following injury, two-way ANOVA analysis with Bonferroni's posthoc analysis was employed.

6.3 RESULTS AND DISCUSSION

Embryonic E18 hippocampal neurons were plated on the surface of MEAs, matured for 22 DIV, and then injured with a focal injury to determine the effect of neuronal damage on network firing patterns. CNNs represent an advantageous model system for the study of injury effects on electrophysiological activity. As the networks mature, they begin to develop stereotypical synchronous bursting behavior that can be used as a benchmark for comparison after the introduction of an injury. In this work, three experimental groups received AraC treatment between 8 DIV and 18 DIV (Groups C2, D2, and D2-tx; Table 1), while two groups received no AraC treatment (Groups C1 and D1). The AraC treatment was introduced as a method of restricting astrocyte proliferation because in CNNs glial cells can overgrow neurons, consume the majority of available media nutrients and release acidic byproducts, leading to CNN death. It was found that in the C1 and D1 groups that were not treated with AraC, regardless of the damage treatment, the CNN quit exhibiting firing activity and perished by 30 - 35 DIV. Because the goal of these experiments was to evaluate the effect of the introduced focal injury on the network activity, and the overgrowth of astrocytes could contribute to altered network firing patterns as the health of the network declined, AraC treatment was introduced in the second set of experiments.

6.3.1 Effect of AraC Treatment on CNN Activity

Interestingly, the firing activity of control cultures was significantly different depending on AraC treatment (Figure 6.2). At 29 DIV, CNNs that did not receive AraC exhibited firing activity that was organized into densely packed superbursts, consisting of periods of high activity followed by

periods of silence extending for seconds (Figure 6.2a). Within the superburst, the activity is organized into smaller bursts lasting for 10 - 50 ms with short periods of silence between bursts (Figure 6.2c). Superbursting activity occurs normally during CNN development [252, 262] and recapitulates spontaneous activity that occurs *in vivo*, which is thought to be involved in strengthening of synaptic connections [263, 264]. Cultures that underwent AraC treatment between 8 DIV and 18 DIV did not display the superbursting behavior at any point during the course of the experiment; however, they did exhibit bursting behavior that is organized into a less stereotyped pattern (Figure 6.2b). The average firing rate measured across all electrodes in the CNN was higher in the AraC-treated culture than the untreated culture (Figure 6.3a), while the IBF (i.e. the firing rate within bursts) was higher (Figure 6.3d) and BD was lower (Figure 6.3c), reflecting the dense organization of firing activity into stereotyped bursting events. Although the AraC treatment resulted in a significant reorganization of bursting patterns, the cross-grid correlation was not significantly different (Figure 6.3b), implying that the widespread synaptic connections across the CNN developed normally and could create the highly correlated bursting activity between cells in the network that is characteristic of CNNs [251, 252, 265].

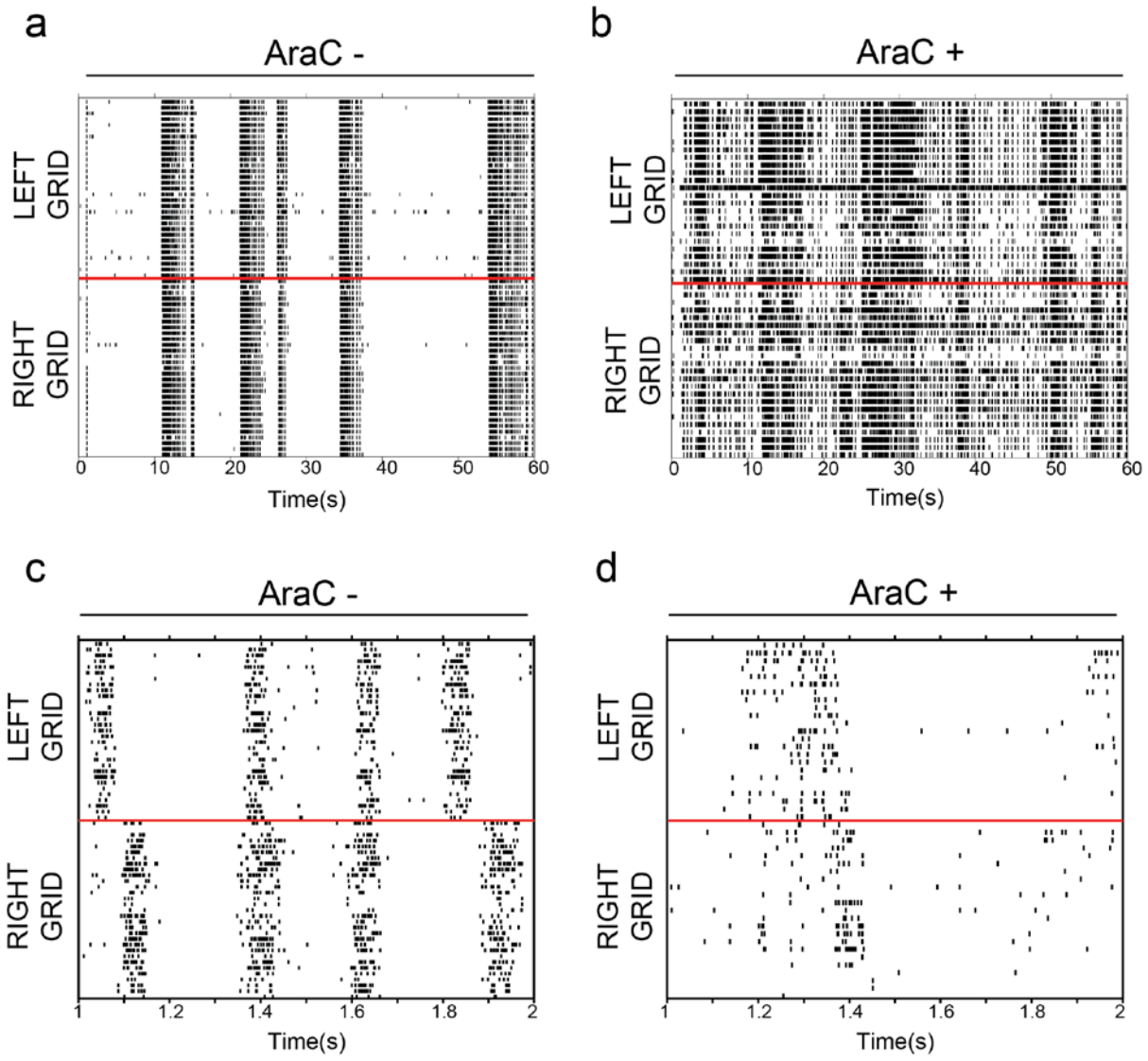

Figure 6.2. AraC Treatment Alters the Pattern of Neuronal Firing Activity. Representative raster plots of control CNN network activity at 29 DIV that received no AraC treatment (a, c) or that received 5 μM AraC between 8 DIV and 18 DIV (b, d). Red line delineates electrodes on the left grid of the MEA from electrodes on the right grid of the MEA.

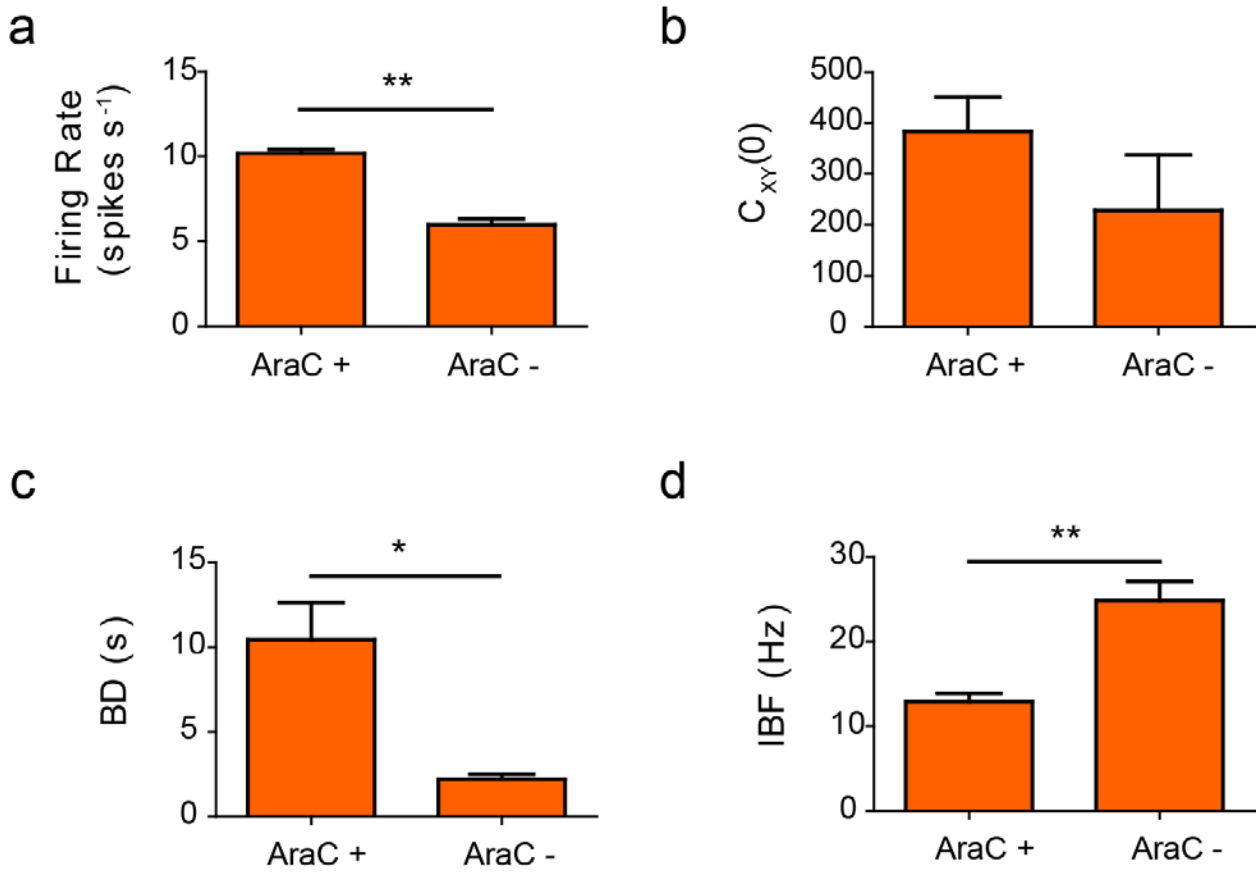

Figure 6.3. Effect of AraC Treatment on the Firing Behavior of CNNs. Comparison of (a) firing rate, (b) cross-grid correlation coefficient ($C_{XY}(0)$), (c) burst duration (BD), and (d) intra-burst frequency (IBF) at 29 DIV in cultures that were treated with AraC between 8 and 18 DIV (AraC+) or that received no AraC treatment (AraC-). * $p < 0.05$; ** $p < 0.01$.

Astrocytes were historically considered "support" cells of the CNS, with a limited role in signaling that leads to the transmission and integration of information [266]. In recent years, accumulating evidence depicts astrocytes in a more active signaling role that couples with neuron activity. While they cannot fire action potentials like their neuronal counterparts, astrocytes do exhibit spontaneous and activity-evoked Ca^{2+} oscillations [267, 268] that can elicit the release of "gliotransmitters" such as neuropeptides, amino acid neurotransmitters, and growth factors [269]. Gliotransmission impacts neuronal synaptic transmission, and glutamate release

from astroglia activates local neurons in a highly synchronous way, indicating that astrocytes play a role in the development of synchronous firing behavior in neurons [270, 271]. In the cultures that were treated with AraC between 8 DIV and 18 DIV, astrocyte growth was restricted and resulted in a largely different network firing patterns, demonstrating the importance of glia in the development of neuron activity. For the future development of the CNN damage model, the extent of astrocyte restriction must be carefully considered because unrestricted growth leads to unhealthy networks during long-term cultures, while smaller populations of astrocytes hold less influence over the formation of synaptic connections and neuronal firing patterns, ultimately resulting in different activity patterns in the mature networks.

6.3.2 Effect of Damage on CNN Firing Activity

Mature CNNs were damaged with a focal injury inflicted with an elastomeric stamp at 22 DIV. The damage site was located approximately equidistant between the two electrode grids. In one group, D1, the damage site was 9 mm^2, which covered approximately 20% of the total culture area, and was considered a severe injury. In a second group, D2, the damage site was 1 mm^2, which covered approximately 2.2% of the total culture area, and was considered a mild injury. In both groups, all cells that were growing under the damage site were completely ablated after the injury. The effects of the injuries on the firing activity of the CNN were evaluated for the first 7 DPI. Experimental group D1 did not receive AraC treatment at any point during the course of the experiment and was compared with control C1, which also did not receive AraC treatment (Table 1), to determine the effect of damage on the activity of the CNN. Likewise, group D2 that was treated with AraC between 8 DIV and 18 DIV was compared with control C2 that also received the same AraC treatment.

6.3.2.1 Severe Damage

Severe damage resulted in a marked interruption in the superbursting activity exhibited by C1 (Figure 6.4a). While correlated bursting activity persists discretely on each grid separately, cross-grid bursts are no longer present and a large amount of firing activity exists outside of correlated bursts. The average firing rate across the entire dish was not significantly different between D1 and C1 (Figure 6.4b). However, all mean values of D1 were below those of C1, suggesting that a trend exists and with a higher sample size, significant differences may emerge. The cross-grid correlation coefficient declined over the first 3 DPI, stabilized around 25% of the pre-injury value, then exhibited a slight increase at 7 DPI (Figure 6.4c). These data reflect the deteriorating connections between the cells in the network, possibly a result of cells continuing to die following damage *via* delayed apoptotic pathways initiated by the insult [272]. Similarly, the BR decreased and stabilized at approximately 60% of the pre-injury value, reflecting the disruption in connectivity following injury (Figure 6.4d). The increase in cross-grid correlation at 7 DPI may be an artifact of the intra-culture variation in activity that occurs across different days [252], especially because of the low sample size (n = 2), but it may also indicate the potential of the surviving cells to reestablish connectivity. It should be noted that the D1 cultures completely ceased to exhibit any firing activity soon after 7 DPI, either because of damage sustained during the injury or because of the overgrowth of unrestricted astroglia, so the longer-term response to injury could not be monitored.

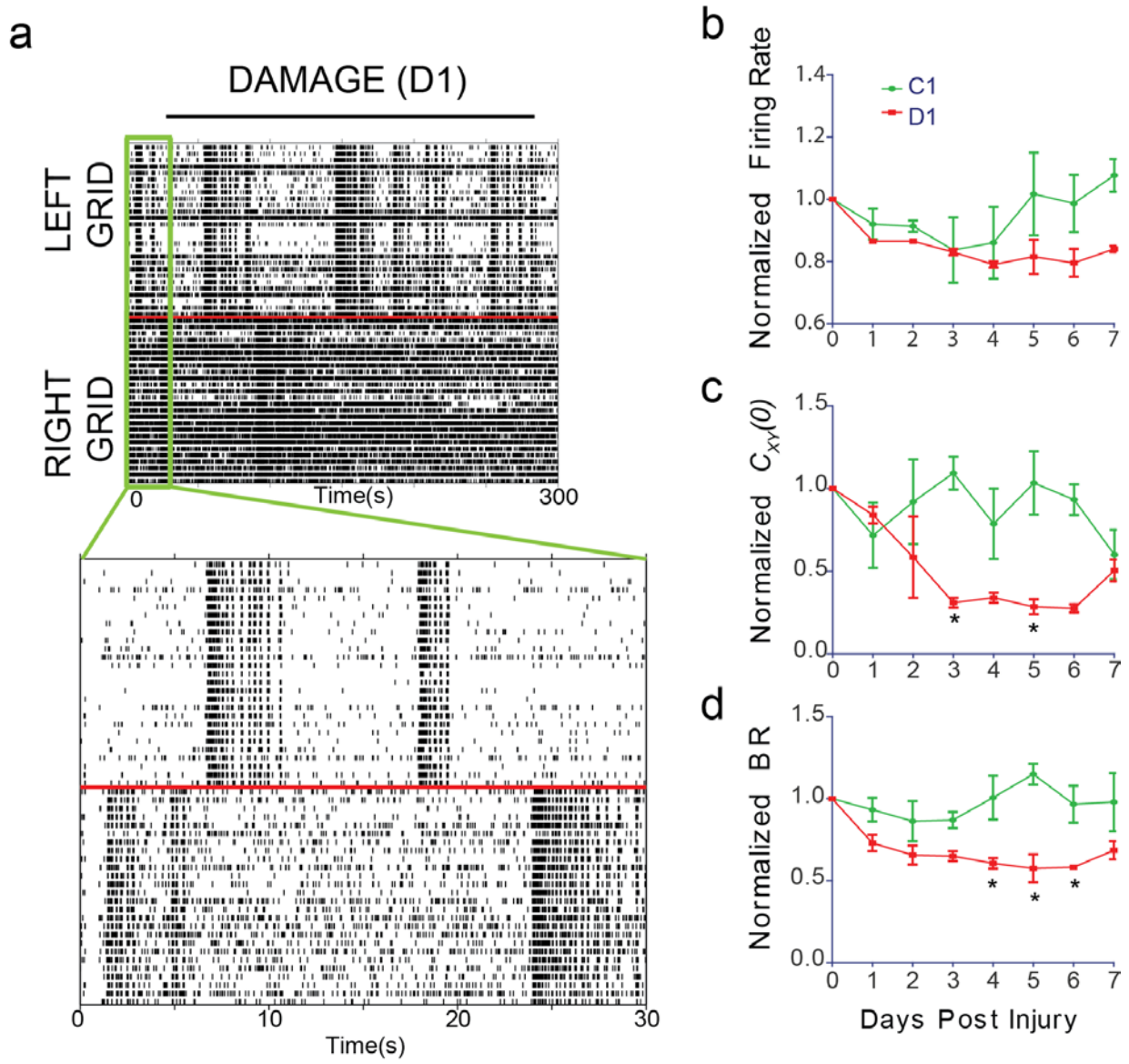

Figure 6.4. Effect of Severe Focal Injury on CNN Firing Activity. (a) Representative raster plots of CNN activity at 7 DPI (29 DIV) exhibiting the interruption in superbursting behavior and decrease in correlated activity. Red line delineates electrodes on the left grid of the MEA from electrodes on the right grid of the MEA. (b) Normalized average firing rate across all electrodes of the MEA, (c) normalized cross-grid correlation coefficient ($C_{XY}(0)$), and (d) normalized burst rate (BR) over the first 7 DPI for control (C1) and damage (D1). All data points are normalized to the pre-damage activity at 22 DIV. * indicates significant difference from C1; $p < 0.05$.

6.3.2.2 Mild Damage

To address the poor long-term survival of the D1 cultures that may arise from unrestricted astroglial overgrowth in combination with the severe damage that ablated 20% of the total culture area, AraC treatment was given to limit the amount of astrocytes in the CNN and a milder damage (2.2%) was introduced to injure the networks. Under this damage condition, D2, the networks exhibited a similar disruption in the synchronous behavior that was apparent in D1 (Figure 6.5a). Some of the correlated intra-grid bursting behavior was retained but, as in D2, there was no synchronous cross-grid bursting behavior after injury. Interestingly, some electrodes began recording superburst-like behavior with periods of silence in between periods of high activity; however, unlike true superbursting activity, the high activity period was not organized into small correlated bursts, but instead consisted of disordered firing (Figure 6.5a, left grid activity). The mean firing rate across the entire MEA was lower in D2 than in C2, though the effect was non-significant, perhaps due to the low sample size (Figure 6.6a), and the cross-grid correlation coefficient was significantly lower in D2 at several points throughout the first 7 DPI (Figure 6.6b).

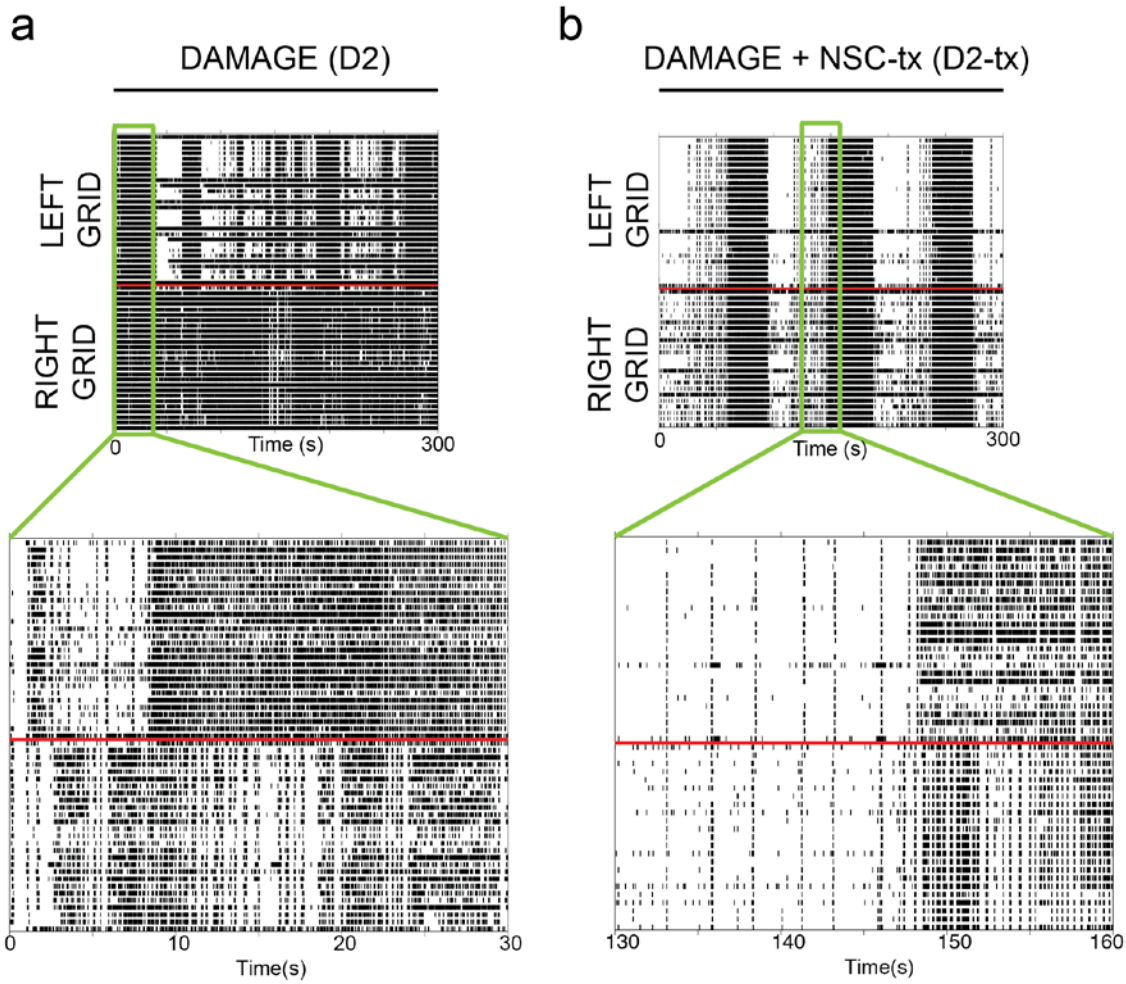

Figure 6.5. Effect of Mild Damage With or Without NSC-Tx on CNN Firing Activity. Representative raster plots of CNN activity 7 DIV after mild damage (a) without NSC-tx (D2) or (b) with NSC-tx (D2-tx). Red line delineates electrodes on the left grid of the MEA from electrodes on the right grid of the MEA. Damage disrupts correlated network-wide bursting activity. In CNNs that received the NSC-tx treatment, network-wide superbursting behavior was initiated, and cross-grid bursting was restored.

Bursting behavior in neuronal networks is driven by GABAergic inhibition provided by interneurons in the circuit and develops as the synaptic inhibitory drive outweighs the excitatory drive [251, 273]. In injured CNNs, it is possible that the GABAergic interneurons are more susceptible to the injury, leading to the dysfunctional bursting behavior observed in both D1 and

D2. In response to prolonged silencing after the introduction of tetrodotoxin, which interrupts spontaneous firing in CNNs, there is a disproportionate decrease in GABA signaling, supporting the hypothesis that GABAergic cells may be more sensitive to injury [274]. Additionally, *in vivo* damage caused by lesion or infarction results in prolonged loss of GABAergic inhibition and dysfunctional circuitry [275-277], again supporting that GABAergic circuits are targeted during damage, and indicating that the model described here may be valid for studying these types of injuries.

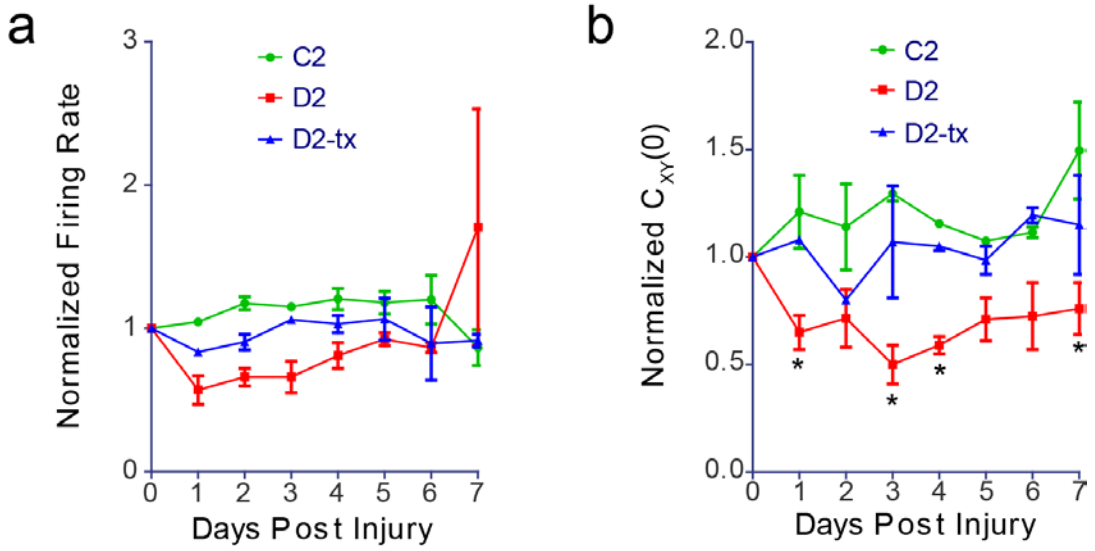

Figure 6.6. Effect of Mild Damage and NSC-Tx on Firing Metrics of CNNs. (a) Normalized average firing rate across all electrodes of the MEA and (b) normalized cross-grid correlation coefficient ($C_{XY}(0)$) over the first 7 DPI for control (C2), damage (D2), and damage with NSC-tx (D2-tx). All data points are normalized to the pre-damage activity at 22 DIV. * indicates significant difference from C2; $p < 0.05$.

The dynamics of the injury were different in experimental groups D1 and D2, with the more severely damaged D1 exhibiting dysfunctional firing metrics for at least 6 DPI (Figure 6.4), while the more mildly injured D2 showed a possible trend toward recovering to pre-injury values

within the 7 DPI period (Figure 6.6). These data indicate the potential of this injury model to provide scalable damage to the CNN, with larger crush injuries resulting in more severely dysfunctional circuitry. However, it should be noted that these two damage groups received different AraC treatments, resulting in differences in the size of astrocyte populations in the culture, which could have an effect on their response to injury. Astrocytes contain glutamate transporters that can provide protection against excitotoxic glutamate release [278, 279], although the expression of astrocytic glutamate transporters is downregulated following injury [280], making it difficult to determine how significant the effect of AraC treatment was in the injury response of D1 and D2 cultures. Future studies are warranted to evaluate any neuroprotective effects of astroglia in this injury model.

6.3.2.3 NSC Transplantation

To evaluate the potential of NSCs as a therapy to restore damaged circuitry following neuronal injury, embryonic-derived NSCs were transplanted into the damaged CNN 3 h after injury and the resulting network activity was evaluated for 7 d. Immediately following injury, there was an improvement in both the firing rate and the cross-grid correlation coefficient compared to D2, which was not treated with NSCs (Figure 6.6). This effect persisted during the entire 7 DPI, with both metrics higher than D2 and slightly lower, but not significantly different than C2. In cultures that received the NSC-tx, the activity pattern displayed superburst-like activity, with periods of increased activity that were not organized into bursts as seen in D2 (Figure 6.5b). However, these superburst-like periods were highly correlated across the two grids of the MEA, suggesting that some connections were either protected from the damage, or restored after the damage. Additionally, outside of the superburst-like periods, there were very short, highly correlated bursts of activity that were present on both electrode grids and generally preceded the

onset of the superburst-like period. In healthy developing CNNs, the network undergoes a period of superbursting activity prior to transitioning to mature stable bursting behavior characterized by abrupt repetitive bursting [252, 262]. Immature superbursting is thought to be associated with neural plasticity, as the network connections are being formed and strengthened [263, 264]. The superburst-like activity that both D2 and D2-tx display may be indicative of plasticity occurring in the damaged networks after injury.

The existence of these highly correlated activity patterns indicate that the NSCs had a therapeutic effect on the damaged network and have the potential to repair the dysfunctional circuitry. The origin of the therapeutic effect is likely due to released factors from the NSCs, rather than the production of newborn neurons integrating into the damaged network because the effect is present as soon as 1 DPI, which would be too soon for the NSCs to differentiate into neurons that are functionally mature [138]. NSCs secrete neurotrophic factors and can protect damaged neurons from oxidative stress and degeneration in disease states or injury *in vivo* and *in vitro* [281, 282], supporting the hypothesis that a neuroprotective effect may also occur in the D2-tx CNNs. However, it is possible that at later time points, some of the NSCs will differentiate into functional cells and integrate into the CNN to further repair the circuitry, and experiments are currently underway to investigate this possibility.

These results indicate that this *in vitro* damage model has the potential to develop into a highly flexible platform for studying neuronal injury and regeneration, especially if coupled with the GO/CP nanocomposite described in *Chapters 2 – 5*. The multifaceted injury pathways involve dysfunctions in a multitude of chemical signals, along with the impaired electrical signaling described here. By modifying the electrodes of the device with the nanocomposite material, the platform can be enabled with the capability to detect chemical signaling to further

elucidate the injury cascade, or to release therapeutic agents as a method to test efficacy of novel drug molecules.

6.4 CONCLUSIONS

This work explored a novel *in vitro* platform for modeling neuronal injury that has the ability to monitor the electrophysiological activity of a network of neurons over time after the introduction of an injury. CNNs display stereotyped bursting behavior as they mature that can be used as a benchmark for evaluating the effects of damage on cell physiology. The pattern of bursting behavior is highly sensitive to the amount of astroglial cells present in the culture, demonstrating that astrocytes exhibit influence over the formation and maintenance of synaptic connections between neurons. Following injury, the firing rate, cross-grid correlation coefficient and burst rate are reduced, while treatment with NSCs can restore the activity to a level that is similar to undamaged cultures. While these results must be considered carefully because of the low sample size in each group (n = 2), they underscore the potential of this model for studying neuronal injury and regeneration. This work lays the foundation for future development and characterization of the MEA-based injury platform that can function as a reduced model of the complex pathophysiology that occurs following neuronal injury.

7.0 CONCLUSION

7.1 SUMMARY OF RESULTS

This dissertation describes the development of a conductive neural biomaterial and its versatile applications in the field of neural interfacing. The material consists of graphene oxide (GO) nanosheets doped into conducting polymer (CP) films that are deposited onto the surface of metal or carbon electrodes to improve interfacing capabilities with neurons and neural stem cells (NSCs). The GO/CP nanocomposite demonstrated good biocompatibility with both neurons and NSCs and could be easily modified with bioactive molecules to influence cell growth. The unique electrochemical properties of the GO/CP composite enabled highly controllable, on-demand drug delivery. The chemical properties contributed by the GO nanosheets created a platform for highly sensitive and selective dopamine (DA) detection. With the goal of developing a customizable device that incorporates the neural interfacing capabilities of the GO/CP, this body of work concludes with the characterization of a repeatable *in vitro* cultured neuronal network (CNN) damage model based on multielectrode arrays (MEAs) for investigating the pathobiology of neuronal injury. The studies described in this dissertation demonstrate the hugely versatile applications that are possible for the GO/CP nanocomposite material, and are indicative of the potential impact that this neural biomaterial can have on the fields of bioengineering and medicine.

Chapter 2 introduced the GO/CP nanocomposite material and its ability to act as a biocompatible substrate for neural cell culture. The GO nanosheets were successfully incorporated into an electrochemically synthesized poly(3,4-ethylenedioxythiophene) (PEDOT) film as dopants and the resulting nanocomposite film demonstrated great electrical properties. Primary neurons cultured on the surface of the nanocomposite material showed no decrease in viability, very minimal cell death and exhibited healthy morphology that included plentiful neurite outgrowth and branching. As compared to conventional PEDOT films that were doped with poly(styrenesulfonate) (PSS), the GO/PEDOT nanocomposite displayed the interesting ability to improve the extent of neurite outgrowth, a property that may result from the unique morphology of the nanocomposite film. With a simple carbodiimide chemistry procedure that utilized the free carboxylic acid groups contributed by the GO nanosheets, the surface of the nanocomposite film could be decorated with functional laminin peptide p20 which further improved the neurite outgrowth of the neurons cultured on the surface of the nanocomposite.

To build on the results of *Chapter 2* that demonstrated the great scaffolding potential of the nanocomposite, *Chapter 3* explored the response of NSCs cultured on the surface of GO/PEDOT films. The nanocomposite exhibited a huge benefit over conventional PEDOT/PSS films in its ability to drive NSC differentiation towards the neuronal phenotype. Further studies are warranted to unravel the mechanism behind the improved neuronal differentiation, which could include effects caused by chemical or biophysical properties imparted by the nanocomposite film. When functionalized with either interferon-γ (IFNγ) or platelet-derived growth factor (PDGF), the nanocomposite could selectively drive differentiation toward the neuronal or oligodendroglial lineages. This result emphasizes the customizability of the nanocomposite as a scaffolding material and demonstrates that along with its subtle intrinsic cues

that may be driving NSC behavior, it has the potential to be tailored with chemical modifications to direct a wide variety of biological processes.

With *Chapter 2* and *Chapter 3* describing the ability of GO/CP nanocomposite to provide physical or immobilized chemical cues to cells, *Chapter 4* focuses on the exceptional ability of GO/CP nanocomposite films to act as highly controlled, on-demand drug delivery systems. Conventional CPs have the ability to controllably release anionic drug molecules in response to electrical stimulation, as a result of their unique doping and redox properties. With the addition of GO nanosheets as co-dopants along with drug molecules, the drug delivery system can release larger quantities of drug in response to the same magnitude electrical stimulation. The GO nanosheets act as drug nanocarriers, shuttling a larger quantity of drug molecules into the CP film during synthesis and improving the drug load, ultimately leading to the increased payload delivery. This result has significance for future *in vivo* applications of the delivery system, in which voltage magnitudes must be carefully controlled so the resident tissue is not harmed by the electrical release stimulation. While drug release from conventional CP systems can be modulated by changing the type of electrical stimulation applied through the film, the GO nanosheets provide an additional level of adjustability to the system. Altering the size of the nanosheets prior to deposition into the CP film results in additional changes in drug loading and release. Clinically, very specific dosage requirements exist and can vary across different applications or over time within the same treatment. This work has demonstrated that the GO/CP drug release platform has the potential to meet these varied dosage needs.

In *Chapter 5*, the focus of the interfacing application changed from the presentation of chemical cues to the detection of chemical signals. The performance of the GO/PEDOT nanocomposite as a sensitive and selective electrochemical DA sensor was evaluated. Electrodes

modified with the nanocomposite detect DA, an important neurotransmitter in the CNS, with significantly higher sensitivity than unmodified electrodes. This implies that the nanocomposite material could be useful for *in vivo* detection of DA, where concentrations of the neurochemical exist in the nanomolar to low micromolar range. Additionally, interfering signal from ascorbic acid (AA) was minimized at the nanocomposite surface as a result of an improved electrocatalyzation that separated the signals of the two analytes. Mechanistic studies suggested that both of these improvements arose as a result of interactions between the analytes and GO nanosheets that were present at the surface of the nanocomposite, clearly demonstrating the benefit of the nanomaterial.

Chapter 6 described a novel neuronal injury platform based on a commercially available MEA that has the capability of monitoring the dynamic effects of injury on the firing patterns of cultured neurons. CNNs display a stereotypical pattern of highly correlated bursting behavior that develops after a few weeks in culture. After the introduction of a focal injury to the CNN, this behavior became dysfunctional, with deficits in the firing rate, correlation level, and bursting patterns of the cultured cells. Transplantation of a population of NSCs into the injury site protected the CNN firing activity, suggesting that the cells had a therapeutic effect on the damaged network. This work produced a framework for future studies that will further characterize the effect of damage on the network activity and provide a platform for studying the effects of damage on the pathophysiology of neural networks.

7.2 FUTURE DIRECTIONS AND PRELIMINARY DATA

7.2.1 Surface Patterning to Direct Cell Growth

The ability of the GO/CP nanocomposite to act as a highly versatile scaffolding material suggests the possibility that it can be adapted for multifunctional surface patterning, in which several bioactive cues are presented at distinct areas on the same culture surface. Surface patterning technologies have been investigated as methods to pattern cells within a culture to evaluate cell-cell contacts or to study the interaction between cells and gradients of cues in their environment [283]. In these studies, a variety of engineering techniques such as lithography, microfluidic, and micro-contact printing are used to attract or confine cell growth to specific regions. To improve on these methods, a system that has the ability to not only direct cell growth *via* chemical signaling, but also to probe their electrical responsiveness is currently under development in our laboratory.

We have developed a method of fabricating patterned cell culture electrode arrays using photolithography and they are being investigated as a high-throughput method of testing cell interactions with biomolecules. The system consists of a sensor chip that contains 16 sets of interdigitated stimulating electrodes, each set within a separate cell culture well (Figure 7.1a). Each electrode in the pair can be individually addressed and separately patterned with CP. In a preliminary experiment, one electrode was patterned with a GO/PEDOT nanocomposite loaded with γ-aminobutyric acid (GABA), an inhibitory neurotransmitter involved in neuronal differentiation and maturation during development, and the second electrode was deposited with PEDOT/PSS (Figure 7.1b). NSCs seeded on the surface of the patterned electrodes in differentiation media for 4 d exhibited markedly increased neuronal differentiation and neurite

outgrowth on the GO/PEDOT-GABA electrode, compared to the PEDOT/PSS electrode (Figure 7.1b). These data demonstrate the potential that this system has for patterning cell growth by providing spatially specific cues to the cells as immobilized molecules on the surface of the electrodes. In this case, GABA molecules were loaded into the CP film as co-dopants with GO nanosheets, but this method is limited to small molecules that carry a negative charge, which function best as dopants. Future work will include covalent immobilization of cues on the surface of the electrodes using the carbodiimide conjugation method described in *Chapter 2* and *Chapter 3*, which will enable the use of larger molecules, such as mitogens or extracellular matrix proteins.

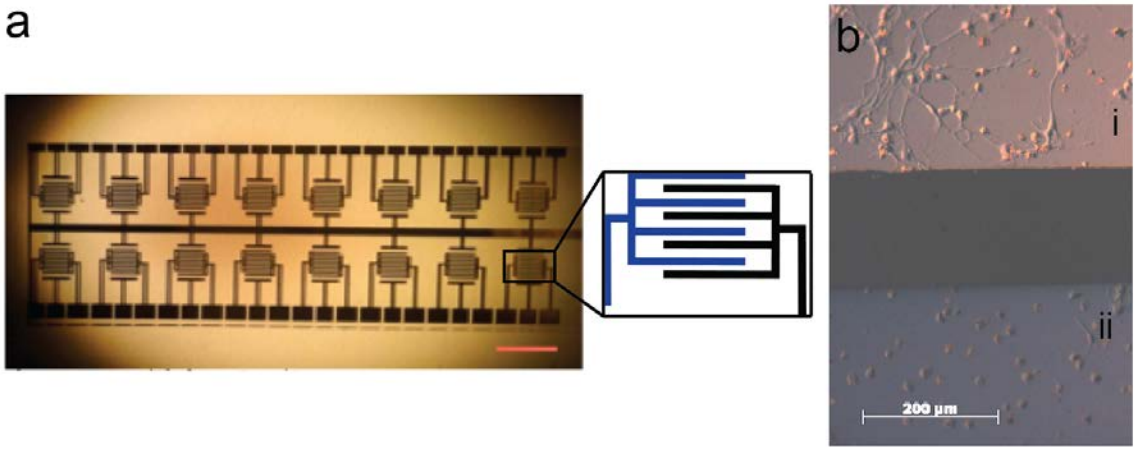

Figure 7.1. Cell Patterning on Electrode Arrays. (a) Image of the patterned cell culture array showing the 16 separate cell culture locations. Scale bar measure 10 mm. Inset shows the interdigitated electrode pattern at each cell culture location. (b) Brightfield image of NSCs on the surface of patterned electrodes after 4 d in differentiation media. Electrode (i) is modified with GO/PEDOT-GABA and electrode (ii) is modified with PEDOT/PSS. Cells on electrode (i) exhibit more neuronal differentiation, indicated by the extensive neurite outgrowth, compared to cells on electrode (ii) where most cells are spheroid in shape and few have extended neurites.

Using this cell culture array platform, or MEAs patterned with microelectrodes, a plethora of experiments could be designed that integrate cell patterning along with electrical stimulation and recording of cultured neuronal networks or NSCs. Important points to consider when patterning immobilized cues on the surface of functional electrodes are 1) how electrical stimulation will affect the molecule, and 2) how the molecule will affect the recording ability of the electrode. There is a possibility that a current passing through the electrode will destabilize the linkage between the molecule and the film surface. Additionally, depending on the type of biomolecule used, there is a possibility that the electrical stimulation could denature or degrade the molecule, rendering it inactive. Future work must establish the stability of candidate biomolecules in response to electrical stimulation, ensuring the feasibility of this method of surface patterning in conjunction with electrical stimulation. Additionally, after the cross-linking procedure, the electrical properties of the CP film must be monitored to ensure that the modified electrodes will be able to successfully record electrical signals from populations of cells growing on their surface. A common way to evaluate the performance of a recording electrode is by measuring the 1 kHz impedance value, which should be less than 1 MΩ to obtain a reliable neural signal [4]. The deposition of a non-conductive molecule at the surface of the electrode can increase the impedance value of the electrode by blocking charge transfer between the electrolyte and electrode surface. Impedance data collected after the covalent immobilization of a small peptide p20 on the surface of a microwire electrode slightly increased the 1 kHz impedance value, but it still remained well below the 1 MΩ cutoff (Figure 2.8a). There is a possibility that larger biomolecules, such as IFNγ or PDGF investigated in *Chapter 3*, could have a more significant effect on the impedance, resulting in poor electrical recording performance. Future

work investigating these potential pitfalls is warranted to ensure the success of the integrated cell patterning and electrical recording/stimulation platform.

7.2.2 Controlled Drug Release from GO/CP Nanocomposite

A major limitation of CP-based drug release platforms is that the system generally functions best with anionic drug molecules. In traditional CP-based drug release, the anionic drug molecules incorporate into the CP film as dopants. This mechanism provides a great system for controlled release of anionic drug molecules, but achieving release of cationic or neutral species is more difficult. One approach that has been successful in achieving cationic drug release is to synthesize a CP film that is doped with a large, immobile dopant, such as PSS, and then load the cationic drug into the intact film during reduction of the backbone [36, 284, 285]. Because the large dopant is immobile and cannot move out of the film, the cationic drug molecule will move in to balance the charge. In the case of neutral drug molecules, one successful method utilized was to create CP films doped with biotin that was then bound to streptavidin, enabling the loading of biotinylated NGF [286], which could then be released in response to electrical stimulation. In both of these methods, drug loading is limited to the surface of the CP, potentially decreasing the quantity of drug that can be release from the film. Additionally, in the case of the biotin/streptavidin-mediated drug loading and release, the drug molecules must be biotinylated, a process that can potentially interrupt their bioactivity.

The GO/CP drug delivery system described in *Chapter 4* has the potential to enable the incorporation and release of both cationic and neutral drug molecules. The GO nanosheets can act as "nanocarriers" by adsorbing the drug molecules *via* electrostatic or hydrophobic interactions and then shuttling them into the CP film during synthesis. Preliminary work being

carried out in our laboratory is exploring the possibility of using this GO/CP system for loading and delivering acetylcholine (ACh), the active neurotransmitter at neuromuscular junctions. The results have thus far been promising, indicating the successful loading and release of cationic ACh. Future work will investigate the ability of the GO/CP nanocomposite to load and release neutral drug molecules, as well as the potential of the system to perform selective release of dual-loaded drug molecules exhibiting different charges.

7.2.3 *In vivo* DA Detection with GO/CP-Modified Electrodes

While macroelectrodes are sufficient for assaying DA concentrations in large volume biological samples as a general screening tool for disease states [220, 221], these electrodes cannot be used *in vivo* to obtain spatially or temporally precise information about DA levels because of their large size. Carbon fiber microelectrodes (CFMEs) are the gold standard used for *in vivo* analysis of DA signaling within the CNS [222]. The concentration of DA within the CNS ranges from nanomolar to low micromolar, requiring highly sensitive analytical methods. Traditional CFMEs can reach this sensitivity level when their surface area is sufficiently high, a property that is controlled by the length of the CFME. However, as the length of the CFME increases to meet minimum sensitivity requirements, the size of the population of cells from which the electrode assays also increases, resulting in the low spatial specificity of current DA analysis methods. Consequently, there is a growing interest in electrode modifications that can improve the sensitivity to DA oxidation while maintaining or decreasing the total size of the electrode.

Our laboratory is currently applying the GO/CP nanocomposite film to CFMEs for use in *in vivo* applications. GO/PEDOT nanocomposite films were deposited onto the CFME and, interestingly, exhibited a very different morphology than what was observed on the

macroelectrode under similar synthesis parameters (Figure 7.2a; refer to Figure 5.1a for macroelectrode morphology). This difference implies that the GO/CP electrodeposition process varies significantly depending on the size of the electrode despite the polymerization procedure being analogous. We hypothesis that this effect occurs 1) based on the differing geometry of the electrodes, with the CFME exhibiting a cylindrical shape, while the macroelectrode exhibits a disc shape or 2) based on the relative size ratio between the electrodes and the GO nanosheets, which would be much lower in the case of the CFMEs, creating a different deposition pattern. However, the true mechanism behind the differences is unknown and will be the subject of future investigation.

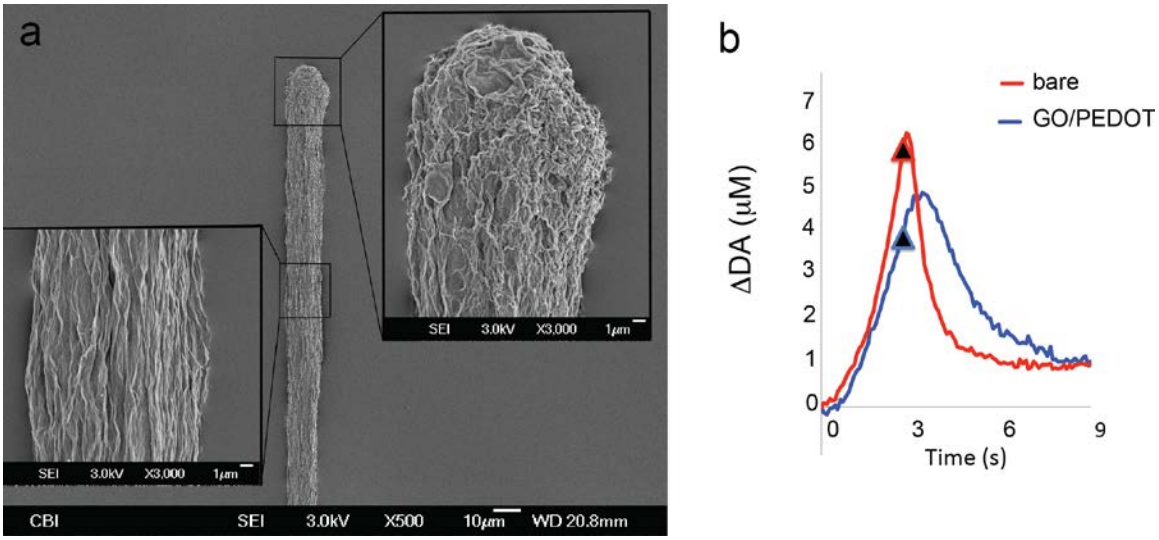

Figure 7.2. *In vivo* detection of DA signals using GO/CP-modified CFMEs. (a) SEM image of the GO/PEDOT-modified CFME showing a wrinkled-sheet morphology. (b) Recorded DA signal in the striatum of rat in response to electrical stimulation to the ipsilateral medial forebrain bundle. Stimulation begins at t = 0 and ends at the arrow marker on the curves. Bare electrode (*n* = 3); GO/PEDOT electrode (*n* = 1).

Using the GO/CP-modified CFMEs, preliminary *in vivo* data was collected from the striatum of an anesthetized Sprague-Dawley rat at collaborator Dr. Adrian Michael's laboratory in the Department of Chemistry at the University of Pittsburgh. The change in DA signal was monitored using fast scan cyclic voltammetry after the application of electrical stimulation to the ipsilateral medial forebrain bundle, which contains nigrostriatal DA fibers that project to the striatum [287]. The preliminary results indicate that the GO/CP nanocomposite has the sensitivity required to detect *in vivo* DA signals (Figure 7.2b). With future work to optimize the deposition parameters of the nanocomposite onto CFMEs, it is possible that we may achieve the boosted sensitivity toward DA that was observed using the GO/CP-modified macroelectrodes.

7.2.4 Neural Recording and Stimulation with GO/CP

The work described in this dissertation focuses on the chemical interfacing abilities of the GO/CP nanocomposite, but the material must also have the ability to stimulate and record electrical signals to function as a successful neural interfacing material. The electrical properties of the GO/CP nanocomposite described here and by others [161-163] indicate that the material should be able to record electrical activity from neurons with high signal-to-noise ratio, but none have yet demonstrated this capability, either *in vitro* or *in vivo*. We have begun preliminary work to evaluate the neural recording performance of the GO/CP both *in vitro* with CNNs cultured on MEAs and *in vivo* with microwire electrodes implanted into the visual cortex of mice. The GO/CP-modified microwire electrodes have successfully recorded spontaneous and visually-evoked activity from the visual cortex, but it has yet to be determined whether the GO/CP-modified microwires exhibit higher signal-to-noise ratios than the unmodified microwires. Future work to compare the performance of the GO/CP-modified electrodes to bare electrodes is

planned and will characterize the full benefit of using the nanocomposite as a multimodal neural interfacing material.

Electrical stimulation of neural tissue holds great therapeutic potential for a variety of neurological disorders and is currently utilized in clinical applications such as deep brain stimulation for treatment of Parkinson's disease [288] or auditory nerve stimulation in cochlear implant technologies [289]. Nanostructured polymer materials have been explored as modifications to stimulating neural electrodes as a means of improving the surface area and charge injection capability, which results in safer stimulation paradigms for biological tissues [4, 290]. The GO/PEDOT nanocomposite exhibits rough surface morphology (Figures 2.2, 3.1, and 5.1a) and low impedance (Figures 2.8a and 5.1c) indicating that the material may demonstrate a large charge injection capacity that will reduce the voltage excursion of the stimulation and reduce potential damage to surrounding tissue. Future studies characterizing the performance of GO/CP-modified microelectrodes for neural stimulation are planned to assess its full potential as a neural interfacing material.

7.2.5 Continued Development of CNN Damage Platform

While the results reported in *Chapter 6* regarding the use of the MEA-based CNN as an *in vitro* damage and regeneration model were promising, the sample size for each experimental group was low and must be increased to establish a more confident assessment of the injury and possible repair by NSCs. Additionally, there are several injury characterizations that would assist in validating the model. For example, following an injury to the CNS, secondary molecular pathways are initiated that lead to continuing cell necrosis and apoptosis after the initial insult [257]. As a method to determine the validity of this *in vitro* model, the extent of degeneration

around the injury should be evaluated, along with the viability of the surviving cells, reactive oxygen species production and other characteristic markers of CNS injury. Qualitative assessment of the injury site after the injury revealed that the size of the "dead zone," where there were no cells growing, increased for at least the first week after injury. Additionally, cells exhibiting morphology associated with astrocytes were seen to infiltrate the damage zone, potentially to create a glial scar around the damage site [291]. Inhibitory factors released from the glial scar *in vivo* are thought to impede neurons from regenerating following injury, making the glial scar a focus of study in regenerative medicine [292]. If a glial scar is, in fact, forming in the *in vitro* injury model, it could provide a valuable platform for studying the physiology of the scar and testing the effect of potential interventions.

NSC transplantation following injury to the CNS *in vivo* can result in functional recovery, but the mechanism of the therapeutic effect is thought to be largely due to released neurotrophic factors protecting existing cells from damage rather than cell replacement bridging damaged circuitry [281, 282]. Our *in vitro* transplantation results support the idea of neuroprotection *via* secreted factors because improved CNN activity is observed as soon as 1 day post injury (DPI), too soon for NSCs to differentiate into functional neurons [98]. To confirm that NSCs are secreting protective factors, damaged CNNs will be treated with NSC conditioned media or neurotrophic factors to evaluate the protective effect on CNN activity. While our data suggest that the immediate effects are due to secreted factors, NSCs may differentiate into functional cells that will have effects at longer time periods, possibly by integrating into the damaged circuitry. Current experiments are underway to evaluate the therapeutic effects of NSCs on damaged CNNs for up to 20 DPI. The transplanted NSCs will be tracked using live-cell fluorescent labeling coupled with endpoint immunocytochemistry to evaluate their survival and

differentiation patterns with the goal of providing information that will lead to more effective cellular therapies for the treatment of CNS injury.

7.2.6 Concluding Remarks: Towards a Highly Customizable Platform for the Multimodal Study of Neuronal Injury

The CNS is a hugely complicated organ system, considered by some to be the "last frontier" in science because of the relatively limited amount of understanding we currently have about its physiology. This dissertation presents a body of work that demonstrates the highly versatile applications of GO/CP nanocomposite-modified electrodes within the field of neural engineering that can be used to create a window into the intricate processes that form a basis for human behavior and cognition. This work, along with the described *in vitro* regeneration model, provides a framework for studying the complex pathology of neuronal injury or disease in a simplified, controllable fashion. By combining the full functionality of the GO/CP nanocomposite material with the MEA-based regeneration model, a multimodal platform for studying injury can be created that has the ability to monitor electrical and chemical changes following injury, in conjunction with testing the efficacy of various soluble or immobilized therapeutics that can be presented to the dish in a highly temporally and spatially precise manner. Various parameters in the platform (injury severity, cell type, chemical cues) can be tuned, making the device a powerful research tool for elucidating the pathology of neuronal injury and regeneration.

APPENDIX A

A.1 SUPPORTING INFORMATION FOR CHAPTER 4

To verify that both GO nanosheets and DEX were incorporated into the PPy film, Fourier transform IR (FTIR) spectroscopy was performed on the pure GO nanosheets, and GO/PPy nanocomposite films with or without DEX as a co-dopant (Figure A1.1). The GO nanosheet spectrum exhibits characteristic peaks arising from oxygen-containing moieties (carboxylic C=O: 1736 cm^{-1}; O-H deformation: 1406 cm^{-1}; C-O-H stretch: 1221 cm^{-1}; C-O-C stretching vibration: 1043 cm^{-1})[90]. The electrodeposited GO/PPy film spectrum contains a carboxylic carbonyl peak at 1705 cm^{-1}, attributable to GO, along with characteristic PPy peaks at 1472 cm^{-1} (C-N stretching vibration) and 964 cm^{-1} (N-H wag), confirming the successful incorporation of the GO nanosheets into the polymer[161]. The spectrum of the film synthesized in the presence of both GO and DEX molecules (GO/PPy-DEX) exhibits an additional carbonyl peak at 1657 cm^{-1} that arises from the carbonyl group conjugated to the double bond framework of the DEX molecule, along with a peak at 1146 cm^{-1}, assigned to the DEX phosphate group[293].

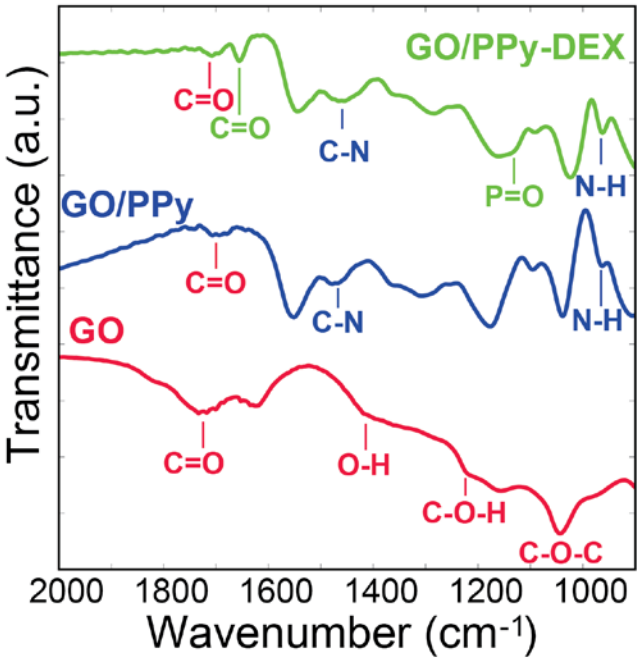

Figure A1.1. FTIR spectra of GO nanosheets, unloaded GO/PPy, and DEX-loaded GO/PPy. On each spectrum, peaks labeled in red are contributed by GO, blue by PPy, and green by DEX.

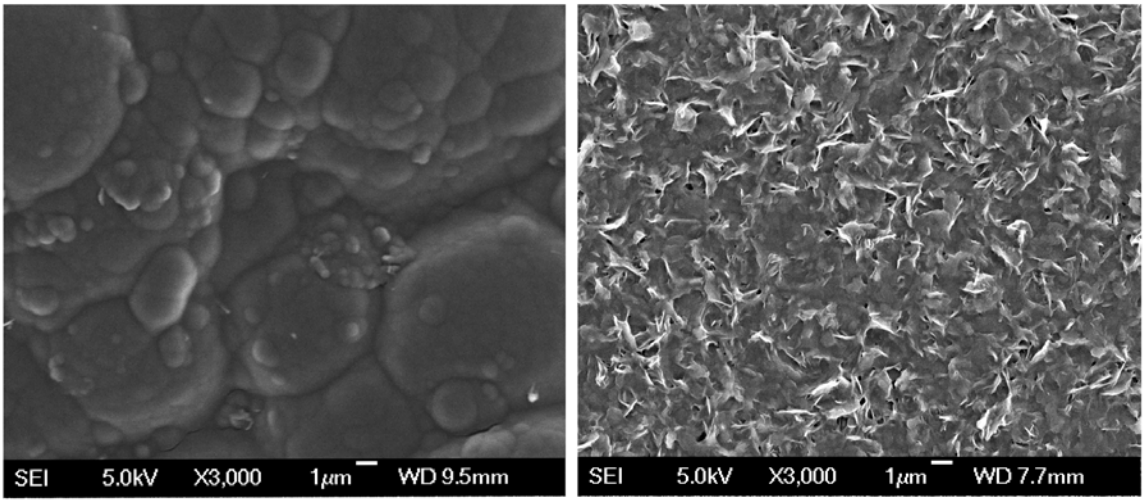

Figure A1.2. Surface morphology of DEX-loaded PPy films. Representative SEM images of a conventional DEX-loaded PPy film (left) and a DEX-loaded GO/PPy nanocomposite film (right). The conventional film exhibits a much smoother morphology than the nanocomposite that contains rough sheet-like protrusions at its surface.

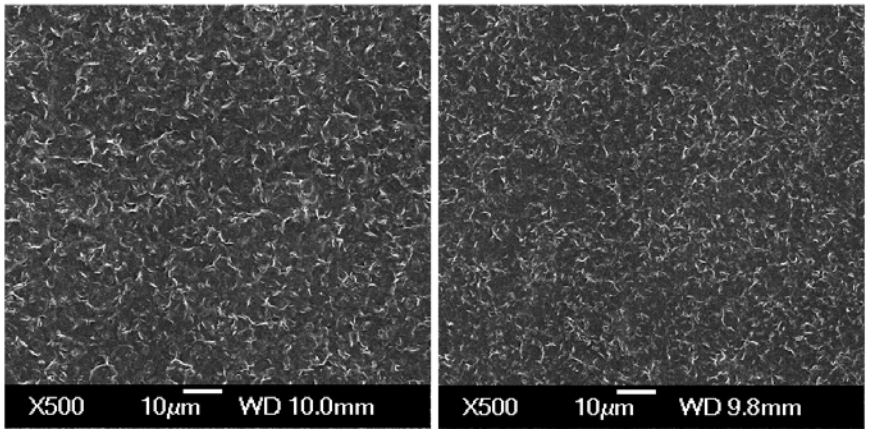

Figure A1.3. Stability of the DEX-loaded GO/PPy nanocomposite film. SEM images of the GO/PPy-DEX film before (left panel) and after (right panel) 1000 release stimulations (-0.5 V for 5 s, followed by 0.5 V for 5 s). There is no visible cracking or delamination of the film post-stimulation, demonstrating the good stability of the film.

BIBLIOGRAPHY

[1] Beck EC. Electrophysiology and Behavior. Annu Rev Psychol. 1975;26:233-62.

[2] Mukamel R, Fried I. Human intracranial recordings and cognitive neuroscience. Annu Rev Psychol. 2012;63:511-37.

[3] Strumwasser F. Long-term recording from single neurons in brain of unrestrained mammals. Science. 1958;127:469-70.

[4] Cogan SF. Neural stimulation and recording electrodes. Annu Rev Biomed Eng. 2008;10:275-309.

[5] Schwartz AB, Cui XT, Weber DJ, Moran DW. Brain-controlled interfaces: Movement restoration with neural prosthetics. Neuron. 2006;52:205-20.

[6] Merrill DR, Bikson M, Jefferys JG. Electrical stimulation of excitable tissue: design of efficacious and safe protocols. J Neurosci Meth. 2005;141:171-98.

[7] Letheby H. On the production of a blue substance by the eletrolysis of sulphate of aniline. J Chem Soc. 1862;15:161-3.

[8] Angelopoulos M. Conducting polymers in microelectronics. IBM J Res Dev. 2001;45:57-75.

[9] Feng C, Wan Q, Lv Z, Yue X, Chen Y, Wei C. One-step fabrication of membraneless microbial fuel cell cathode by electropolymerization of polypyrrole onto stainless steel mesh. Biosens Bioelectron. 2011.

[10] Gerard M, Chaubey A, Malhotra BD. Application of conducting polymers to biosensors. Biosens Bioelectron. 2002;17:345-59.

[11] Janata J, Josowicz M. Conducting polymers in electronic chemical sensors. Nature Mater. 2003;2:19-24.

[12] Luo SC. Conducting polymers as biointerfaces and biomaterials: A perspective for a special issue of polymer reviews. Polym Rev. 2013;53:303-10.

[13] Ateh DD, Navsaria HA, Vadgama P. Polypyrrole-based conducting polymers and interactions with biological tissues. J R Soc Interface. 2006;3:741-52.

[14] Cui X, Hetke JF, Wiler JA, Anderson DJ, Martin DC. Electrochemical deposition and characterization of conducting polymer polypyrrole/PSS on multichannel neural probes. Sensor Actuat A-Physical. 2001;93:8-19.

[15] Cui XT, Zhou DD. Poly (3,4-ethylenedioxythiophene) for chronic neural stimulation. IEEE T Neur Sys Reh. 2007;15:502-8.

[16] Green RA, Lovell NH, Wallace GG, Poole-Warren LA. Conducting polymers for neural interfaces: challenges in developing an effective long-term implant. Biomaterials. 2008;29:3393-9.

[17] Ludwig KA, Langhals NB, Joseph MD, Richardson-Burns SM, Hendricks JL, Kipke DR. Poly(3,4-ethylenedioxythiophene) (PEDOT) polymer coatings facilitate smaller neural recording electrodes. J Neur Eng. 2011;8:014001.

[18] Richardson-Burns SM, Hendricks JL, Foster B, Povlich LK, Kim DH, Martin DC. Polymerization of the conducting polymer poly(3,4-ethylenedioxythiophene) (PEDOT) around living neural cells. Biomaterials. 2007;28:1539-52.

[19] Venkatraman S, Hendricks J, King ZA, Sereno AJ, Richardson-Burns S, Martin D, et al. In vitro and in vivo evaluation of PEDOT microelectrodes for neural stimulation and recording. IEEE T Neur Sys Reh. 2011;19:307-16.

[20] Inzelt G. Conducting polymers : a new era in electrochemistry. 1st ed. New York: Springer; 2008.

[21] Malinauskas A. Chemical deposition of conducting polymers. Polymer. 2001;42:3957-72.

[22] Heinze J, Frontana-Uribe BA, Ludwigs S. Electrochemistry of conducting polymers--persistent models and new concepts. Chem Rev. 2010;110:4724-71.

[23] Niu L, Kvarnstrom C, Froberg K, Ivaska A. Electrochemically controlled surface morphology and crystallinity in poly(3,4-ethylenedioxythiophene) films. Synthetic Met. 2001;122:425-9.

[24] Castagnola V, Bayon C, Descamps E, Bergaud C. Morphology and conductivity of PEDOT layers produced by different electrochemical routes. Synthetic Met. 2014;189:7-16.

[25] Chiang CK, Fincher CR, Park YW, Heeger AJ, Shirakawa H, Louis EJ, et al. Electrical conductivity in doped polyacetylene. Phys Rev Lett. 1977;39:1098-101.

[26] Gill WD, Bludau W, Geiss RH, Grant PM, Greene RL, Mayerle JJ, et al. Structure and electronic properties of polymeric sulfur nitride (SN)x modified by bromine. Physical Rev Lett. 1977;38:1305.

[27] Walatka VV, Labes MM. Polysulfur nitiride - A one-dimensional chain with a metallic ground state. Phys Rev Lett. 1973;31:1139-42.

[28] Wallace GG. Conductive electroactive polymers : intelligent polymer systems. 3rd ed. Boca Raton: CRC Press; 2009.

[29] Bredas JL, Street GB. Polarons, bipolarons, and solitons in conducting polymers. Accounts Chem Res. 1985;18:309-15.

[30] Han D-H, Lee HJ, Park S-M. Electrochemistry of conductive polymers XXXV: Electrical and morphological characteristics of polypyrrole films prepared in aqueous media studied by current sensing atomic force microscopy. Electrochim Acta. 2005;50:3085-92.

[31] King ZA, Shaw CM, Spanninga SA, Martin DC. Structural, chemical and electrochemical characterization of poly(3,4-Ethylenedioxythiophene) (PEDOT) prepared with various counter-ions and heat treatments. Polymer. 2011;52:1302-8.

[32] Kontturi K, Pentti P, Sundholm G. Polypyrrole as a model membrane for drug delivery. J Electroanal Chem. 1998;453:231-8.

[33] Miller LL, Zinger B, Zhou QX. Electrically controlled release of Fe(Cn)6(4-) from polypyrrole. J Am Chem Soc. 1987;109:2267-72.

[34] Svirskis D, Travas-Sejdic J, Rodgers A, Garg S. Electrochemically controlled drug delivery based on intrinsically conducting polymers. J Control Release. 2010;146:6-15.

[35] Thompson BC, Moulton SE, Ding J, Richardson R, Cameron A, O'Leary S, et al. Optimising the incorporation and release of a neurotrophic factor using conducting polypyrrole. J Control Release. 2006;116:285-94.

[36] Tybrandt K, Larsson KC, Kurup S, Simon DT, Kjall P, Isaksson J, et al. Translating electronic currents to precise acetylcholine-induced neuronal signaling using an organic electrophoretic delivery device. Adv Mater. 2009;21:4442-6.

[37] Yue Z, Moulton SE, Cook M, O'Leary S, Wallace GG. Controlled delivery for neuro-bionic devices. Adv Drug Deliver Rev. 2013;65:559-69.

[38] Asplund M, von Holst H, Inganas O. Composite biomolecule/PEDOT materials for neural electrodes. Biointerphases. 2008;3:83-93.

[39] Collier JH, Camp JP, Hudson TW, Schmidt CE. Synthesis and characterization of polypyrrole-hyaluronic acid composite biomaterials for tissue engineering applications. J Biomed Mater Res. 2000;50:574-84.

[40] Cui X, Lee VA, Raphael Y, Wiler JA, Hetke JF, Anderson DJ, et al. Surface modification of neural recording electrodes with conducting polymer/biomolecule blends. J Biomed Mater Res. 2001;56:261-72.

[41] Cui X, Wiler J, Dzaman M, Altschuler RA, Martin DC. In vivo studies of polypyrrole/peptide coated neural probes. Biomaterials. 2003;24:777-87.

[42] Green RA, Lovell NH, Poole-Warren LA. Impact of co-incorporating laminin peptide dopants and neurotrophic growth factors on conducting polymer properties. Acta Biomater. 2010;6:63-71.

[43] Warren LF, Walker JA, Anderson DP, Rhodes CG. A study of conducting polymer morphology: the effect of dopant anions upon order. J Electrochem Soc. 1989;136:2286-95.

[44] Zhang L, Stauffer WR, Jane EP, Sammak PJ, Cui XT. Enhanced differentiation of embryonic and neural stem cells to neuronal fates on laminin peptides doped polypyrrole. Macromol Biosci. 2010;10:1456-64.

[45] Balint R, Cassidy NJ, Cartmell SH. Conductive polymers: Towards a smart biomaterial for tissue engineering. Acta Biomater. 2014.

[46] Bendrea AD, Cianga L, Cianga I. Review paper: Progress in the field of conducting polymers for tissue engineering applications. J Biomater Appl. 2011;26:3-84.

[47] Ravichandran R, Sundarrajan S, Venugopal JR, Mukherjee S, Ramakrishna S. Applications of conducting polymers and their issues in biomedical engineering. J R Soc Interface. 2010;7 Suppl 5:S559-79.

[48] Weber SG. Signal-to-noise ratio in microelectrode-array-based electrochemical detectors. Anal Chem. 1989;61:295-302.

[49] Abidian MR, Ludwig KA, Marzullo TC, Martin DC, Kipke DR. Interfacing conducting polymer nanotubes with the central nervous system: chronic neural recording using poly (3,4-ethylenedioxythiophene) nanotubes. Adv Mater. 2009;21:3764-70.

[50] Stauffer WR, Cui XT. Polypyrrole doped with 2 peptide sequences from laminin. Biomaterials. 2006;27:2405-13.

[51] Novoselov KS, Geim AK, Morozov SV, Jiang D, Zhang Y, Dubonos SV, et al. Electric field effect in atomically thin carbon films. Science. 2004;306:666-9.

[52] Park S, Ruoff RS. Chemical methods for the production of graphenes. Nat Nanotechnol. 2009;4:217-24.

[53] Dreyer DR, Park S, Bielawski CW, Ruoff RS. The chemistry of graphene oxide. Chem Soc Rev. 2010;39:228-40.

[54] Hummers WS, Offeman RE. Preparation of Graphitic Oxide. J Am Chem Soc. 1958;80:1339.

[55] Stankovich S, Dikin DA, Piner RD, Kohlhaas KA, Kleinhammes A, Jia Y, et al. Synthesis of graphene-based nanosheets via chemical reduction of exfoliated graphite oxide. Carbon. 2007;45:1558-65.

[56] Park S, Ruoff RS. Chemical methods for the production of graphenes. Nat Nanotechnol. 2009;4:217-24.

[57] He HY, Riedl T, Lerf A, Klinowski J. Solid-state NMR studies of the structure of graphite oxide. J Phys Chem. 1996;100:19954-8.

[58] Gao W, Alemany LB, Ci LJ, Ajayan PM. New insights into the structure and reduction of graphite oxide. Nat Chem. 2009;1:403-8.

[59] Pyun J. Graphene Oxide as Catalyst: Application of Carbon Materials beyond Nanotechnology. Angew Chem Int Edit. 2011;50:46-8.

[60] Stergiou DV, Diamanti EK, Gournis D, Prodromidis MI. Comparitive study of different types of graphenes as electrocatalysts for ascorbic acid. Electrochem Commun. 2010;12:1307-9.

[61] Dhakshinamoorthy A, Alvaro M, Concepcion P, Fornes V, Garcia H. Graphene oxide as an acid catalyst for the room temperature ring opening of epoxides. Chem Commun. 2012;48:5443-5.

[62] Dreyer DR, Jia HP, Bielawski CW. Graphene oxide: a convenient carbocatalyst for facilitating oxidation and hydration reactions. Angew Chem Int Edit. 2010;49:6813-6.

[63] Chen D, Feng HB, Li JH. Graphene oxide: preparation, functionalization, and electrochemical applications. Chem Rev. 2012;112:6027-53.

[64] Wang Y, Li Z, Wang J, Li J, Lin Y. Graphene and graphene oxide: biofunctionalization and applications in biotechnology. Trend Biotechnol. 2011;29:205-12.

[65] Zhang Y, Nayak TR, Hong H, Cai WB. Graphene: a versatile nanoplatform for biomedical applications. Nanoscale. 2012;4:3833-42.

[66] Bolotin KI, Sikes KJ, Jiang Z, Klima M, Fudenberg G, Hone J, et al. Ultrahigh electron mobility in suspended graphene. Solid State Comm. 2008;146:351-5.

[67] Eda G, Fanchini G, Chhowalla M. Large-area ultrathin films of reduced graphene oxide as a transparent and flexible electronic material. Nat Nanotechnol. 2008;3:270-4.

[68] Gilgunn PJ, Khilwani R, Kozai TDY, Weber DJ, Cui XT, Erdos G, et al. An ultra-compliant, scalable neural probe with molded biodissolvable delivery vehicle. Proc IEEE Micr Elect. 2012:56-9.

[69] Chen CH, Lin CT, Hsu WL, Chang YC, Yeh SR, Li LJ, et al. A flexible hydrophilic-modified graphene microprobe for neural and cardiac recording. Nanomedicine-UK. 2013;9:600-4.

[70] Chiu C, He X, Liang H. Surface modification of a neural sensor using graphene. Electrochim Acta. 2013;94:42-8.

[71] Hong SW, Lee JH, Kang SH, Hwang EY, Hwang Y-S, Lee MH, et al. Enhanced neural cell adhesion and neurite outgrowth on graphene-based biomimetic substrates. Biomed Res Int. 2014;2014:212149.

[72] Kim SM, Joo P, Ahn G, Cho IH, Kim DH, Song WK, et al. Transparent conducting films based on reduced graphene oxide multilayers for biocompatible neuronal interfaces. J Biomed Nanotechnol. 2013;9:403-8.

[73] Li N, Zhang XM, Song Q, Su RG, Zhang Q, Kong T, et al. The promotion of neurite sprouting and outgrowth of mouse hippocampal cells in culture by graphene substrates. Biomaterials. 2011;32:9374-82.

[74] Zhou K, Thouas GA, Bernard CC, Nisbet DR, Finkelstein DI, Li D, et al. Method to impart electro- and biofunctionality to neural scaffolds using graphene-polyelectrolyte multilayers. ACS Appl Mater Interfaces. 2012;4:4524-31.

[75] Lu CH, Hsiao YS, Kuo CW, Chen P. Electrically tunable organic bioelectronics for spatial and temporal manipulation of neuron-like pheochromocytoma (PC-12) cells. Biochim Biophys Acta. 2013;1830:4321-8.

[76] Heo C, Yoo J, Lee S, Jo A, Jung S, Yoo H, et al. The control of neural cell-to-cell interactions through non-contact electrical field stimulation using graphene electrodes. Biomaterials. 2011;32:19-27.

[77] Tang ML, Song Q, Li N, Jiang ZY, Huang R, Cheng GS. Enhancement of electrical signaling in neural networks on graphene films. Biomaterials. 2013;34:6402-11.

[78] Tu Q, Pang L, Chen Y, Zhang Y, Zhang R, Lu B, et al. Effects of surface charges of graphene oxide on neuronal outgrowth and branching. Analyst. 2014;139:105-15.

[79] Tu Q, Pang L, Wang L, Zhang Y, Zhang R, Wang J. Biomimetic choline-like graphene oxide composites for neurite sprouting and outgrowth. ACS Appl Mater Interfaces. 2013;5:13188-97.

[80] Luo X, Weaver CL, Tan S, Cui XT. Pure graphene oxide doped conducting polymer nanocomposite for bio-interfacing. J Mater Chem B. 2013;1:1340-8.

[81] Weaver CL, Larosa JM, Luo X, Cui XT. Electrically Controlled Drug Delivery from Graphene Oxide Nanocomposite Films. ACS Nano. 2014.

[82] Huang X, Yin ZY, Wu SX, Qi XY, He QY, Zhang QC, et al. Graphene-based materials: synthesis, characterization, properties, and applications. Small. 2011;7:1876-902.

[83] Loh KP, Bao QL, Eda G, Chhowalla M. Graphene oxide as a chemically tunable platform for optical applications. Nat Chem. 2010;2:1015-24.

[84] Zhu Y, Murali S, Cai W, Li X, Suk JW, Potts JR, et al. Graphene and graphene oxide: synthesis, properties, and applications. Adv Mater. 2010;22:3906-24.

[85] Alwarappan S, Boyapalle S, Kumar A, Li CZ, Mohapatra S. Comparative study of single-, few-, and multi layered graphene toward enzyme conjugation and electrochemical response. J Phys Chem C. 2012;116:6556-9.

[86] Alwarappan S, Erdem A, Liu C, Li CZ. Probing the electrochemical properties of graphene nanosheets for biosensing applications. J Phys Chem C. 2009;113:8853-7.

[87] Alwarappan S, Joshi RK, Ram MK, Kumar A. Electron transfer mechanism of cytochrome c at graphene electrode. Appl Phys Lett. 2010;96.

[88] Alwarappan S, Liu C, Kumar A, Li CZ. Enzyme-doped graphene nanosheets for enhanced glucose biosensing. J Phys Chem C. 2010;114:12920-4.

[89] Kalbacova M, Broz A, Kalbac M. Influence of the fetal bovine serum proteins on the growth of human osteoblast cells on graphene. J Biomed Mater Res A. 2012;100A:3001-7.

[90] Zhu CZ, Zhai JF, Wen D, Dong SJ. Graphene oxide/polypyrrole nanocomposites: one-step electrochemical doping, coating and synergistic effect for energy storage. J Mater Chem. 2012;22:6300-6.

[91] Depan D, Girase B, Shah JS, Misra RDK. Structure-process-property relationship of the polar graphene oxide-mediated cellular response and stimulated growth of osteoblasts on hybrid chitosan network structure nanocomposite scaffolds. Acta Biomater. 2011;7:3432-45.

[92] Pan YZ, Sahoo NG, Li L. The application of graphene oxide in drug delivery. Expert Opin Drug Del. 2012;9:1365-76.

[93] Ruiz ON, Fernando KAS, Wang BJ, Brown NA, Luo PG, McNamara ND, et al. Graphene oxide: a nonspecific enhancer of cellular growth. ACS Nano. 2011;5:8100-7.

[94] Zhou M, Zhai YM, Dong SJ. Electrochemical sensing and biosensing platform based on chemically reduced graphene oxide. Anal Chem. 2009;81:5603-13.

[95] Hu W, Peng C, Lv M, Li X, Zhang Y, Chen N, et al. Protein corona-mediated mitigation of cytotoxicity of graphene oxide. ACS Nano. 2011;5:3693-700.

[96] Wang K, Ruan J, Song H, Zhang JL, Wo Y, Guo SW, et al. Biocompatibility of graphene oxide. Nano Res Lett. 2011;6.

[97] Lee WC, Lim CH, Shi H, Tang LA, Wang Y, Lim CT, et al. Origin of enhanced stem cell growth and differentiation on graphene and graphene oxide. ACS Nano. 2011;5:7334-41.

[98] Singh SK, Singh MK, Kulkarni PP, Sonkar VK, Gracio JJA, Dash D. Amine-modified graphene. Thrombo-protective safer alternative to graphene oxide for biomedical applications. ACS Nano. 2012;6:2731-40.

[99] Wojtoniszak M, Chen XC, Kalenczuk RJ, Wajda A, Lapczuk J, Kurzewski M, et al. Synthesis, dispersion, and cytocompatibility of graphene oxide and reduced graphene oxide. Colloid Surface B. 2012;89:79-85.

[100] Istamboulie G, Sikora T, Jubete E, Ochoteco E, Marty JL, Noguer T. Screen-printed poly(3,4-ethylenedioxythiophene) (PEDOT): A new electrochemical mediator for acetylcholinesterase-based biosensors. Talanta. 2010;82:957-61.

[101] Rozlosnik N. New directions in medical biosensors employing poly(3,4-ethylenedioxy thiophene) derivative-based electrodes. Anal Bioanal Chem. 2009;395:637-45.

[102] Akoudad S, Roncali J. Modification of the electrochemical and electronic properties of electrogenerated poly(3,4-ethylenedioxythiophene) by hydroxymethyl and oligo(oxyethylene)substituents. Electrochem Commun. 2000;2:72-6.

[103] Ali EM, Kantchev EAB, Yu HH, Ying JY. Conductivity shift of polyethylenedioxythiophenes in aqueous solutions from side-chain charge perturbation. Macromolecules. 2007;40:6025-7.

[104] Arias-Pardilla J, Otero TF, Blanco R, Segura JL. Synthesis, electropolymerization and oxidation kinetics of an anthraquinone-functionalized poly(3,4-ethylenedioxythiophene). Electrochim Acta. 2010;55:1535-42.

[105] Luo SC, Ali EM, Tansil NC, Yu HH, Gao S, Kantchev EAB, et al. Poly(3,4-ethylenedioxythiophene) (PEDOT) nanobiointerfaces: thin, ultrasmooth, and functionalized PEDOT films with in vitro and in vivo biocompatibility. Langmuir. 2008;24:8071-7.

[106] Povlich LK, Cho JC, Leach MK, Corey JM, Kim J, Martin DC. Synthesis, copolymerization and peptide-modification of carboxylic acid-functionalized 3,4-ethylenedioxythiophene (EDOTacid) for neural electrode interfaces. BBA-Gen Subjects. 2013;1830:4288-93.

[107] Segura JL, Gomez R, Blanco R, Reinold E, Bauerle P. Synthesis and electronic properties of anthraquinone-, tetracyanoanthraquinodimethane-, and perylenetetracarboxylic diimide-functionalized poly(3,4-ethylenedioxythiophenes). Chem Mater. 2006;18:2834-47.

[108] Xie H, Luo SC, Yu HH. Electric-field-assisted growth of functionalized poly(3,4-ethylenedioxythiophene) nanowires for label-free protein detection. Small. 2009;5:2611-7.

[109] Roncali J. Electrogenerated functional conjugated polymers as advanced electrode materials. J Mater Chem. 1999;9:1875-93.

[110] Brisset H, Navarro AE, Moustrou C, Perepichka IF, Roncali J. Electrogenerated conjugated polymers incorporating a ferrocene-derivatized-(3,4-ethylenedioxythiophene). Electrochem Commun. 2004;6:249-53.

[111] Doherty WJ, Wysocki RJ, Armstrong NR, Saavedra SS. Electrochemical copolymerization and spectroelectrochemical characterization of 3,4-ethylenedioxythiophene and 3,4-ethylenedioxythiophene-methanol copolymers on indium-tin oxide. Macromolecules. 2006;39:4418-24.

[112] Yildiz E, Camurlu P, Tanyeli C, Akhmedov I, Toppare L. A soluble conducting polymer of 4-(2,5-di(thiophen-2-yl)-1H-pyrrol-1-yl)benzenamine and its multichromic copolymer with EDOT. J Electroanal Chem. 2008;612:247-56.

[113] Abidian MR, Martin DC. Multifunctional nanobiomaterials for neural interfaces. Adv Funct Mater. 2009;19:573-85.

[114] Kim DH, Richardson-Burns SM, Hendricks JL, Sequera C, Martin DC. Effect of immobilized nerve growth factor on conductive polymers: electrical properties and cellular response. Adv Funct Mater. 2007;17:79-86.

[115] Jeong H-K, Lee YP, Lahaye RJWE, Park M-H, An KH, Kim IJ, et al. Evidence of graphitic AB stacking order of graphite oxides. J Am Chem Soc. 2008;130:1362-6.

[116] Shen JF, Hu YZ, Shi M, Lu X, Qin C, Li C, et al. Fast and facile preparation of graphene oxide and reduced graphene oxide nanoplatelets. Chem Mater. 2009;21:3514-20.

[117] Agarwal S, Zhou X, Ye F, He Q, Chen GC, Soo J, et al. Interfacing live cells with nanocarbon substrates. Langmuir. 2010;26:2244-7.

[118] Lv M, Zhang Y, Liang L, Wei M, Hu W, Li X, et al. Effect of graphene oxide on undifferentiated and retinoic acid-differentiated SH-SY5Y cells line. Nanoscale. 2012;4:3861-6.

[119] Ameen S, Akhtar MS, Shin HS. Hydrazine chemical sensing by modified electrode based on in situ electrochemically synthesized polyaniline/graphene composite thin film. Sensor Actuat B-Chem. 2012;173:177-83.

[120] Liesi P, Narvanen A, Soos J, Sariola H, Snounou G. Identification of a neurite outgrowth-promoting domain of laminin using synthetic peptides. FEBS Lett. 1989;244:141-8.

[121] Matsuzawa M, Liesi P, Knoll W. Chemically modifying glass surfaces to study substratum-guided neurite outgrowth in culture. J Neurosci Meth. 1996;69:189-96.

[122] Mohanty N, Berry V. Graphene-based single-bacterium resolution biodevice and DNA transistor: interfacing graphene derivatives with nanoscale and microscale biocomponents. Nano Lett. 2008;8:4469-76.

[123] Chen D, Li L, Guo L. An environment-friendly preparation of reduced graphene oxide nanosheets via amino acid. Nanotechnology. 2011;22:325601.

[124] Asplund M, Thaning E, Lundberg J, Sandberg-Nordqvist AC, Kostyszyn B, Inganas O, et al. Toxicity evaluation of PEDOT/biomolecular composites intended for neural communication electrodes. Biomed Mater. 2009;4:045009.

[125] Cui X, Martin DC. Electrochemical deposition and characterization of poly(3,4-ethylenedioxythiophene) on neural microelectrode arrays. Sensors Actuat A-Physical. 2003;89:92-102.

[126] Huber M, Heiduschka P, Klenle S, Pavlidis C, Mack J, Walk T, et al. Modification of glassy carbon surfaces with synthetic laminin-derived peptides for nerve cell attachment and neurite growth. J Biomed Mater Res. 1998;41:278-88.

[127] Powell SK, Kleinman HK. Neuronal laminins and their cellular receptors. Int J Biochem Cell Bio. 1997;29:401-14.

[128] Khan SP, Auner GG, Newaz GM. Influence of nanoscale surface roughness on neural cell attachment on silicon. Nanomedicine-UK. 2005;1:125-9.

[129] Walsh JF, Manwaring ME, Tresco PA. Directional neurite outgrowth is enhanced by engineered meningeal cell-coated substrates. Tissue Eng. 2005;11:1085-94.

[130] Hsiao M-C, Liao S-H, Yen M-Y, Liu P-I, Pu N-W, Wang C-A, et al. Preparation of covalently functionalized graphene using residual oxygen-containing functional groups. ACS Appl Mater Interfaces. 2010;2:3092-9.

[131] Jeong H-K, Noh H-J, Kim J-Y, Jin MH, Park CY, Lee YH. X-ray absorption spectroscopy of graphite oxide. EPL. 2008;82:67004.

[132] Xiao SJ, Textor M, Spencer ND, Wieland M, Keller B, Sigrist H. Immobilization of the cell-adhesive peptide arg-gly-asp-cys (RGDC) on titanium surfaces by covalent chemical attachment. J Mater Sci Mater Med. 1997;8:867-72.

[133] Pancrazio JJ. Neural interfaces at the nanoscale. Nanomedicine-UK. 2008;3:823-30.

[134] Peng C, Jin J, Chen GZ. A comparative study on electrochemical co-deposition and capacitance of composite films of conducting polymers and carbon nanotubes. Electrochim Acta. 2007;53:525-37.

[135] Alvarez-Buylla A, Garcia-Verdugo JM. Neurogenesis in adult subventricular zone. J Neurosci. 2002;22:629-34.

[136] Taupin P, Gage FH. Adult neurogenesis and neural stem cells of the central nervous system in mammals. J Neurosci Res. 2002;69:745-9.

[137] Kempermann G, Gast D, Kronenberg G, Yamaguchi M, Gage FH. Early determination and long-term persistence of adult-generated new neurons in the hippocampus of mice. Development. 2003;130:391-9.

[138] Song HJ, Stevens CF, Gage FH. Neural stem cells from adult hippocampus develop essential properties of functional CNS neurons. Nature Neurosci. 2002;5:438-45.

[139] van Praag H, Schinder AF, Christie BR, Toni N, Palmer TD, Gage FH. Functional neurogenesis in the adult hippocampus. Nature. 2002;415:1030-4.

[140] Andressen C. Neural stem cells: from neurobiology to clinical applications. Curr Pharm Biotechnol. 2013;14:20-8.

[141] Gage FH, Temple S. Neural stem cells: generating and regenerating the brain. Neuron. 2013;80:588-601.

[142] Lindvall O, Kokaia Z, Martinez-Serrano A. Stem cell therapy for human neurodegenerative disorders-how to make it work. Nature Med. 2004;10 Suppl:S42-50.

[143] Vishwakarma SK, Bardia A, Tiwari SK, Paspala SAB, Khan AA. Current concept in neural regeneration research: NSCs isolation, characterization and transplantation in

various neurodegenerative diseases and stroke. J Adv Res. 2013; DOI: 10.1016/j.jare.2013.04.005.

[144] Faigle R, Song H. Signaling mechanisms regulating adult neural stem cells and neurogenesis. Biochim Biophys Acta. 2013;1830:2435-48.

[145] Keung AJ, Dong M, Schaffer DV, Kumar S. Pan-neuronal maturation but not neuronal subtype differentiation of adult neural stem cells is mechanosensitive. Sci Rep. 2013;3:1817.

[146] Keung AJ, Kumar S, Schaffer DV. Presentation counts: microenvironmental regulation of stem cells by biophysical and material cues. Annu Review Cell Dev Bi. 2010;26:533-56.

[147] Palmer TD, Willhoite AR, Gage FH. Vascular niche for adult hippocampal neurogenesis. J Comp Neurol. 2000;425:479-94.

[148] Song H, Stevens CF, Gage FH. Astroglia induce neurogenesis from adult neural stem cells. Nature. 2002;417:39-44.

[149] Wade A, McKinney A, Phillips JJ. Matrix regulators in neural stem cell functions. Biochim Biophys Acta. 2014. DOI: 10.1016/j.bbagen.2014.01.017.

[150] Ananthanarayanan B, Little L, Schaffer DV, Healy KE, Tirrell M. Neural stem cell adhesion and proliferation on phospholipid bilayers functionalized with RGD peptides. Biomaterials. 2010;31:8706-15.

[151] Nakajima M, Ishimuro T, Kato K, Ko IK, Hirata I, Arima Y, et al. Combinatorial protein display for the cell-based screening of biomaterials that direct neural stem cell differentiation. Biomaterials. 2007;28:1048-60.

[152] Willerth SM, Rader A, Sakiyama-Elbert SE. The effect of controlled growth factor delivery on embryonic stem cell differentiation inside fibrin scaffolds. Stem Cell Res. 2008;1:205-18.

[153] Aizawa Y, Leipzig N, Zahir T, Shoichet M. The effect of immobilized platelet derived growth factor AA on neural stem/progenitor cell differentiation on cell-adhesive hydrogels. Biomaterials. 2008;29:4676-83.

[154] Leipzig ND, Xu C, Zahir T, Shoichet MS. Functional immobilization of interferon-gamma induces neuronal differentiation of neural stem cells. J Biomed Mater Res A. 2010;93:625-33.

[155] Kennedy HJ. New developments in understanding the mechanisms and function of spontaneous electrical activity in the developing mammalian auditory system. JARO. 2012;13:437-45.

[156] Kilb W, Kirischuk S, Luhmann HJ. Electrical activity patterns and the functional maturation of the neocortex. Eur J Neurosci. 2011;34:1677-86.

[157] Yamamoto N, Lopez-Bendito G. Shaping brain connections through spontaneous neural activity. Eur J Neurosci. 2012;35:1595-604.

[158] Guimard NK, Gomez N, Schmidt CE. Conducting polymers in biomedical engineering. Prog Polym Sci. 2007;32:876-921.

[159] Salto C, Saindon E, Bolin M, Kanciurzewska A, Fahlman M, Jager EW, et al. Control of neural stem cell adhesion and density by an electronic polymer surface switch. Langmuir. 2008;24:14133-8.

[160] Bechara S, Wadman L, Popat KC. Electroconductive polymeric nanowire templates facilitates in vitro C17.2 neural stem cell line adhesion, proliferation and differentiation. Acta Biomater. 2011;7:2892-901.

[161] Deng M, Yang X, Silke M, Qiu WM, Xu MS, Borghs G, et al. Electrochemical deposition of polypyrrole/graphene oxide composite on microelectrodes towards tuning the electrochemical properties of neural probes. Sensor Actuat B-Chem. 2011;158:176-84.

[162] Osterholm A, Lindfors T, Kauppila J, Damlin P, Kvarnstrom C. Electrochemical incorporation of graphene oxide into conducting polymer films. Electrochim Acta. 2012;83:463-70.

[163] Tian H, Liu J, Wei D, Kang X, Zhang C, Du J, et al. Graphene oxide doped conducting polymer nanocomposite film for electrode-tissue interface. Biomaterials. 2013.

[164] Yang F, Xu CY, Kotaki M, Wang S, Ramakrishna S. Characterization of neural stem cells on electrospun poly(L-lactic acid) nanofibrous scaffold. J Biomater Sci Polymer. 2004;15:1483-97.

[165] Zanden C, Erkenstam NH, Padel T, Wittgenstein J, Liu J, Georg Kuhn H. Stem cell responses to plasma surface modified electrospun polyurethane scaffolds. Nanomedicine-UK. 2014.

[166] Barreto JA, O'Malley W, Kubeil M, Graham B, Stephan H, Spiccia L. Nanomaterials: applications in cancer imaging and therapy. Adv Mater. 2011;23:H18-40.

[167] Sharifi S, Behzadi S, Laurent S, Forrest ML, Stroeve P, Mahmoudi M. Toxicity of nanomaterials. Chem Soc Rev. 2012;41:2323-43.

[168] Zhang L, Gu FX, Chan JM, Wang AZ, Langer RS, Farokhzad OC. Nanoparticles in medicine: therapeutic applications and developments. Clin Pharm Ther. 2008;83:761-9.

[169] Bianco A. Graphene: safe or toxic? The two faces of the medal. Angew Chem. 2013;52:4986-97.

[170] Liu Y, Luo Y, Wu J, Wang Y, Yang X, Yang R, et al. Graphene oxide can induce in vitro and in vivo mutagenesis. Sci Rep-UK. 2013.

[171] Zhang YB, Ali SF, Dervishi E, Xu Y, Li ZR, Casciano D, et al. Cytotoxicity effects of graphene and single-wall carbon nanotubes in neural phaeochromocytoma-derived PC12 cells. ACS Nano. 2010;4:3181-6.

[172] Li N, Zhang Q, Gao S, Song Q, Huang R, Wang L, et al. Three-dimensional graphene foam as a biocompatible and conductive scaffold for neural stem cells. Sci Rep-UK. 2013;3.

[173] Park SY, Park J, Sim SH, Sung MG, Kim KS, Hong BH, et al. Enhanced differentiation of human neural stem cells into neurons on graphene. Adv Mater. 2011;23:H263-7.

[174] Chen S, Lewallen M, Xie T. Adhesion in the stem cell niche: biological roles and regulation. Development. 2013;140:255-65.

[175] Harnett EM, Alderman J, Wood T. The surface energy of various biomaterials coated with adhesion molecules used in cell culture. Colloid Surface B. 2007;55:90-7.

[176] Kandel ER. Principles of neural science. 5th ed. New York: McGraw-Hill; 2013.

[177] Yang F, Murugan R, Wang S, Ramakrishna S. Electrospinning of nano/micro scale poly(L-lactic acid) aligned fibers and their potential in neural tissue engineering. Biomaterials. 2005;26:2603-10.

[178] Ren YJ, Zhang H, Huang H, Wang XM, Zhou ZY, Cui FZ, et al. In vitro behavior of neural stem cells in response to different chemical functional groups. Biomaterials. 2009;30:1036-44.

[179] Stevens MM, George JH. Exploring and engineering the cell surface interface. Science. 2005;310:1135-8.

[180] Scadden DT. The stem-cell niche as an entity of action. Nature. 2006;441:1075-9.

[181] Wong G, Goldshmit Y, Turnley AM. Interferon-gamma but not TNF alpha promotes neuronal differentiation and neurite outgrowth of murine adult neural stem cells. Exp Neurol. 2004;187:171-7.

[182] Hu JG, Fu SL, Wang YX, Li Y, Jiang XY, Wang XF, et al. Platelet-derived growth factor-AA mediates oligodendrocyte lineage differentiation through activation of extracellular signal-regulated kinase signaling pathway. Neuroscience. 2008;151:138-47.

[183] Murugan AV, Quintin M, Delville MH, Campet G, Vijayamohanan K. Entrapment of poly(3,4-ethylenedioxythiophene) between VS2 layers to form a new organic-inorganic intercalative nanocomposite. J Mater Chem. 2005;15:902-9.

[184] Kong J, Yu S. Fourier transform infrared spectroscopic analysis of protein secondary structures. Acta Bioch Bioph Sin. 2007;39:549-59.

[185] Ibrahim M, Nada A, Kamal DE. Density functional theory and FTIR spectroscopic study of carboxyl group. Indian J Pure Ap Phy. 2005;43:911-7.

[186] LaVan DA, McGuire T, Langer R. Small-scale systems for in vivo drug delivery. Nat Biotechnol. 2003;21:1184-91.

[187] Staples M. Microchips and controlled-release drug reservoirs. Wires Nanomed Nanobi. 2010;2:400-17.

[188] Timko BP, Kohane DS. Materials to Clinical Devices: Technologies for Remotely Triggered Drug Delivery. Clin Ther. 2012;34:S25-S35.

[189] Mura S, Nicolas J, Couvreur P. Stimuli-responsive nanocarriers for drug delivery. Nature Mater. 2013;12:991-1003.

[190] Timko BP, Dvir T, Kohane DS. Remotely triggerable drug delivery systems. Adv Mater. 2010;22:4925-43.

[191] Balmert SC, Little SR. Biomimetic delivery with micro- and nanoparticles. Adv Mater. 2012;24:3757-78.

[192] Bianco A, Kostarelos K, Prato M. Applications of carbon nanotubes in drug delivery. Curr Opin Chem Biol. 2005;9:674-9.

[193] Yang K, Feng L, Shi X, Liu Z. Nano-graphene in biomedicine: theranostic applications. Chem Soc Rev. 2013;42:530-47.

[194] Li M, Yang XJ, Ren JS, Qu KG, Qu XG. Using graphene oxide high near-infrared absorbance for photothermal treatment of alzheimer's disease. Adv Mater. 2012;24:1722-8.

[195] Sanchez VC, Jachak A, Hurt RH, Kane AB. Biological interactions of graphene-family nanomaterials: an interdisciplinary review. Chem Res Toxicol. 2012;25:15-34.

[196] Tao Y, Lin YH, Huang ZZ, Ren JS, Qu XG. Incorporating graphene oxide and gold nanoclusters: a synergistic catalyst with surprisingly high peroxidase-like activity over a broad pH range and its application for cancer cell detection. Adv Mater. 2013;25:2594-9.

[197] Sun XM, Liu Z, Welsher K, Robinson JT, Goodwin A, Zaric S, et al. Nano-graphene oxide for cellular imaging and drug delivery. Nano Res. 2008;1:203-12.

[198] Yang XY, Zhang XY, Liu ZF, Ma YF, Huang Y, Chen Y. High-efficiency loading and controlled release of doxorubicin hydrochloride on graphene oxide. J Phys Chem C. 2008;112:17554-8.

[199] Depan D, Shah J, Misra RDK. Controlled release of drug from folate-decorated and graphene mediated drug delivery system: Synthesis, loading efficiency, and drug release response. Mat Sci Eng C-Mater. 2011;31:1305-12.

[200] Ma XX, Tao HQ, Yang K, Feng LZ, Cheng L, Shi XZ, et al. A functionalized graphene oxide-iron oxide nanocomposite for magnetically targeted drug delivery, photothermal therapy, and magnetic resonance imaging. Nano Res. 2012;5:199-212.

[201] Yang XY, Wang YS, Huang X, Ma YF, Huang Y, Yang RC, et al. Multi-functionalized graphene oxide based anticancer drug-carrier with dual-targeting function and pH-sensitivity. J Mater Chem. 2011;21:3448-54.

[202] Yang XY, Zhang XY, Ma YF, Huang Y, Wang YS, Chen YS. Superparamagnetic graphene oxide-Fe3O4 nanoparticles hybrid for controlled targeted drug carriers. J Mater Chem. 2009;19:2710-4.

[203] Zhang JL, Yang HJ, Shen GX, Cheng P, Zhang JY, Guo SW. Reduction of graphene oxide via L-ascorbic acid. Chem Commun. 2010;46:1112-4.

[204] Liu HW, Hu SH, Chen YW, Chen SY. Characterization and drug release behavior of highly responsive chip-like electrically modulated reduced graphene oxide-poly(vinyl alcohol) membranes. J Mater Chem. 2012;22:17311-20.

[205] Luo XL, Cui XT. Electrochemically controlled release based on nanoporous conducting polymers. Electrochem Commun. 2009;11:402-4.

[206] Si P, Chen HL, Kannan P, Kim DH. Selective and sensitive determination of dopamine by composites of polypyrrole and graphene modified electrodes. Analyst. 2011;136:5134-8.

[207] Si WM, Lei W, Zhang YH, Xia MZ, Wang FY, Hao QL. Electrodeposition of graphene oxide doped poly(3,4-ethylenedioxythiophene) film and its electrochemical sensing of catechol and hydroquinone. Electrochim Acta. 2012;85:295-301.

[208] Li Y, Wu Y. Coassembly of graphene oxide and nanowires for large-area nanowire alignment. J Am Chem Soc. 2009;131:5851-7.

[209] Vernitskaya TV, Efimov ON. Polypyrrole: A conducting polymer (synthesis, properties, and applications). Russ Chem Rev. 1997;66:489-505.

[210] Unemura K, Kume T, Kondo M, Maeda Y, Izumi Y, Akaike A. Glucocorticoids decrease astrocyte numbers by reducing glucocorticoid receptor expression in vitro and in vivo. J Pharmacol Sci. 2012;119:30-9.

[211] Russier J, Treossi E, Scarsi A, Perrozzi F, Dumortier H, Ottaviano L, et al. Evidencing the mask effect of graphene oxide: a comparative study on primary human and murine phagocytic cells. Nanoscale. 2013;5:11234-47.

[212] Luo J, Kim J, Huang J. Material processing of chemically modified graphene: some challenges and solutions. Accounts Chem Res. 2013;46:2225-34.

[213] Kolind K, Leong KW, Besenbacher F, Foss M. Guidance of stem cell fate on 2D patterned surfaces. Biomaterials. 2012;33:6626-33.

[214] Yim EK, Leong KW. Significance of synthetic nanostructures in dictating cellular response. Nanomedicine-UK. 2005;1:10-21.

[215] Zhang B, Xiao Y, Hsieh A, Thavandiran N, Radisic M. Micro- and nanotechnology in cardiovascular tissue engineering. Nanotechnology. 2011;22:494003.

[216] Wise RA. Dopamine, learning and motivation. Nat Rev Neurosci. 2004;5:483-94.

[217] Lotharius J, Brundin P. Pathogenesis of Parkinson's disease: Dopamine, vesicles and alpha-synuclein. Nat Rev Neurosci. 2002;3:932-42.

[218] Yang CR, Seamans JK, Gorelova N. Developing a neuronal model for the pathophysiology of schizophrenia based on the nature of electrophysiological actions of dopamine in the prefrontal cortex. Neuropsychopharmacol. 1999;21:161-94.

[219] Volkow ND, Fowler JS, Wang GJ, Swanson JM. Dopamine in drug abuse and addiction: results from imaging studies and treatment implications. Mol Psychiatr. 2004;9:557-69.

[220] Noelker C, Hampel H, Dodel R. Blood-based protein biomarkers for diagnosis and classification of neurodegenerative diseases: current progress and clinical potential. Mol Diagn Ther. 2011;15:83-102.

[221] Eisenhofer G, Tischler AS, de Krijger RR. Diagnostic tests and biomarkers for pheochromocytoma and extra-adrenal paraganglioma: from routine laboratory methods to disease stratification. Endocr Pathol. 2012;23:4-14.

[222] Robinson DL, Hermans A, Seipel AT, Wightman RM. Monitoring rapid chemical communication in the brain. Chem Rev. 2008;108:2554-84.

[223] Bicker J, Fortuna A, Alves G, Falcao A. Liquid chromatographic methods for the quantification of catecholamines and their metabolites in several biological samples--a review. Anal Chim Acta. 2013;768:12-34.

[224] Lee NS, Hsieh YZ, Paisley RF, Morris MD. Surface-enhanced Raman spectroscopy of the catecholamine neurotransmitters and related compounds. Anal Chem. 1988;60:442-6.

[225] Liu D, Wang Z, Jiang X. Gold nanoparticles for the colorimetric and fluorescent detection of ions and small organic molecules. Nanoscale. 2011;3:1421-33.

[226] Westerink BH. Analysis of biogenic amines in microdialysates of the brain. J Chromatogr B. 2000;747:21-32.

[227] Kuila T, Bose S, Khanra P, Mishra AK, Kim NH, Lee JH. Recent advances in graphene-based biosensors. Biosens Bioelectron. 2011;26:4637-48.

[228] Liu Y, Dong X, Chen P. Biological and chemical sensors based on graphene materials. Chem Soc Rev. 2012;41:2283-307.

[229] Tang L, Wang Y, Li Y, Feng H, Lu J, Li J. Preparation, structure, and electrochemical properties of reduced graphene sheet films. Adv Funct Mater. 2009;19:2782-9.

[230] Li J, Yang J, Yang ZJ, Li YF, Yu SH, Xu Q, et al. Graphene-Au nanoparticles nanocomposite film for selective electrochemical determination of dopamine. Anal Methods-UK. 2012;4:1725-8.

[231] Zhu X, Liu Q, Zhu XH, Li CL, Xu MT, Liang Y. Reduction of graphene oxide via ascorbic acid and its application for simultaneous detection of dopamine and ascorbic acid. Int J Electrochem Sc. 2012;7:5172-84.

[232] Duan YY, Clark GM, Cowan RSC. Factors determining and limiting the impedance behavior of implanted bio-electrodes. Proc SPIE. 2001;4235:498-508.

[233] Karp FB, Bemotski NA, Valdes TI, Bohringer KF, Ratner BD. Foreign body response investigated with an implanted biosensor by in situ electrical impedance spectroscopy. IEEE Sens J. 2008;8:104-12.

[234] Deakin MR, Kovach PM, Stutts KJ, Wightman RM. Heterogeneous mechanisms of the oxidation of catechols and ascorbic-acid at carbon electrodes. Anal Chem. 1986;58:1474-80.

[235] Saraceno RA, Pack JG, Ewing AG. Catalysis of slow charge-transfer reactions at polypyrrole-coated glassy-carbon electrodes. J Electroanal Chem. 1986;197:265-78.

[236] Engstrom RC, Strasser VA. Characterization of electrochemically pretreated glassy-carbon electrodes. Anal Chem. 1984;56:136-41.

[237] Hu IF, Karweik DH, Kuwana T. Activation and deactivation of glassy-carbon electrodes. J Electroanal Chem. 1985;188:59-72.

[238] Bagherzadeh M, Heydari M. Electrochemical detection of dopamine based on pre-concentration by graphene nanosheets. Analyst. 2013;138:6044-51.

[239] Rochefort A, Wuest JD. Interaction of substituted aromatic compounds with graphene. Langmuir. 2009;25:210-5.

[240] Armstrong J, Barlow RB. The ionization of phenolic amines, including apomorphine, dopamine and catecholamines and an assessment of zwitterion constants. British J Pharmacol. 1976;57:501-16.

[241] Konkena B, Vasudevan S. Understanding aqueous dispersibility of graphene oxide and reduced graphene oxide through pK(a) measurements. J Phys Chem Lett. 2012;3:867-72.

[242] Bagri A, Mattevi C, Acik M, Chabal YJ, Chhowalla M, Shenoy VB. Structural evolution during the reduction of chemically derived graphene oxide. Nat Chem. 2010;2:581-7.

[243] Brezina M, Koryta J, Loucka T, Marsikova D. Adsorption and kinetics of oxidation of ascorbic acid at platinum electrodes. J Electroanal Chem. 1972;40:13-7.

[244] Karabinas P, Jannakoudakis D. Kinetic-parameters and mechanism of the electrochemical oxidation of l-ascorbic-acid on platinum-electrodes in acid-solutions. J Electroanal Chem. 1984;160:159-67.

[245] Rueda M, Aldaz A, Sanchez-Burgos F. Oxidation of l-ascorbic acid on a gold electrode. Electrochim Acta. 1978;23:419-24.

[246] Langlois JA, Rutland-Brown W, Wald MM. The epidemiology and impact of traumatic brain injury: a brief overview. J Head Trauma Rehabil. 2006;21:375-8.

[247] Algattas H, Huang JH. Traumatic Brain Injury pathophysiology and treatments: early, intermediate, and late phases post-injury. Int J Mol Sci. 2014;15:309-41.

[248] Tran LV. Understanding the pathophysiology of traumatic brain injury and the mechanisms of action of neuroprotective interventions. J Trauma Nurs. 2014;21:30-5.

[249] Kumaria A, Tolias CM. In vitro models of neurotrauma. British Journal Neurosurg. 2008;22:200-6.

[250] Morrison B, 3rd, Elkin BS, Dolle JP, Yarmush ML. In vitro models of traumatic brain injury. Ann Rev Biomed Eng. 2011;13:91-126.

[251] van Pelt J, Wolters PS, Corner MA, Rutten WL, Ramakers GJ. Long-term characterization of firing dynamics of spontaneous bursts in cultured neural networks. IEEE T Bio-Med Eng. 2004;51:2051-62.

[252] Wagenaar DA, Pine J, Potter SM. An extremely rich repertoire of bursting patterns during the development of cortical cultures. BMC Neurosci. 2006;7:11.

[253] Yu Z, Graudejus O, Tsay C, Lacour SP, Wagner S, Morrison B, 3rd. Monitoring hippocampus electrical activity in vitro on an elastically deformable microelectrode array. J Neurotrauma. 2009;26:1135-45.

[254] Yu Z, Lacour SP, Tsay C, Wagner S, Morrison B. A new tool to study post-traumatic neuronal dysfunction: Stretchable microelectrode arrays. J Neurotrauma. 2006;23:998.

[255] Harting MT, Sloan LE, Jimenez F, Baumgartner J, Cox CS, Jr. Subacute neural stem cell therapy for traumatic brain injury. J Surg Res. 2009;153:188-94.

[256] Brewer GJ, Price PJ. Viable cultured neurons in ambient carbon dioxide and hibernation storage for a month. Neuroreport. 1996;7:1509-12.

[257] Hovda DA, Lee SM, Smith ML, Von Stuck S, Bergsneider M, Kelly D, et al. The neurochemical and metabolic cascade following brain injury: moving from animal models to man. J Neurotrauma. 1995;12:903-6.

[258] Kozai TD, Langhals NB, Patel PR, Deng X, Zhang H, Smith KL, et al. Ultrasmall implantable composite microelectrodes with bioactive surfaces for chronic neural interfaces. Nature Mater. 2012;11:1065-73.

[259] Ludwig KA, Uram JD, Yang J, Martin DC, Kipke DR. Chronic neural recordings using silicon microelectrode arrays electrochemically deposited with a poly(3,4-ethylenedioxythiophene) (PEDOT) film. J Neural Eng. 2006;3:59-70.

[260] Chiappalone M, Bove M, Vato A, Tedesco M, Martinoia S. Dissociated cortical networks show spontaneously correlated activity patterns during in vitro development. Brain Res. 2006;1093:41-53.

[261] Eytan D, Minerbi A, Ziv N, Marom S. Dopamine-induced dispersions of correlations between action potentials in networks of cortical neurons. J Neurophysiol. 2004;92:1871-24.

[262] Stephens CL, Toda H, Palmer TD, DeMarse TB, Ormerod BK. Adult neural progenitor cells reactivate superbursting in mature neural networks. Exp Neurol. 2012;234:20-30.

[263] Ben-Ari Y. Developing networks play a similar melody. Trend Neurosci. 2001;24:353-60.

[264] Dupont E, Hanganu IL, Kilb W, Hirsch S, Luhmann HJ. Rapid developmental switch in the mechanisms driving early cortical columnar networks. Nature. 2006;439:79-83.

[265] Pine J. Recording action potentials from cultured neurons with extracellular microcircuit electrodes. J Neurosci Meth. 1980;2:19-31.

[266] Peters A, Palay SL, Webster Hd. The fine structure of the nervous system : the neurons and supporting cells. Philadelphia: Saunders; 1976.

[267] Chen J, Backus KH, Deitmer JW. Intracellular calcium transients and potassium current oscillations evoked by glutamate in cultured rat astrocytes. J Neurosci. 1997;17:7278-87.

[268] Pasti L, Volterra A, Pozzan T, Carmignoto G. Intracellular calcium oscillations in astrocytes: a highly plastic, bidirectional form of communication between neurons and astrocytes in situ. J Neurosci. 1997;17:7817-30.

[269] Martin D. Synthesis and release of neuroactive substrances by glial cells. Glia. 1992;5:81-94.

[270] Fellin T. Communication between neurons and astrocytes: relevance to the modulation of synaptic and network activity. J Neurochem. 2009;108:533-44.

[271] Newman EA. New roles for astrocytes: regulation of synaptic transmission. Trend Neurosci. 2003;26:536-42.

[272] Werner C, Engelhard K. Pathophysiology of traumatic brain injury. British J Anaesth. 2007;99:4-9.

[273] Corner MA, van Pelt J, Wolters PS, Baker RE, Nuytinck RH. Physiological effects of sustained blockade of excitatory synaptic transmission on spontaneously active developing neuronal networks--an inquiry into the reciprocal linkage between intrinsic biorhythms and neuroplasticity in early ontogeny. Neurosci Biobehav Rev. 2002;26:127-85.

[274] Ramakers GJ, van Galen H, Feenstra MG, Corner MA, Boer GJ. Activity-dependent plasticity of inhibitory and excitatory amino acid transmitter systems in cultured rat cerebral cortex. Int J Dev Neurosci. 1994;12:611-21.

[275] Imbrosci B, Mittmann T. Functional consequences of the disturbances in the GABA-mediated inhibition induced by injuries in the cerebral cortex. Neural Plast. 2011;2011:614329.

[276] Li H, Prince DA. Synaptic activity in chronically injured, epileptogenic sensory-motor neocortex. J Neurophysiol. 2002;88:2-12.

[277] Paz JT, Christian CA, Parada I, Prince DA, Huguenard JR. Focal cortical infarcts alter intrinsic excitability and synaptic excitation in the reticular thalamic nucleus. J Neurosci. 2010;30:5465-79.

[278] Brown DR. Neurons depend on astrocytes in a coculture system for protection from glutamate toxicity. Mol Cell Neurosci. 1999;13:379-89.

[279] Rosenberg PA, Aizenman E. Hundred-fold increase in neuronal vulnerability to glutamate toxicity in astrocyte-poor cultures of rat cerebral cortex. Neurosci Lett. 1989;103:162-8.

[280] Yi JH, Hazell AS. Excitotoxic mechanisms and the role of astrocytic glutamate transporters in traumatic brain injury. Neurochem Int. 2006;48:394-403.

[281] Carletti B, Piemonte F, Rossi F. Neuroprotection: the emerging concept of restorative neural stem cell biology for the treatment of neurodegenerative diseases. Curr Neuropharmacol. 2011;9:313-7.

[282] Llado J, Haenggeli C, Maragakis NJ, Snyder EY, Rothstein JD. Neural stem cells protect against glutamate-induced excitotoxicity and promote survival of injured motor neurons through the secretion of neurotrophic factors. Mol Cell Neurosci. 2004;27:322-31.

[283] Goubko CA, Cao XD. Patterning multiple cell types in co-cultures: A review. Mat Sci Eng C-Mater. 2009;29:1855-68.

[284] Miller LL, Zhou QX. Poly(N-methylpyrrolylium) poly(styrenesulfonate). A conductive, electrically switchable cation exchanger that cathodically binds and anodically releases dopamine. Macromolecules. 1987;20:1594-7.

[285] Hepel M, Mahdavi F. Application of the electrochemical quartz crystal microbalance for electrochemically controlled binding and release of chlorpromazine from conductive polymer matrix. Microchem J. 1997;56:54-64.

[286] George PM, LaVan DA, Burdick JA, Chen C-Y, Liang E, Langer R. Electrically controlled drug delivery from biotin-doped conductive polypyrrole. Adv Mater. 2006;18:577-81.

[287] Wightman RM, Amatore C, Engstrom RC, Hale PD, Kristensen EW, Kuhr WG, et al. Real-time characterization of dopamine overflow and uptake in the rat striatum. Neurosci. 1988;25:513-23.

[288] Oh MY, Hodaie M, Kim SH, Alkhani A, Lang AE, Lozano AM. Deep brain stimulator electrodes used for lesioning: proof of principle. Neurosurg. 2001;49:363-7; discussion 7-9.

[289] Sparreboom M, van Schoonhoven J, van Zanten BG, Scholten RJ, Mylanus EA, Grolman W, et al. The effectiveness of bilateral cochlear implants for severe-to-profound deafness in children: a systematic review. Otol Neurotol. 2010;31:1062-71.

[290] Luo X, Weaver CL, Zhou DD, Greenberg R, Cui XT. Highly stable carbon nanotube doped poly(3,4-ethylenedioxythiophene) for chronic neural stimulation. Biomaterials. 2011;32:5551-7.

[291] Li Y, Li D, Ibrahim A, Raisman G. Repair involves all three surfaces of the glial cell. Prog Brain Res. 2012;201:199-218.

[292] Kawano H, Kimura-Kuroda J, Komuta Y, Yoshioka N, Li HP, Kawamura K, et al. Role of the lesion scar in the response to damage and repair of the central nervous system. Cell Tissue Res. 2012;349:169-80.

[293] Rodrigues LB, Leite HF, Yoshida MI, Saliba JB, Cunha AS, Faraco AAG. In vitro release and characterization of chitosan films as dexamethasone carrier. Int J Pharm. 2009;368:1-6.